COMMUNICATION

An effective strategy of magnetic stem cell delivery for spinal cord injury therapy†

Dmitry Tukmachev,[a,b] Oleg Lunov,*[c] Vitalii Zablotskii,[c] Alexandr Dejneka,[c] Michal Babic,[d] Eva Syková[a] and Šárka Kubinová*[a,c]

Spinal cord injury (SCI) is a condition that results in significant mortality and morbidity. Treatment of SCI utilizing stem cell transplantation represents a promising therapy. However, current conventional treatments are limited by inefficient delivery strategies of cells into the injured tissue. In this study, we designed a magnetic system and used it to accumulate stem cells labelled with superparamagnetic iron oxide nanoparticles (SPION) at a specific site of a SCI lesion. The loading of stem cells with engineered SPIONs that guarantees sufficient attractive magnetic forces was achieved. Further, the magnetic system allowed rapid guidance of the SPION-labelled cells precisely to the lesion location. Histological analysis of cell distribution throughout the cerebrospinal channel showed a good correlation with the calculated distribution of magnetic forces exerted onto the transplanted cells. The results suggest that focused targeting and fast delivery of stem cells can be achieved using the proposed non-invasive magnetic system. With future implementation the proposed targeting and delivery strategy bears advantages for the treatment of disease requiring fast stem cell transplantation.

Spinal cord injury (SCI) represents a devastating condition that leads to a dramatic disability, loss of voluntary movement, tactile sensibility, and is accompanied by chronic pain and spasticity.[1,2] Currently there is no available restorative therapy for SCI, only prevention is identified as the best medicine.[2,3] The transplantation of stem cells, particularly mesenchymal stem cells (MSCs), holds considerable potential as effective SCI therapies.[2–4] Despite the noticed therapeutic benefits, stem cell transplantation, in general, has a number of serious limitations related to the low efficiency of delivery, retention and

engraftment of cells.[5,6] To achieve a significant therapeutic benefit, minimally invasive but highly effective delivery strategies are a crucial aspect of cell transplantation. Interestingly, intrathecal injection of stem cells has considerable advantages (higher efficacy of delivery, better retention and survival of stem cells) over intravenous injection as a means of cell transplantation.[7–9] Moreover, it has been demonstrated that repetitive, but not single intrathecal administration of MSCs contributes to their migration into the central lesion and aids functional recovery after SCI in rats.[10] Effective cell targeting is therefore highly desirable in order to promote the homing of transplanted cells to the site of injury. In this regard, the use of magnetic nanomaterials represents novel effective treatment, particularly in SCI.[11] Several research lines have demonstrated the efficient loading of stem cells with superparamagnetic iron oxide nanoparticles (SPIONs) and have shown that magnetically guided cell delivery is able to boost cell retention, engraftment as well as the functional benefit of the cell therapy.[12–14] Indeed, magnetic forces have already been successfully used in directing SPION-labelled cells to a vascular graft,[15] intra-arterial stents,[16] the femoral artery,[17] bone,[18] cartilage,[19] and the retina.[20] However, in the case of SCI, studies on magnetically guided cell delivery have not been thoroughly performed. In fact, only two research groups have shown the therapeutic potential of the magnetic delivery of SPION-labelled cells to the SCI lesion site.[21–23] A common disadvantage of all the previous strategies of cell delivery that utilize magnetic systems[16,17,24,25] is their inappropriate focusing ability. Indeed, magnetic cell capturing takes place in the vicinity of a magnetic pole where the magnetic field gradient is at its maximal value. Since a magnet cannot be placed directly into the lesion site, the focusing ability of such systems is rather limited and not convenient for efficient stem cell transplantation.

Here we propose a new magnetic system consisting of two cylindrical NdFeB magnets (1 cm diameter and 5 cm height, out-of-plane remanent magnetization values 1.2 T) placed on a ring-shaped holder with the alike poles facing toward each other. A specific feature of the proposed magnetic system is

[a]Institute of Experimental Medicine, ASCR, 14200 Prague, Czech Republic. E-mail: sarka.k@biomed.cas.cz; Fax: +420-241062706; Tel: +420-241062635
[b]Department of Neuroscience, 2nd Faculty of Medicine, Charles University, 14220 Prague, Czech Republic
[c]Institute of Physics, ASCR, 18221 Prague, Czech Republic. E-mail: lunov@fzu.cz; Fax: +420-286581448; Tel: +420-266052131
[d]Institute of Macromolecular Chemistry, ASCR, 16206 Prague, Czech Republic
†Electronic supplementary information (ESI) available: Experimental procedures. See DOI: 10.1039/c4nr05791k
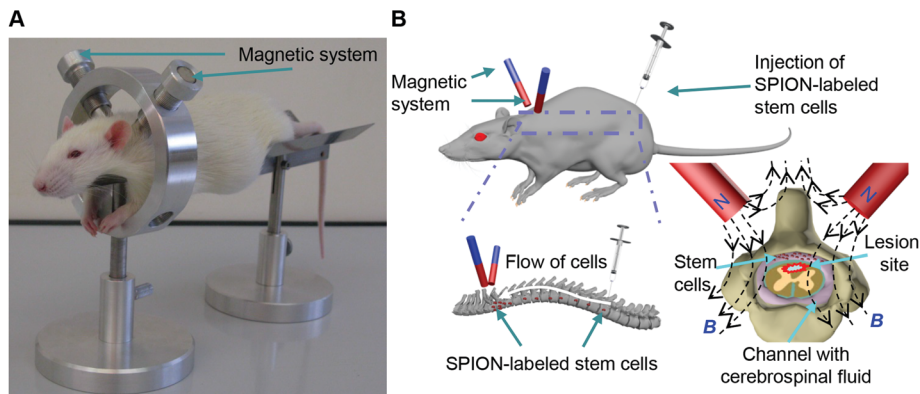
Fig. 1 Magnetic system for MSC targeting into SCI. (A) *In vivo* application of the non-invasive magnetic system for MSC targeting into SCI of a rat. (B) Schematic representation of the magnetic targeting strategy.

the existence of a focusing zone – *trapping area* – where both the horizontal and vertical magnetic force components (*X*- and *Z*-components) are almost zero (Fig. 1 and 2). This focusing zone is located just between the two maxima of the planar components (parallel to the *X–Z*-axis) of the magnetic gradient force (Fig. 2A–C). Thus, the magnetically labelled cells have to be focused namely in this trapping area. The existence of the trapping area (with zero magnetic forces) is determined by two reasons: (i) the maximums of the planar and vertical components of the magnetic field (MF) gradient must reach close

to the magnets' edges; (ii) in the mirror symmetry plane of the system the planar and vertical components of the MF gradients have opposite directions and compensate for each other. Fig. 2 shows the magnetic force distributions in the *X–Z*-plane between two magnets with opposing magnetisations that were calculated analytically using the explicit expressions for the magnetic stray fields produced by a uniformly magnetized magnet.[25] The area outlined by the ellipse represents the focusing zone for the given configuration of the magnetic poles and their geometry. In this study we exploit this mag-
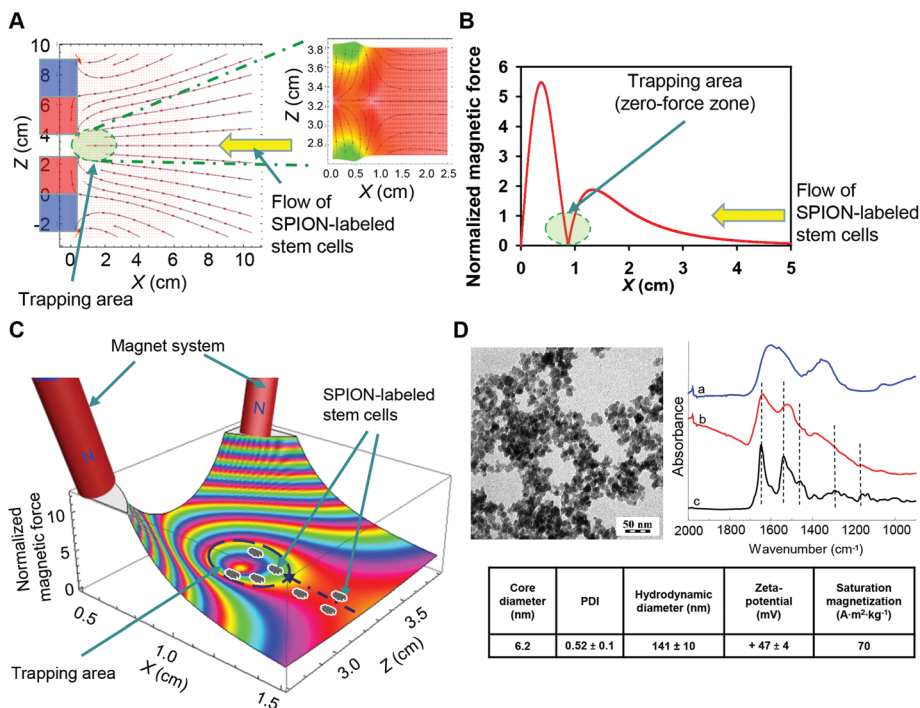

Fig. 2 Spatial distribution of the magnetic gradient forces between the magnets of the designed magnetic system. (A) Calculated vector field plot of the magnetic gradient force (*X–Z*-plane – the vertical cross-section of the spinal cord). The insert represents an enlarged region of the trapping area (zero-force zone). The arrows show the directions of the magnetic gradient forces ($f_m \propto \nabla B^2$) applied to a cell (where *B* is the magnetic induction). (B) Modulus of magnetic gradient force, $\left|(\vec{B}\vec{\nabla})\vec{B}\right|$, normalized to $(\mu_0 M_r)^2 r^{-1}$, as a function of the *X*-coordinate which is along the cerebrospinal channel (M_r represents the remanent magnetization and $\mu_0 M_r = 1.2$ T for the used magnets, magnet radius *r* = 0.5 cm). In (A) and (B) the focusing area is shown by the green ellipses. (C) 3D plot of the normalized magnetic gradient force (*X–Z*-plane). (D) Physicochemical properties of SPIONs.

netic system to enhance the efficacy of stem cell delivery using rat models of SCI. The experiments were carried out in following groups of animals: SPION-labelled MSCs exposed to MF, non-labelled MSCs exposed to MF and SPION-labelled MSCs without exposure to MF. One week after the induction of the lesion, 5×10^5 cells were injected intrathecally at the L5–L6 level, at a distance of 10 cm from the lesion site (Fig. 1A and B). Subsequently, the above-described external magnetic system was placed around the rat, under the top of the vertebral column above the lesion site at Th10, for two hours to improve cell retention and attachment (Fig. 1A and B). For MSCs labelling the poly-L-lysine-coated SPIONs were chosen as non-toxic and non-inducing pathophysiological effects nanoparticles as described in our previously performed biocompatibility screening.[26–28]

First, we tested whether the MSCs labelled with SPIONs (Fig. 2D) can be efficiently attracted by a magnet *in vitro* (Fig. 3A). Second, *in vivo* experiments (which scheme is depicted in Fig. 1) showed dramatic increase of SPION-labelled cell retention at the lesion site (Fig. 3B and 4B, C). On the other hand, cells without SPIONs and cells loaded with SPIONs but with no magnets exhibited practically homogenous distribution through the spinal cord channel (Fig. 3B). This means that the lesion itself, which releases various chemoattractants, is not able to retain the transplanted cells and therefore enhance their homing to the damaged

tissue area. It is worth noting that the cell distribution in the vicinity of the lesion site (Fig. 3B) was quantitatively consistent with the calculated magnetic gradient force distribution (Fig. 2B and C): SPION-labelled cells accumulated maximally in the trapping area of the magnetic system (Fig. 3B and 4A). Moreover, the number of SPION-labelled cells in the centre of the lesion was significantly higher when compared to the control groups (Fig. 3). Furthermore, very few cells were detected in the cranial direction from the magnetic gradient force (Fig. 3B and 4A), which verifies the capture of the SPION-labelled cells within the MF. In contrast, non-labelled cells used with MF and SPION-labelled cells without MF revealed a homogeneous distribution without any apparent effect of the MF on cell accumulation at SCI lesion site (Fig. 3B). Aside from this, the use of the magnetic system resulted in a significant increase in SPION-labelled cell accumulation directly in the lesion site in comparison to no MF application (Fig. 4B and C). The ratio (E) between the number of cells captured in the lesion site and the total number of cells in the operating range of the spinal cord may serve as a convenient measure of the efficiency of cell delivery. From Fig. 3B the ratio E was calculated for three studied animal groups: $E = 45\%$ for the SPION-labelled MSCs exposed to MF; $E = 14\%$ for the non-labelled MSCs exposed to MF and $E = 13\%$ for the SPION-labelled MSCs without exposure to MF. Thus, there is an obvious advantage of the proposed magnetic delivery strategy
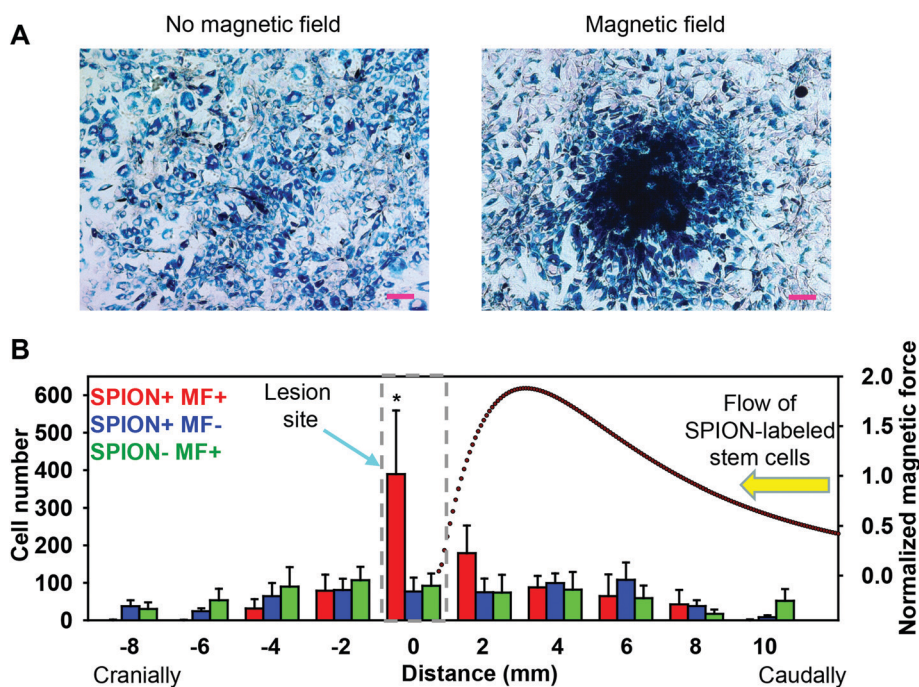
Fig. 3 Distributions of SPION-labelled cells and non-labelled cells with and without the magnetic field. (A) Attraction of SPION-labelled cells to a cylindrical magnet *in vitro*. MSCs were labelled with SPIONs at a concentration of 15.4 µg mL^{-1} and exposed to an external magnetic field for 48 h. Cells were stained for intracellular iron using Prussian blue. Scale bar: 100 µm. (B) Numbers of the captured SPION-labelled cells and non-labelled cells in the rat model as a function of the distance from the lesion site of the SCI. After the induction of the lesion, SPION-labelled MSCs were injected intrathecally at the L5–L6 level, at a distance of 10 cm from the lesion site. Thereafter, animals were subjected to the magnetic system exposure for 2 h in longitudinal spinal cord segments. The dotted curves represent the respective magnetic gradient force distribution taken from Fig. 2B. Data are expressed as mean ± SEM, *$P < 0.05$.
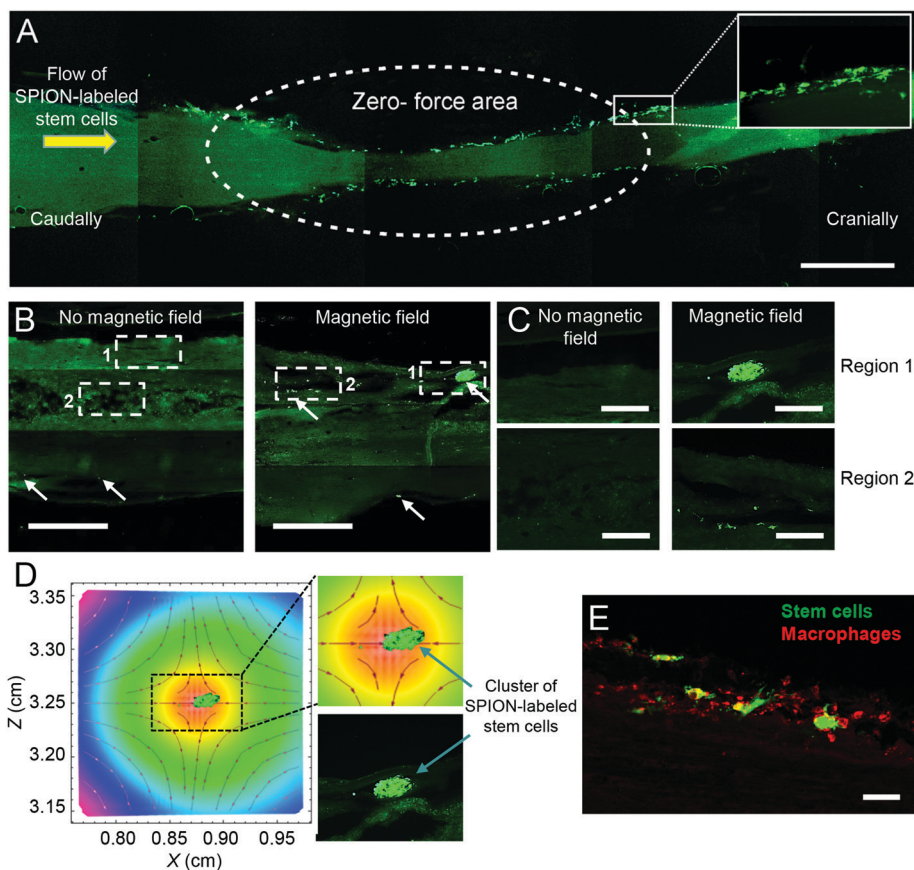
Fig. 4 Longitudinal spinal cord sections of the targeted SPIONs-labelled MSCs. (A) Spinal cord sections of SPION-labelled MSCs captured in the trapping area of the magnetic system. Scale bar – 1 mm. (B) Longitudinal sections of the lesion site showing MSC distribution within the lesion with or without exposure to the magnetic field. The arrows show clusters of delivered SPION-labelled MSCs on the surface of the spinal cord (region 1) and SPION labelled MSCs that migrated in the deeper area of the lesion (region 2). Scale bar – 500 μm. (C) Higher magnification of regions 1 and 2 of (B). Upon application of the magnetic field system, one can clearly see clusters of delivered SPION-labelled MSCs on the surface of the spinal cord (region 1) and in the deeper area of the lesion (region 2). Scale bar – 100 μm. (D) Overlay vector field of the calculated magnetic gradient force (X–Z-plane) with a cluster of accumulated cells. The binary image was generated from the respective fluorescent picture using ImageJ software (NIH). A representative enlarged region of the magnetic gradient force distribution (Fig. 2A) was calculated in accordance with the magnetic system positioning. The insert shows a zoomed in section of the indicated region. (E) Immunofluorescence staining of MSCs and macrophage infiltration in the lesion site. Macrophages were stained for the CD68 marker. Scale bar – 50 μm.

resulting in a 3-fold increase of the ratio E. Furthermore, migration of stem cells from the cerebrospinal fluid into tissue has been associated with a better prognosis of SCI treatment.[29] Interestingly, the application of MF for 2 h resulted in stem cell infiltration into the tissue (Fig. 4B and C). Finally, the designed magnetic system targeted SPION-labelled cells to the trapping area (Fig. 4D), as revealed by superimposing the immunofluorescence images with the calculated normalized magnetic force distribution (Fig. 4D). However, after stem cell delivery to the lesion site, an adverse reaction occurred. Microglia/macrophages attacked the SPION-labelled stem cells (Fig. 4E). Thus, the long-term effects of transplanted SPION-labelled stem cells should be investigated in more detail in future studies. Consequently, because of the obvious advantages of the stem cell-based SCI therapy, we should look further for a pharmacological (or any other) strategy to counteract the impact of SPION-derived adverse effects *in vivo*. In future studies, the efficacy of such a magnetic targeting strategy and the possibilities of reaching therapeutic concentrations should be assessed together with the physiological and biological factors that decrease the number of captured living cells at the lesion site.

Conclusions

A minimally invasive magnetic targeting strategy enabling fast cell retention after intrathecal transplantation was designed and tested *in vivo*. Its main advantage is the ability to reach a significantly higher concentration of SPION-labelled stem cells into the vicinity of a lesion site. We succeeded in efficiently delivering stem cells to lesions within the animal anaesthesia time period, 2 hours. In our experiments, in contrast to the control non-magnetic groups, the SPION-labelled cells were able to migrate from the trapping area to the lesion site (Fig. 4C). It is worth noting that the efficacy of stem cell transplantation to the lesion site is low and variable,[30] with typical

delivery time to SCI varying from 12 to 24 h.[22,31,32] Therefore, the application of our magnetic system for targeted stem cell delivery into SCI lesions demonstrates the potential benefits of fast and efficient cell delivery. The proposed strategy can be used for stem cell-based treatments of not only traumatic SCIs, but also for non-traumatic SCI or neurodegenerative diseases.[33,34] The fate and regenerative capacity of magnetically labelled MSCs after their forced accumulation near the lesion would be a challenging direction for further study.

Acknowledgements

Notes and references

1 E. J. Bradbury and S. B. McMahon, *Nat. Rev. Neurosci.*, 2006, **7**, 644–653.

2 S. Thuret, L. D. F. Moon and F. H. Gage, *Nat. Rev. Neurosci.*, 2006, **7**, 628–643.

3 A. Antonic, E. S. Sena, J. S. Lees, T. E. Wills, P. Skeers, P. E. Batchelor, M. R. Macleod and D. W. Howells, *PLoS Biol.*, 2013, **11**, e1001738.

4 A. P. Pego, S. Kubinova, D. Cizkova, I. Vanicky, F. M. Mar, M. M. Sousa and E. Sykova, *J. Cell Mol. Med.*, 2012, **16**, 2564–2582.

5 I. L. Weissman, *Science*, 2000, **287**, 1442–1446.

6 A. Al Kindi, Y. Ge, D. Shum-Tim and R. C. J. Chiu, *Front. Biosci.*, 2008, **13**, 2421–2434.

7 S. Pluchino, A. Quattrini, E. Brambilla, A. Gritti, G. Salani, G. Dina, R. Galli, U. Del Carro, S. Amadio, A. Bergami, R. Furlan, G. Comi, A. L. Vescovi and G. Martino, *Nature*, 2003, **422**, 688–694.

8 S. F. Wu, Y. Suzuki, M. Kitada, K. Kataoka, M. Kitaura, H. Chou, Y. Nishimura and C. Ide, *Neurosci. Lett.*, 2002, **318**, 81–84.

9 A. Bakshi, C. Hunter, S. Swanger, A. Lepore and I. Fischer, *J. Neurosurg: Spine*, 2004, **1**, 330–337.

10 D. Cizkova, I. Novotna, L. Slovinska, I. Vanicky, S. Jergova, J. Rosocha and J. Radonak, *J. Neurotrauma*, 2011, **28**, 1951–1961.

11 J. Y. Tyler, X. M. Xu and J. X. Cheng, *Nanoscale*, 2013, **5**, 8821–8836.

12 N. Landazuri, S. Tong, J. Suo, G. Joseph, D. Weiss, D. J. Sutcliffe, D. P. Giddens, G. Bao and W. R. Taylor, *Small*, 2013, **9**, 4017–4026.

13 A. C. Vandergriff, T. M. Hensley, E. T. Henry, D. L. Shen, S. Anthony, J. Y. Zhang and K. Cheng, *Biomaterials*, 2014, **35**, 8528–8539.

14 K. Cheng, D. Shen, M. T. Hensley, R. Middleton, B. Sun, W. Liu, G. De Couto and E. Marban, *Nat. Commun.*, 2014, **5**, 4880.

15 S. V. Pislaru, A. Harbuzariu, G. Agarwal, T. Witt, R. Gulati, N. P. Sandhu, C. Mueske, M. Kalra, R. D. Simari and G. S. Sandhu, *Circulation*, 2006, **114**, 314–318.

16 B. Polyak, I. Fishbein, M. Chorny, I. Alferiev, D. Williams, B. Yellen, G. Friedman and R. J. Levy, *Proc. Natl. Acad. Sci. U. S. A.*, 2008, **105**, 698–703.

17 J. Riegler, A. Liew, S. O. Hynes, D. Ortega, T. O'Brien, R. M. Day, T. Richards, F. Sharif, Q. A. Pankhurst and M. F. Lythgoe, *Biomaterials*, 2013, **34**, 1987–1994.

18 S. Panseri, C. Cunha, T. D'Alessandro, M. Sandri, A. Russo, G. Giavaresi, M. Marcacci, C. T. Hung and A. Tampieri, *PLoS One*, 2012, **7**, e38710.

19 G. Kamei, T. Kobayashi, S. Ohkawa, W. Kongcharoensombat, N. Adachi, K. Takazawa, H. Shibuya, M. Deie, K. Hattori, J. L. Goldberg and M. Ochi, *Am. J. Sports Med.*, 2013, **41**, 1255–1264.

20 A. Yanai, U. O. Hafeli, A. L. Metcalfe, P. Soema, L. Addo, C. Y. Gregory-Evans, K. Po, X. Shan, O. L. Moritz and K. Gregory-Evans, *Cell Transplant.*, 2012, **21**, 1137–1148.

21 K. Nishida, N. Tanaka, K. Nakanishi, N. Kamei, T. Hamasaki, S. Yanada, Y. Mochizuki and M. Ochi, *Neuro-Report*, 2006, **17**, 1269–1272.

22 V. Vanecek, V. Zablotskii, S. Forostyak, J. Ruzicka, V. Herynek, M. Babic, P. Jendelova, S. Kubinova, A. Dejneka and E. Sykova, *Int. J. Nanomed.*, 2012, **7**, 3719–3730.

23 T. Hamasaki, N. Tanaka, N. Kamei, O. Ishida, S. Yanada, K. Nakanishi, K. Nishida, Y. Oishi, S. Kawamata, N. Sakai and M. Ochi, *Spine*, 2007, **32**, 2300–2309.

24 U. O. Häfeli, K. Gilmour, A. Zhou, S. Lee and M. E. Hayden, *J. Magn. Magn. Mater.*, 2006, **311**, 323–329.

25 V. Zablotskii, J. M. Pastor, S. Larumbe, J. I. Pérez-Landazábal, V. Recarte and C. Gómez-Polo, *AIP Conf. Proc.*, 2010, **1311**, 152–157.

26 B. Novotna, P. Jendelova, M. Kapcalova, P. Rossner, K. Turnovcova, Y. Bagryantseva, M. Babic, D. Horak and E. Sykova, *Toxicol. Lett.*, 2012, **210**, 53–63.

27 O. Lunov, T. Syrovets, B. Buchele, X. Jiang, C. Rocker, K. Tron, G. U. Nienhaus, P. Walther, V. Mailander, K. Landfester and T. Simmet, *Biomaterials*, 2010, **31**, 5063–5071.

28 O. Lunov, T. Syrovets, C. Rocker, K. Tron, G. U. Nienhaus, V. Rasche, V. Mailander, K. Landfester and T. Simmet, *Biomaterials*, 2010, **31**, 9015–9022.

29 E. Sykova and P. Jendelova, *Cell Death Differ.*, 2007, **14**, 1336–1342.

30 B. Neuhuber, B. T. Himes, J. S. Shumsky, G. Gallo and I. Fischer, *Brain Res.*, 2005, **1035**, 73–85.

31 L. Fan, F. Du, B. C. Cheng, H. Peng and S. Q. Liu, *Chin. J. Traumatol.*, 2008, **11**, 94–97.

32 V. Donega, C. H. Nijboer, G. van Tilborg, R. M. Dijkhuizen, A. Kavelaars and C. J. Heijnen, *Exp. Neurol.*, 2014, **261C**, 53–64.

33 E. Sykova, A. Homola, R. Mazanec, H. Lachmann, S. L. Konradova, P. Kobylka, R. Padr, J. Neuwirth, V. Komrska, V. Vavra, J. Stulik and M. Bojar, *Cell Transplant.*, 2006, **15**, 675–687.

34 S. Forostyak, P. Jendelova and E. Sykova, *Biochimie*, 2013, **95**, 2257–2270.

An effective strategy of magnetic stem cell delivery for spinal cord injury therapy

Dmitry Tukmachev,[ab] Oleg Lunov,[*c] Vitalii Zablotskii,[c] Alexandr Dejneka,[c] Michal Babic,[d] Eva Sykova,[ab] Sarka Kubinova,[*ab]

[a]Institute of Experimental Medicine, ASCR, Prague, Czech Republic

[b]Department of Neuroscience, 2nd Faculty of Medicine, Charles University, Prague, Czech Republic

[c]Institute of Physics, ASCR, Prague, Czech Republic

[d]Institute of Macromolecular Chemistry, ASCR, Prague Czech Republic

Supplementary Information

1. Cell preparation

The preparation of GFP-positive mesenchymal stem cells (MSCs) and labelling with poly-*L*-lysine-coated SPION was done in accordance to previously published methods.[1, 2] To summarise, MSCs were obtained from 4-week-old green fluorescent protein transgenic Sprague-Dowley rats, TgN (acro/act-EGFP) 4Osb. The animals were deeply anesthetized, the femurs and tibias were dissected and the bone marrow was plated on Petri dishes in medium containing DMEM (PAA Laboratories GmbH,Pasching,Austria), 10% FBS (PAA Laboratories GmbH, Pasching, Austria), and Primocin™ (100 μg mL^{-1}) (Lonza Cologne AG, Koln, Germany). Cells were allowed to adhere; non-adherent cells were removed after 48 days by replacing the medium. Adherent cells were cultivated at 37 °C in a humidified atmosphere containing 5 % CO_2, and the medium was changed twice a week. After reaching near-confluency, the cells were harvested by a trypsin/EDTA solution. After 2-3 passages, the cells were labelled with SPION and transplanted into the animals.

2. Cell labelling with SPIONs

Poly-L-lysine-coated (PLL) SPIO nanoparticles were used in this study for cell labelling. The nanoparticles were prepared and characterized as described elsewhere.[2] The diameter of the dry-state particles measured by TEM was 6.2 nm. The hydrodynamic diameter of the used particles, measured by dynamic light scattering, was $D_h = 141 \pm 10$ nm, PDI = 0.52 ± 0.1, zeta potential was $\zeta = 47 \pm 4$ mV. The saturation magnetization of neat particles $M_s \sim 70$ A·m^2·kg^{-1} was obtained by measuring the magnetization curves with SQUID magnetometer. Because the weight of the coating agent is 1 % of the weight of iron oxide, the reduction of M_s by coating can be omitted. The coating of maghemite nanoparticles surface of with PLL was investigated using a Thermo Nicolet Nexus 870 FTIR spectrometer (Madison, WI, USA) in an H_2O-purged environment with DTGS (deuterated triglycine sulfate) detector. The Golden Gate single-reflection ATR system (Specac Ltd., Orpington, Great Britain) was applied to measure the ATR spectra of powdered samples over a wavenumber range 400–4000 cm^{-1}. Typical parameters were as follows: 256 sample scans, resolution 4 cm^{-1}, Happ-Genzel apodization, KBr beamsplitter. The samples for measurements were prepared by freeze-drying of PLL-coated nanoparticles purified by multiple centrifugation and redispersion in ultrapure water (four times at 14 000 rpm for 1 h).

Cultures of MSCs were incubated with SPION (50 μL per 10 mL of culture medium, i.e., 15.4 μg of iron per 1 mL media) 72 hours prior to the experiments. After this, the nanoparticles were washed out and the labelled cells were implanted into the animals.

3. Balloon-induced compression lesion model

The use of animals in this study was approved by the ethics committee of the Institute of Experimental Medicine AS CR (Prague, Czech Republic). A balloon compression lesion was performed in a total of 15 male Wistar rats (280-400 g). In short, the animals were anesthetized with 2 % isoflorane (Forane®, Abbott Laboratories, Queenborough, Great

2

Britain) and shaved on the back from *C7* to *Th1*. Under sterile conditions the skin was cut in the midline from *Th7-Th12*. The soft tissue was removed, as well as the spinous processes of vertebrae *Th8-Th11*. A catheter was filled with saline and connected to a Hamilton syringe. The catheter was inserted into the epidural space and advanced cranially for 1 cm, so that the centre of the balloon rested at the *Th8-Th9* level of the spinal cord. The balloon was rapidly inflated with 15 µL of saline for 5 min. The catheter was then deflated and removed.

4. Cell transplantation

One week after the induction of the lesion, 5×10^5 cells in 50 µL of phosphate-buffered saline were injected intrathecally at the *L5-L6* level, at a distance of 10 cm from the lesion site (Fig. 1A and B). Subsequently, as was described in the main manuscript, the external magnetic system was placed around the rat, under the top of the vertebral column at *Th8–Th9* above the lesion site, for 2 h to improve cell retention and attachment (Fig. 1A and B). Three groups of animals were used with five animals in each group; SPION-labelled MSCs exposed to MF, non-labelled MSCs exposed to MF and SPION-labelled MSCs without exposure to MF. Cell quantification was performed 24 hours after cell transplantation in longitudinal sections.

5. Histology and image analysis

Twenty-four hours after cell transplantation, the animals were intracardially perfused under deep anesthesia (pentobarbital 150 mg kg^{-1}; Sigma, St Louis, MO) with 4 % paraformaldehyde in 0.1 M PBS. The spinal cords were dissected and histologically processed. Cell quantification was performed in longitudinal sections (20 µm) using a fluorescent microscope (Carl Zeiss, Rochester, NY). GFP-positive MSCs were counted in 360 µm thick upper segments of an area 36 mm^2 (18 × 2 mm), with the epicentre of the lesion in the centre of the segment. Image quantifications were performed using ImageJ software (NIH). Cell number was calculated by normalizing corrected total cell fluorescence (CTCF) of the full area of interest to average fluorescence of a single cell. The net average CTCF

intensity of a pixel in the region of interest was calculated for each image utilizing a previously described method.[3] The region placed in an area without fluorescent objects was used for background subtraction. CTCF was determined as the sum of pixel intensity for a single image with the subtracted average signal per pixel for a region selected as the background. Averages of normalized intensity values of at least 10 morphologically indentical cells were calculated to determine the mean fluorescence of a single cell.

6. Cell staining

In order to visualize the SPION labelling in cell culture, cells were fixed in paraformaldehyde and phosphate buffer (PBS) for 15 min, washed with 0.1M PBS and then stained for iron using potassium ferrocyanide (Lachema, Brno, Czech Republic) to produce ferric ferrocyanide (Prussian blue) according to a standard staining protocol. To detect the infiltration of macrophages in the lesion, immunofluorescent staining for CD68 (ED1) (Serotec, Oxford, UK) was performed.

7. Mathematical modelling

The magnetic field and force distributions were calculated with the help of the explicit analytical expressions for magnetic field induction generated by a cylindrical permanent magnet, magnetized along its symmetry axis. For homogeneously magnetized cylinder of the radius, a and length L, the axial (B_z) and radial (B_ρ) components of the magnetic field induction can be calculated as[4]:

$$B_z = -\frac{\mu_0}{4\pi} M \int_0^{2\pi} \int_0^a \left(\frac{R(L/2-z)}{(R^2 + (L/2-z)^2 + \rho^2 - 2R\rho\cos\Phi)^{3/2}} + \frac{R(L/2+z)}{(R^2 + (L/2+z)^2 + \rho^2 - 2R\rho\cos\Phi)^{3/2}} \right) dRd\Phi \quad (1)$$

and

$$B_\rho = -\frac{\mu_0}{4\pi} M \int_0^{2\pi} \int_0^a \left(-\frac{R(2\rho - 2R\cos\Phi)}{2(R^2 + (L/2-z)^2 + \rho^2 - 2R\rho\cos\Phi)^{3/2}} + \frac{R(2\rho - 2R\cos\Phi)}{2(R^2 + (L/2+z)^2 + \rho^2 - 2R\rho\cos\Phi)^{3/2}} \right) dRd\Phi \quad (2)$$

where Φ is the azimuthal angle, z is the coordinate along the symmetry axis of a cylinder, ρ is the radial coordinate, M is the remanent magnetization and μ_0 is the permeability of free space. The vector field of the magnetic gradient shown in Fig. 2 was calculated using equations.1 and 2.

8. Statistical Analysis

The statistical significance of differences in cell counts in the spinal cord lesions between the groups was determined using ANOVA Fisher's LSD and Newman-Keuls tests. Differences were considered statistically significant statistically at $*P < 0.05$.

References

1.   V. Vanecek, V. Zablotskii, S. Forostyak, J. Ruzicka, V. Herynek, M. Babic, P. Jendelova, S. Kubinova, A. Dejneka and E. Sykova, *Int J Nanomedicine*, 2012, **7**, 3719-3730.

2.   M. Babic, D. Horak, M. Trchova, P. Jendelova, K. Glogarova, P. Lesny, V. Herynek, M. Hajek and E. Sykova, *Bioconjug. Chem.*, 2008, **19**, 740-750.

3.   O. Gavet and J. Pines, *Developmental Cell*, 2010, **18**, 533-543.

4.   S. M. Blinder, *Wolfram Demonstrations Project*, 2011, **Magnetic field of a cylindrical bar magnet**.

termis.

Tissue Engineering
& Regenerative Medicine
International Society

ORIGINAL ARTICLE

Injectable Extracellular Matrix Hydrogels as Scaffolds for Spinal Cord Injury Repair

Dmitry Tukmachev, MD,[1,2] Serhiy Forostyak, MD, PhD,[1,2] Zuzana Koci, MS,[1,2] Kristyna Zaviskova, MS,[1,2] Irena Vackova, PhD,[1] Karel Vyborny, MS,[1,2] Ioanna Sandvig, PhD,[3,4] Axel Sandvig, MD, PhD,[3,5] Christopher J. Medberry, PhD,[6] Stephen F. Badylak, DVM, PhD, MD,[6] Eva Sykova, MD, DSc,[1,2] and Sarka Kubinova, PharmD, PhD[1]

Restoration of lost neuronal function after spinal cord injury (SCI) still remains a big challenge for current medicine. One important repair strategy is bridging the SCI lesion with a supportive and stimulatory milieu that would enable axonal rewiring. Injectable extracellular matrix (ECM)-derived hydrogels have been recently reported to have neurotrophic potential *in vitro*. In this study, we evaluated the presumed neuroregenerative properties of ECM hydrogels *in vivo* in the acute model of SCI. ECM hydrogels were prepared by decellularization of porcine spinal cord (SC) or porcine urinary bladder (UB), and injected into a spinal cord hemisection cavity. Histological analysis and real-time qPCR were performed at 2, 4, and 8 weeks postinjection. Both types of hydrogels integrated into the lesion and stimulated neovascularization and axonal ingrowth into the lesion. On the other hand, massive infiltration of macrophages into the lesion and rapid hydrogel degradation did not prevent cyst formation, which progressively developed over 8 weeks. No significant differences were found between SC-ECM and UB-ECM. Gene expression analysis revealed significant downregulation of genes related to immune response and inflammation in both hydrogel types at 2 weeks post SCI. A combination of human mesenchymal stem cells with SC-ECM did not further promote ingrowth of axons and blood vessels into the lesion, when compared with the SC-ECM hydrogel alone. In conclusion, both ECM hydrogels bridged the lesion cavity, modulated the innate immune response, and provided the benefit of a stimulatory substrate for *in vivo* neural tissue regeneration. However, fast hydrogel degradation might be a limiting factor for the use of native ECM hydrogels in the treatment of acute SCI.

Introduction

SPINAL CORD INJURY (SCI) is a devastating disorder that often results in permanent motor and sensory dysfunctions due to the inability of axons to regenerate in the hostile environment of the lesion.[1] Current therapeutic approaches are being combined to activate the intrinsic neuronal regeneration capacity, such as blocking axon growth-inhibitory factors, reducing excitotoxicity and the inflammatory response, administration of neurotrophic factors, or using various types of stem and progenitor cells.[2,3] In addition to these approaches, tissue-engineered scaffolds play an important role in providing supportive substrates that contribute to replacing lost tissue and re-establishing damaged connections after SCI.[4–7]

In terms of SCI repair, biomaterials, with their own intrinsic biological activity that would encourage endoge-

nous tissue repair without the need for additional bioactive molecules such as exogenous growth factors or peptides, may provide high treatment effectivity together with relative ease of application and scalable manufacturing potential.[8]

In contrast to artificial tissue-engineered materials that fail to mimic the complex structure and chemistry of the extracellular microenvironment seen *in vivo*, biological scaffolds composed of native extracellular matrix (ECM) represent structures very similar to those of the uninjured host tissue with advantages, such as a natural three-dimensional (3D) structure, biological activity promoting cell adhesion and proliferation, and biodegradability.[9] The general concept of ECM scaffolds is based on the constructive remodeling process, in which a degradable biomaterial serves as a temporary inductive niche that is completely degraded and gradually

[1]Institute of Experimental Medicine AS CR, Prague, Czech Republic.
[2]2nd Medical Faculty, Charles University, Prague, Czech Republic.
[3]Department of Neuroscience, Norwegian University of Science and Technology, Trondheim, Norway.
[4]John Van Geest Centre for Brain Repair, School of Clinical Neurosciences, University of Cambridge, Cambridge, United Kingdom.
[5]Division of Pharmacology and Clinical Neuroscience, Department of Neurosurgery, Umeå University, Umeå, Sweden.
[6]McGowan Institute for Regenerative Medicine, Pittsburgh, Pennsylvania.

replaced by anatomically appropriate and functional tissue as opposed to scar tissue.[10,11]

Acellular tissue matrices have revealed an intrinsic ability to guide cells to differentiate into tissue-appropriate structures and phenotypes, and are also associated with positive *in vivo* host tissue remodeling and regeneration,[12,13] degradation of ECM-evoked recruitment of endogenous stem and progenitor cells, and modulation of the innate immune response.[14,15] After removal of cellular antigens, ECM scaffolds are considered biocompatible and nonimmunogenic even in allogeneic and xenogeneic settings. Currently, ECM scaffolds are being widely used for various tissue reconstructions, including heart valves, blood vessels, skin, bone, cartilage, trachea, lung, or peripheral nerves. A number of ECM scaffolds derived from a range of source species and tissues have also been approved by the FDA and commercially available for clinical use, for example, in wound healing, soft tissue repair, or heart valve replacement.[10,11]

In contrast to the extensive research on ECM scaffolds used for the reconstruction of various tissues, there are only a few studies addressing biological scaffolds for the repair of SCI based on an acellular muscle scaffold,[16] acellular sciatic nerve,[17] or acellular spinal cord scaffolds.[18] Nevertheless, the shape and conformation of such acellular scaffolds might be restrictive for bridging a chronic spinal cord lesion with an irregular cavity. Thus, in terms of suitability for clinical application, injectable *in situ* gelling hydrogels are more appropriate as these materials can easily conform to the lesion irregularity with minimal tissue damage during delivery.

To meet such requirements, tissue-specific injectable ECM hydrogels, prepared by decellularization of porcine brain, spinal cord (SC-ECM), and porcine urinary bladder (UB-ECM), have been recently described in terms of their composition, biomechanical properties, and neurotrophic properties.[19,20] These materials proved to be advantageous for providing a supportive environment for the *in vitro* neural cell growth. However, experimentally, it is unknown whether these materials can be successfully used for SCI repair, either alone or in combination with various types of cells.

To evaluate the potential neuroregenerative properties of the central nervous system (CNS) and non-CNS-derived materials *in vivo*, this study examined the effects of ECM hydrogels based on SC-ECM and UB-ECM in the model of SCI.

The *in vitro* cell-adhesive properties and neurotrophic potential of the ECM hydrogels were studied on human mesenchymal stem cells derived from Wharton's jelly (hWJ-MSCs) and on dorsal root ganglia (DRG) explant culture, respectively. To evaluate the *in vivo* tissue compatibility, the ECM hydrogels were injected into the spinal cord hemisection in rats and histologically evaluated. The tissue–scaffold interactions were further investigated using real-time qPCR to determine changes in the messenger RNA (mRNA) expression of genes related to the inflammation and immune response, secretion of neurotrophic and growth factors, and astrogliosis.

Materials and Methods

Preparation of ECM hydrogels

The preparation of the ECM hydrogels was based on a previously described procedure.[9,19,21] ECM samples were solubilized with 1.0 mg/mL pepsin in 0.01 N HCl (Sigma-Aldrich, Steinheim, Germany) at a concentration of 10 mg ECM/mL and stirred at room temperature for 48 h to form a pregel solution (pH ~ 2). The pepsin–HCl ECM solution was neutralized to pH 7.4 with 0.1 N NaOH, isotonically balanced with $10\times$ phosphate-buffered saline (PBS), and diluted with $1\times$ PBS to the concentration of 8 mg/mL. To form the hydrogel, the neutralized pregel was placed at 37°C for 45 min. The composition and biomechanical properties of the ECM hydrogels have been described in detail in Crapo *et al.*,[9] Medberry *et al.*,[19] and Wolf *et al.*[21]

Cell culture

Fresh human umbilical cord samples were collected from healthy full-term neonates after spontaneous delivery with the informed consent of the donors using the guidelines approved by the Institutional Ethics Committee at University Hospitals (Pilsen and Prague, Czech Republic). About 10–15 cm per umbilical cord were aseptically transported into sterile PBS (IKEM, Prague, Czech Republic) with antibiotic–antimycotic solution (Sigma-Aldrich) at 4°C.

After removal of blood vessels, the remaining tissue was chopped into small pieces (1–2 mm^3) and transferred to 10-cm Nunc culture dishes (Schoeller, Prague, Czech Republic) containing the complete Alpha-Minimum Essential Medium (East Port, Prague, Czech Republic) supplemented with 5% platelet lysate (IKEM) and gentamicin 10 μg/mL (Sandoz, Prague, Czech Republic), and cultivated at 37°C and 5% CO_2 in a humidified atmosphere.

On day 10, the explants were removed from the culture dishes and the remaining adherent cells were cultured for 3 weeks or until 90% confluence. The medium was changed two times a week. Cells of the third passage were identified by flow cytometry (FACSAria™; Becton Dickinson, San Jose, CA) to confirm their purity. The following antibodies against human antigens were used: CD34, CD45, CD105 (Exbio, Vestec, Czech Republic); CD29, CD73, CD90, CD271, CD31, HLA-ABC, and CD235a (BD Pharmingen, San Jose, CA); CD133 (Miltenyi Biotec, Bergisch Gladbach, Germany). Data analysis was performed using BD FACSDiva software.

In vitro *cell growth and viability*

In vitro cell growth on the surface of hydrogels was characterized using hWJ-MSCs cultures. Cell viability was determined after 1, 3, 7, and 14 days in culture using WST-1 reagent (Roche, Mannheim, Germany). Cells were cultured in 96-well plates (5000 cells/per well) coated with either UB-ECM or SC-ECM hydrogels (90 μL/well) before cell seeding. At the measured time points, 10 μL of WST-1 reagent was added to each well with 100 μL culture media and the plates were incubated for 2 h at 37°C. The absorbance was measured using a Tecan Spectra ELISA plate reader (Tecan Trading, Mannedorf, Switzerland) at 450 nm. Each type of hydrogel was seeded in triplicate; 14 independent experiments in three hydrogel batches were performed for each hydrogel type. Cell viability on the culture plastic was used as a control.

In 3D culture, cells were seeded within the hydrogels by adding concentrated cell suspension in PBS to neutralized liquid pregel solution for a final cell concentration of 2.5×10^6 cells/mL. Cells were thoroughly mixed in the pregel and 200 μL of the suspension was transferred inside the seeding

rings with a diameter of 0.8 cm (Scaffdex, Tampere, Finland) placed in the 24-well plates, and transferred at 37°C for 45 min to form a hydrogel around the cells. Following this, the seeding rings were removed, 1 mL of media was added, and the hydrogel discs were imaged after 4 h, 24 h, 4 days, and 7 days in culture to quantify gel contraction (more details in the Supplementary Data; Supplementary Data are available online at www.liebertpub.com/tea). The cell-seeded hydrogels used for *in vivo* experiments were placed into PBS and incubated at 37°C and 5% CO_2 in a humidified atmosphere for ~4 h before their implantation into the hemisection cavity.

The morphology of the cells on the hydrogels was examined by immunofluorescence staining for actin filaments. After fixation in 4% paraformaldehyde in 0.1 M PBS for 15 min, the cells were washed with 0.1 M PBS and stained with AlexaFluor 568 phalloidin (1:300); the nuclei were visualized using 4′,6-diamidino-2-phenylindole (DAPI) fluorescent dye (all from Invitrogen, Paisley, United Kingdom).

DRG explant culture

Wistar rats (Velaz, Unetice, Czech Republic), aged 3–5 days, were used for DRG extraction. Briefly, their spinal cords were dissected and DRGs from low thoracic and lumbar parts were isolated, placed in cold Hank's Balanced Salt Solution without Ca^{2+}/Mg^{2+} solution (Invitrogen, Waltham, MA), and cleaned of peripheral nerve processes.

DRG explants were then placed on SC-ECM ($n=5$) or UB-ECM ($n=4$) hydrogels in 24-well plates and cultured in Neurobasal medium (Invitrogen) supplemented with 2% B27 (Life Technologies, Carlsbad, CA), 2 mM L-glutamine (Invitrogen), 0.5% NGF (50 ng/mL; PeproTech, Prague, Czech Republic), uridine (17.5 μg/mL; Sigma-Aldrich), and primocin (PeproTech) in humidified atmosphere at 37°C and 5% CO_2. The medium was changed every 3 days.

After 7 days of culture, DRGs were fixed with 4% paraformaldehyde in 0.1 M PBS for 10 min and subjected to immunocytochemical staining for neurofilaments (NF160, 1:200; Abcam, Cambridge, United Kingdom) and cell nuclei (DAPI, 1:1000). Imaging was performed using a Leica fluorescent microscope (Leica DMI 6000B) and TissueGnostics software (TissueGnostics GmbH, Vienna, Austria). The neurite extension area and the longest neurite length were determined using ImageJ software with the Neurite-J plug-in, as described by Torres-Espin *et al.*[22]

Hydrogel injection into the SCI lesion

Male Wistar rats (250–300 g; Velaz) underwent a hemisection at the level of the 8th thoracic vertebra (Th8). The neutralized and isotonically balanced liquid pregel solution of SC-ECM and UB-ECM hydrogels (8 mg/mL) were acutely injected into the spinal cord defect after hemisection and allowed to gelate *in situ*, followed by histological evaluation 2, 4, and 8 weeks after implantation ($n=5$ per group, per time point).

The surgery was performed under adequate pentobarbital (PTB) anesthesia (60 mg/kg). The animals received local injections of mesocain (0.3 mL s.c. at the surgery site) in addition to general anesthesia, as well as gentamicin (0.05 mL i.m.; Sandoz) and atropine (0.2 mL, atropine solution 1:5) (both from BB Pharma, Prague, Czech Republic) injections.

First, a microsection of the skin was made at the level of Th8 spinal process using a scalpel. Then the laminectomy at Th8 was performed using rongeur, and the dura was incised with capsulotomy scissors. A 2 mm long spinal cord segment of the volume ~6 mm^3 was dissected using delicate tissue scissors to generate a hemisection cavity. Then the dissected segment was removed using a small piece of cellulose and fine forceps. The aforementioned instruments were purchased from Medicon® (Tuttlingen, Germany). The dura mater was sutured with 10/0 monofilament nonresorbable thread (B Braun, Aesculap, Melsungen, Germany), and the hydrogels were injected into the cavity in a single injection using an Omnican® Insulin syringe for U-100 Insulin (Melsungen, Germany). The muscles and skin were sutured with 4/0 monofilament nonresorbable thread (4/0 Chirmax, Prague, Czech Republic), and the animals were housed, two rats in a cage, with food and water *ad libitum*.

In the control SCI group ($n=4$) the hemisection defect was filled with saline. In the animal group treated with SC-ECM hydrogel seeded with hWJ-MSCs ($n=4$), the hydrogels were implanted into the hemisection cavity. This animal group received a daily injection of the immunosuppressant cyclosporin A (10 mg/kg, intraperitoneally) (Sandimmune; Novartis, Basel, Switzerland), azathioprine (2 mg/kg, per orally) (Imuran; Aspen Europe GmbH, Bad Oldesloe, Germany), and methylprednisolone (2 mg/kg, i.m.) (Solu-Medrol; Pfizer, Puurs, Belgium) to prevent the rejection of the transplanted cells.

Of the 56 animals that underwent the hemisection, 4 animals died during the operation and 2 animals died 2–4 weeks after operation. All experiments were performed in accordance with the European Communities Council Directive of 24 November 1986 (86/609/EEC), regarding the use of animals in research and were approved by the Ethics Committee of the Institute of Experimental Medicine, Academy of Sciences, Czech Republic (Prague, Czech Republic).

Hindlimb motor function between the first and fourth weeks post-SCI was recorded for the sham-operated control group, SC-ECM alone, and SC-ECM combined with hWJ-MSCs using the Basso–Beattie–Bresnahan (BBB) open field locomotor test[23] (Supplementary Data).

Tissue processing and histology

At 2, 4, and 8 weeks after hydrogel injection, the animals were deeply anesthetized with an intraperitoneal injection of overdose PTB and perfused with PBS followed by 4% paraformaldehyde in 0.1 M PBS. The spinal cord was left in the bone overnight, then removed and postfixed in the same fixative for at least 1 week. A 3 cm long segment of the spinal cord containing the lesioned site was dissected out and transferred to 10% and 30% sucrose. After freezing, the spinal cords were cryosectioned into 40 μm thick longitudinal sections. Hematoxylin–Eosin (H&E) and Masson's Trichrome staining was performed using the standard protocol.

For immunohistological analysis, the following antibodies were used: against neurofilament (NF160, 1:200), endothelial cells (RECA-1, 1:500), astrocytes (Cy3-conjugated mouse Glial Fibrillary Acidic Protein, GFAP, 1:200), all from Sigma-Aldrich; Schwann cells p75 (1:200), serotonin-positive axons (R-SERO, 1:100), oligodendrocytes (OSP, 1:1000), macrophages (ED1, 1:100), M1 macrophages (CD86, Cy5-

conjugated donkey anti-rabbit IgG-PerCp-Cy5,5, 1:2500), human mitochondria (MTCO2, 1:250), all from Abcam; and M2 macrophages (CD206, 1:250), axonal growth cone (GAP43, 1:100), all from Santa Cruz (Heidelberg, Germany). Alexa Fluor® 488-conjugated goat anti-mouse IgG (1:200), Alexa Fluor 594-conjugated goat anti-mouse IgG (1:200) and Alexa Fluor 488-conjugated donkey anti-goat IgG (1:700) were used as secondary antibodies. The nuclei were visualized by using 4′,6-diamidino-2-phenylindole (DAPI) fluorescent dye. Fluorescent micrographs were taken using an AxioCam HRc Axioskop 2 Plus fluorescence microscope (Zeiss, Jena, Germany) and a LSM 510 DUO laser scanning confocal microscope (Zeiss).

For axonal and vessel analysis, multiple images across the entire lesion were taken using a 20× objective. Five images from each sample were selected and the total area of the axons (NF160 staining) and blood vessels (RECA staining) within the lesion area was outlined using ImageJ software (National Institutes of Health, Bethesda, MD) and divided by the area of the lesion to determine the percentage of the lesion that was occupied by new axons or vasculature.

Gene expression analysis

The expressions were studied using quantitative real-time reverse transcription polymerase chain reaction (qPCR) 2, 4, and 8 weeks after the surgery (in all groups $n = 4$). RNA was isolated from paraformaldehyde-fixed frozen tissue sections using the High Pure RNA Paraffin Kit (Roche, Penzberg, Germany), following the manufacturer's recommendations. RNA amounts were quantified using a spectrophotometer (NanoPhotometer™ P-Class, Munchen, Germany). The isolated RNA was reverse transcribed into complementary DNA (cDNA) using the Transcriptor Universal cDNA Master (Roche) and a thermal cycler (T100™ Thermal Cycler; Bio-Rad, Hercules, CA).

The qPCR reactions were performed using cDNA solution, FastStart Universal Probe Master (Roche) and TaqMan® Gene Expression Assays (Life Technologies), (Supplementary Table S1; Supplementary Data are available online at www.liebertpub.com/tea). The qPCR was carried out in a final volume of $10 \mu L$ containing 25 ng of extracted RNA. Amplification was performed on the real-time PCR cycler (StepOnePlus™; Life Technologies). All amplifications were run under the same cycling conditions: 2 min at 50°C, 10 min at 95°C, followed by 40 cycles of 15 s at 95°C and 1 min at 60°C.

All samples were run in duplicate, and a negative control was included in each array. Relative quantification of gene expression was determined using the $\Delta\Delta Ct$ method. Results were analyzed with StepOnePlus software. The gene expression level was normalized on *Gapdh* as a reference gene; control samples from unlesioned spinal cord tissue were used as a calibrator.

Statistical evaluation

The statistical significance of the differences in gene expression between the groups at three time points was determined using two-way repeated measurement analysis of variance (ANOVA) with a Student–Newman–Keuls *post hoc* pair-to-pair test. A one-way ANOVA was used for the comparisons of gene expression between groups with SC-ECM hydrogel at 4-week intervals and cell proliferation (SigmaStat 3.1; Systat Software, Inc., San Jose, CA).

Results

In vitro *cell culture*

The solubilized ECM matrix self-assembles from the pregel form into the hydrogel at 37°C and physiologic pH, as was described in Medberry *et al.*[19] The biocompatibility and
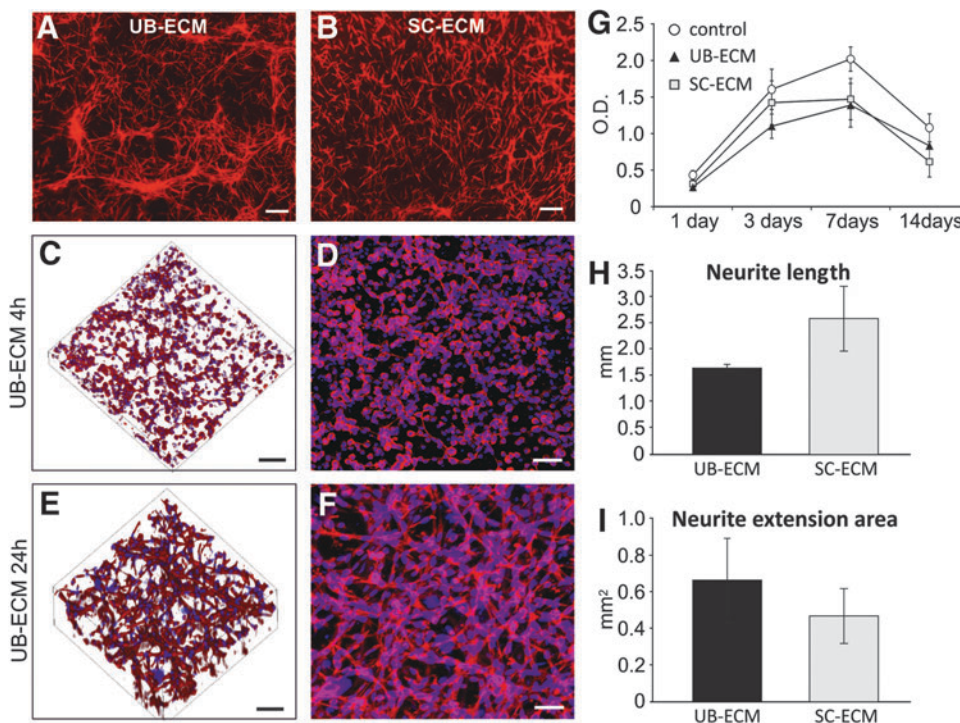
FIG. 1. *In vitro* cell growth on extracellular matrix (ECM) hydrogels. Two-dimensional (2D) cell culture on (A) urinary bladder (UB)-ECM and (B) spinal cord (SC)-ECM hydrogels at 3 days. (C–F) Three-dimensional (3D) cell culture in UB-ECM at (C, D) 4 and (E, F) 24 h. Cells were stained for (A–F) phalloidin and (C–F) cell nuclei (DAPI). (G) Proliferation of human Wharton's jelly-derived mesenchymal stem cells (hWJ-MSCs) on ECM hydrogels using WST-1 assay. (H) Quantification of the highest neurite length and (I) neurite extension area of dorsal root ganglia explants on ECM hydrogels using Neurite-J plug-in for ImageJ software. Scale bar: (A, B) 100 μm, (C–F) 50 μm. Color images available online at www.liebertpub.com/tea
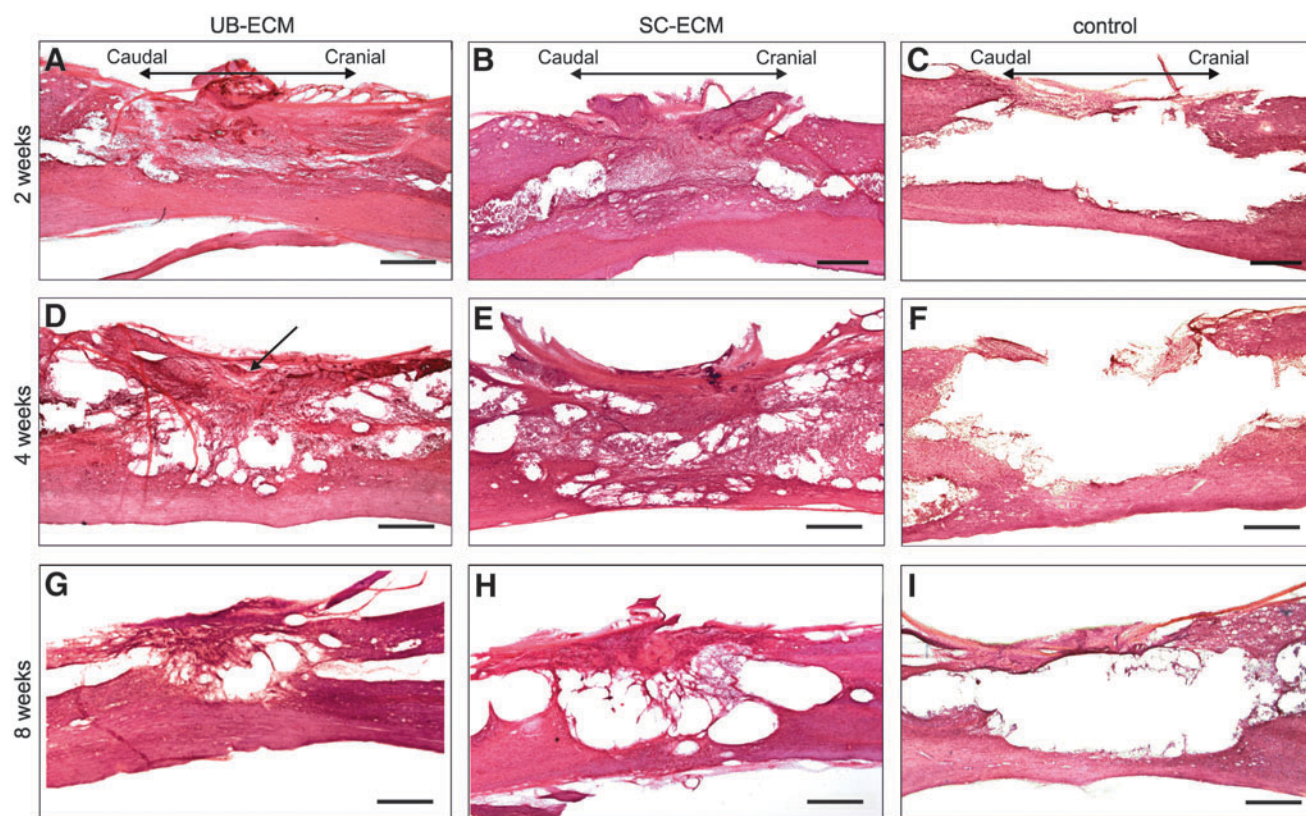
FIG. 2. Representative Hematoxylin–Eosin staining of the spinal cord lesion **(A–C)** 2, **(D–F)** 4, and **(F–I)** 8 weeks after injection of **(A, D, G)** UB-ECM hydrogels; **(B, E, H)** SC-ECM hydrogels. **(C, F, I)** Represent a sham-operated control lesion. **(D)** The *arrow* shows the nondegraded part of the hydrogel. Scale bar: 500 μm. Color images available online at www.liebertpub.com/tea

bioadhesive properties of ECM hydrogels were confirmed by the *in vitro* use of hWJ-MSCs in the two-dimensional (2D) and 3D cell cultures (Fig. 1). Flow cytometry was performed to detect cell purity, while CD markers were found positive for CD29, CD105, CD90, CD73, and HLA-ABC and negative for CD31, CD34, CD45, CD133, CD235a, and CD271. After seeding onto the ECM hydrogels, cells spread and proliferated on both hydrogel types (Fig. 1).

Cell proliferation was determined using the WST-1 assay after 1, 3, 7, and 14 days of the culture. Both ECM hydrogels showed comparable ability to support *in vitro* cell proliferation, which did not significantly differ from the control cell proliferation on tissue culture plastic (TCP). Cell viability increased until day 7, then, after reaching the confluency of the culture, decreased on both hydrogel types as well as on TCP (Fig. 1G).

When seeded in 3D culture (0.5 million cells per 0.2 mL), hWJ-MSC extended their lamellipodia within the hydrogels and formed a 3D network, as is shown in Figure 1C–F after 4 and 24 h. Rapid hydrogel contraction was observed already after 4 h, which progressed during the culture to at least 10% of the initial area after 7 days (Supplementary Fig. S1).

DRG explant culture on ECM hydrogels

DRG explant cultures were used to compare the neurotrophic properties of the CNS and non-CNS-derived ECM hydrogels. After 7 days of culture, neurites densely extended

from the DRG bodies (Supplementary Fig. S2). No significant differences were found between UB-ECM and SC-ECM in both examined parameters, total neurite extension area and longest neurite length (Fig. 1H, I).

Histological evaluation after ECM hydrogel injection

Both UB-ECM and SC-ECM hydrogels were injected into the cavity of the spinal cord hemisection and examined at 2, 4, and 8 weeks. The tissue response to the scaffolds was histologically evaluated by analyzing axonal ingrowth, vascularization, and infiltration of macrophages/microglia, astrocytes, and oligodendrocytes within the injury site.

At 2 weeks after injury, H&E staining of longitudinal spinal cord sections demonstrated that both hydrogel types were biocompatible with the surrounding host tissue and entirely filled the lesion cavity (Fig. 2A, B). The hydrogels were mostly degraded, but still detectable in the lesion area (Supplementary Fig. S3) and were densely populated among the host cells.

By 4 weeks postinjury, small areas of the original hydrogel were still present (Fig. 2D), while the newly formed tissue interconnected with the host tissue, bridging the lesion center. Macrophages massively infiltrated the periphery of the lesion where several small cysts developed due to the rapid degradation of the graft. A similar tissue response was found at 8 weeks, when the hydrogels had fully degraded, which was followed by further progression of cyst formation. In contrast
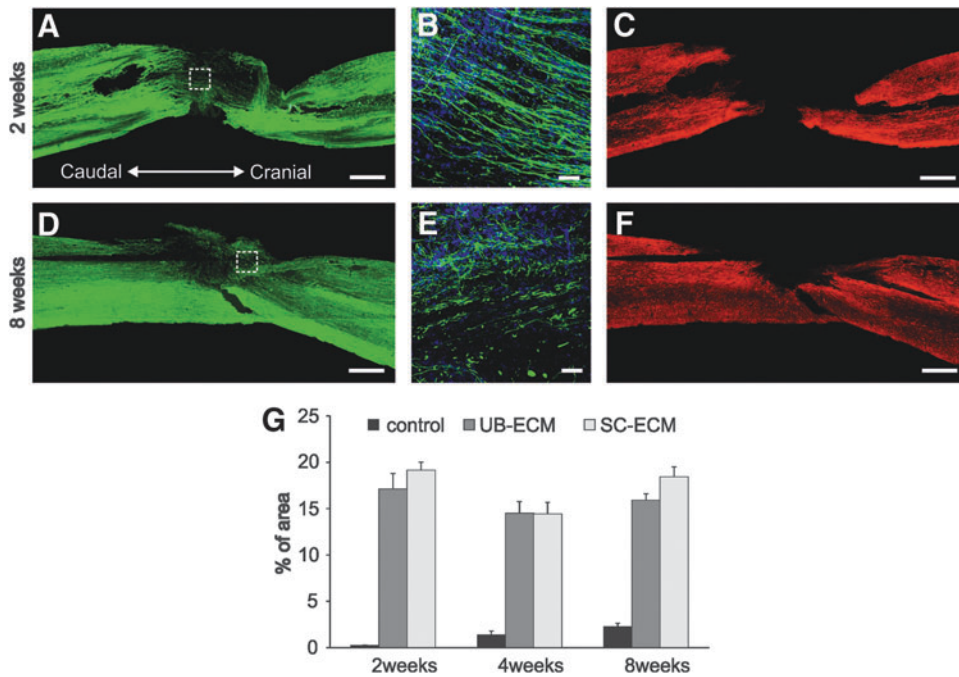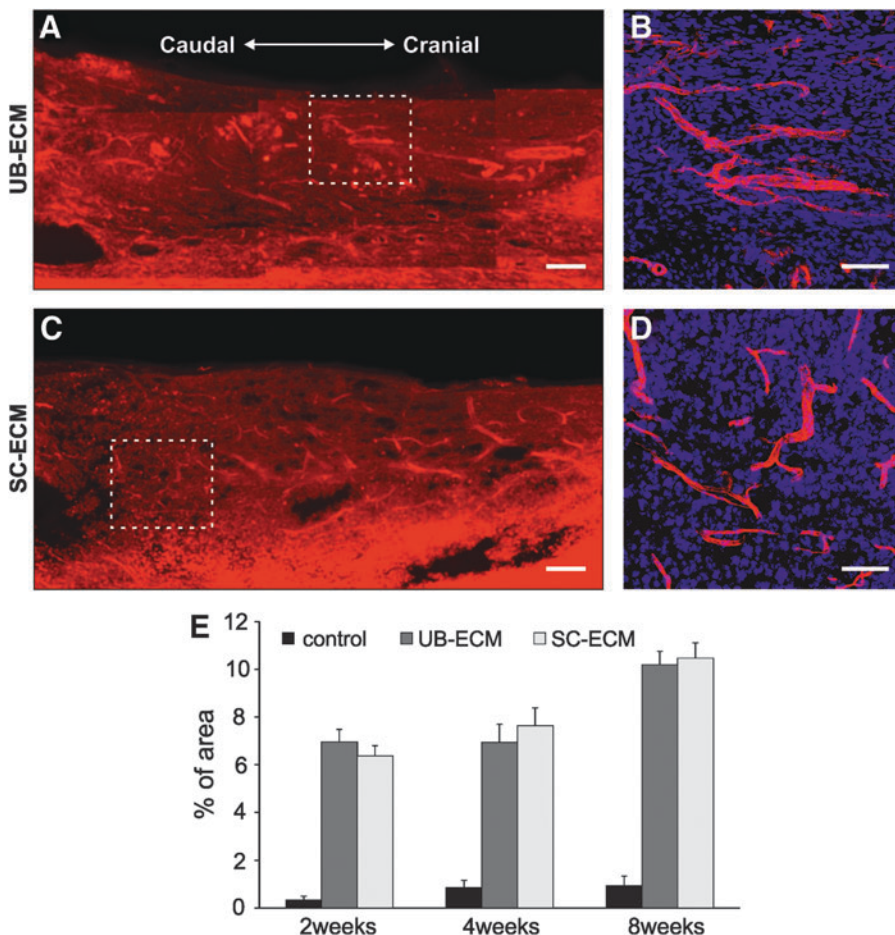
FIG. 3. Representative images of the spinal cord lesion (A–C) 2 and (D–F) 8 weeks after injection of SC-ECM hydrogels. Immunofluorescence staining for (A, B, D, E) neurofilaments (NF160), (C, F) astrocytes (GFAP), and (B, E) cell nuclei (DAPI, blue). Squares (A, D) are also shown under the higher magnification insets (B, E). (G) The effect of ECM hydrogels on the ingrowth of NFs. A significantly higher ingrowth of NFs was found in both the ECM hydrogel groups when compared to the control lesion at all time points. Scale bar: (A, C, D, F) 500 μm; (B, E) 50 μm. Color images available online at www.liebertpub.com/tea

to the tissue remodeling process observed in the lesion after hydrogel injection, large pseudocysts formed in the control sham-treated lesion (Fig. 2C, F, I).

To evaluate axonal ingrowth into the hydrogels, a neurofilament marker (NF160) was used (Fig. 3). Robust ingrowth of NF-positive fibers into the hydrogel-treated lesion was observed from both the rostral and caudal stumps of the lesion, while dense infiltration of NFs was also found in the center of the lesion. Quantification analysis expressed the relative value of NF160 immunopositive area as a percentage

FIG. 4. Representative images of the spinal cord lesion at 2 weeks after injection of (A, B) UBM-ECM and (C, D) SC-ECM hydrogels. (A–D) Immunofluorescence staining for blood vessels (RECA) and (B, D) cell nuclei (DAPI). Squares (A, C) are also shown under higher magnification insets (B, D). (E) An effect of ECM hydrogels on vascularization. A significantly higher ingrowth of blood vessels was found in both ECM hydrogel groups when compared to the control lesion at all time points. Scale bar: (A, C) 500 μm; (B, D) 50 μm. Color images available online at www.liebertpub.com/tea

FIG. 5. Representative immunofluorescence staining for **(A, B)** macrophages (ED1, *green*) and astrocytes (GFAP, *red*) in **(A)** UB-ECM at 2 weeks and **(B)** SC-ECM seeded with hWJ-MSCs at 4 weeks. Confocal micrographs of the staining for **(C)** serotonin-positive axons (5-HT, *red*) and blood vessels (RECA, *green*) in SC-ECM at 4 weeks; **(D)** serotonin-positive axons (5-HT, *red*), blood vessels (RECA, *green*), and cell nuclei (DAPI, *blue*) in SC-ECM seeded with WJ-MSCs at 4 weeks; **(E)** M1 macrophages (CD86, *red*) and M2 macrophages (CD206, *green*) in UB-ECM hydrogel at 2 weeks; **(F)** oligodendrocytes (OSP, *green*) and cell nuclei (DAPI, *blue*) in SC-ECM at 4 weeks; **(G)** neuronal growth cones (GAP 43, *red*) and cell nuclei (DAPI, *blue*) in SC-ECM at 4 weeks; **(H)** Schwann cells (p75, *red*) and cell nuclei (DAPI, *blue*) in SC-ECM at 4 weeks. The *dotted line* in **(C, D, E, F, H)** describes the border between ECM hydrogel and neural tissue (NT). Scale bar: **(A, B)** 500 μm; **(C, H)** 100 μm; **(D–F)** 50 μm; **(G)** 25 μm. Color images available online at www.liebertpub.com/tea
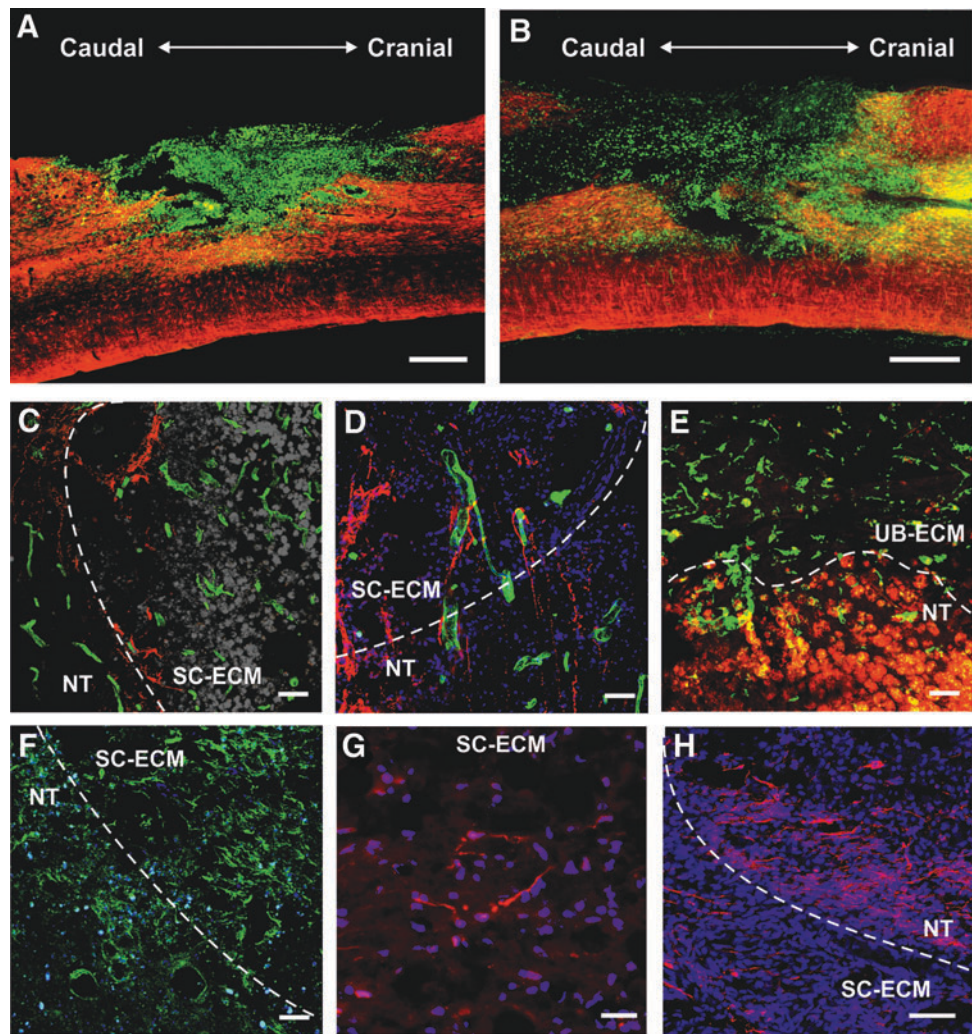
of the lesion area. The ingrowth of NFs was maximal at 2 weeks in both hydrogel groups and did not further increase at later time points. No differences in the NFs area were found between SC-ECM and UB-ECM hydrogels at all time points (Fig. 3G). Despite the isotropic structure of the ECM hydrogels, the ingrowing axons linearly bridged the SCI lesion while forming multiple bundles organized in the longitudinal direction along the spinal cord (Fig. 3B).

Astrocytes, evaluated by immunofluorescence staining for GFAP, did not migrate inside the lesion and thus served as a clear demarcation of the lesion area (Fig. 3C, F). Only a few astrocytic processes grew into the graft from the lesion border (Fig. 3F).

In terms of neovascularization, a number of blood vessels (RECA staining) grew into the hydrogel-treated lesions and formed a dense network (Fig. 4A–D). The area of blood vessels gradually increased with time, but no differences in blood vessel density were found between the UB-ECM and SC-ECM hydrogels at any time point (Fig. 4E).

The host tissue remodeling response was characterized by robust infiltration of CD68^{+} cells throughout the entire lesion area (Fig. 5A, B), which populated the hydrogels at all time points, and remained in the lesion site after the hydrogel had degraded. As is apparent from the staining for

M1 and M2 macrophages in Figure 5E, macrophages at the interface of the ECM hydrogel and the host tissue were predominantly of the M1 phenotype (CD86 staining), while M2 phenotype macrophages (CD206 staining) were mostly present within the hydrogel area.

Infiltration of serotonin-positive axons (Fig. 5C, D) was observed from the rostral part of the hydrogels, but these axons did not spread across the lesion. Infiltration of oligodendrocytes (OSP staining, Fig. 5F) within the lesion site indicated that myelination occurred in some of the regenerated axons. Newly sprouted axonal fibers were also detected using GAP43 staining (Fig. 5G). Numerous endogenous Schwann cells that migrated from the nerve roots were detected within the lesion site as well as in the surrounding tissue (Fig. 5H).

Histological evaluation of implanted ECM hydrogels combined with hWJ-MSCs

To evaluate the potential of ECM hydrogels as a cell vehicle, the SC-ECM hydrogels were mixed with hWJ-MSCs (0.5 million cells per 0.2 mL), and the cell–hydrogel constructs containing ∼15,000 cells were acutely implanted into the hemisection cavity. Four weeks after
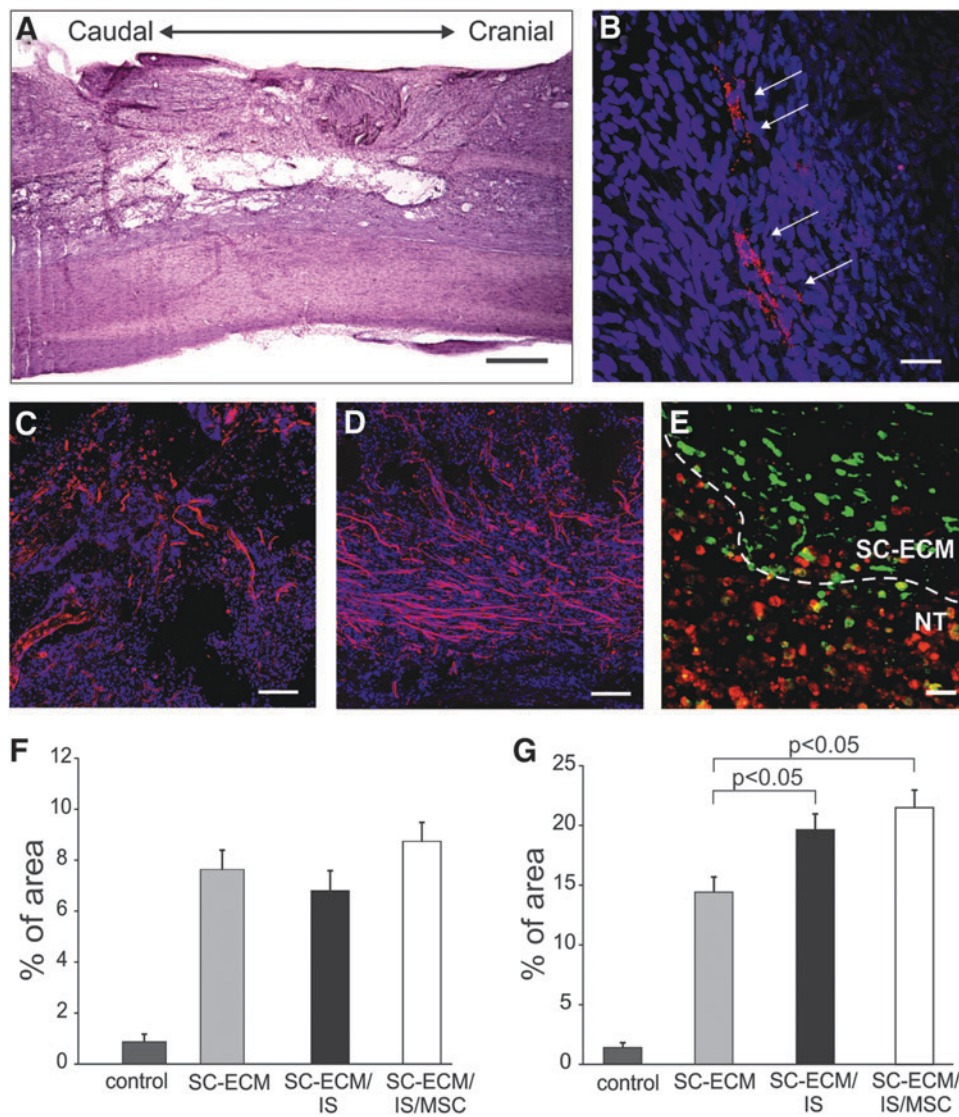
FIG. 6. Representative images of the spinal cord lesion after implantation of SC-ECM seeded with hWJ-MSCs at 4 weeks. **(A)** Hematoxylin–Eosin staining. Confocal micrographs of the staining for **(B)** human mitochondria (MTCO2); **(C)** blood vessels (RECA); **(D)** neurofilaments (NF160) and **(B–D)** cell nuclei (DAPI, *blue*); **(E)** M1 macrophages (CD86, *red*) and M2 macrophages (CD206, *green*). The *dotted line* describes the border between ECM hydrogel and NT. An effect of the SC-ECM hydrogels seeded with hWJ-MSCs on the ingrowth of **(F)** blood vessels and **(G)** neurofilaments. (IS)—animal groups that received immunosuppression. Scale bar: **(A)** 500 μm, **(B, E)** 50 μm, **(C, D)** 100 μm. Color images available online at www.liebertpub.com/tea

surgery, the grafts were densely infiltrated with endogenous tissue, while cysts had developed at the graft–tissue interface (Fig. 6A). Only very few surviving cells, positive for human mitochondria MTCO2 marker, were detected in the lesion (Fig. 6B). Transplanted cells did not further promote the ingrowth of NF-positive fibers or blood vessels. However, an increase in NF-positive fibers was found in those animal groups that received immunosuppression (Fig. 6F, G). As in the empty ECM hydrogels, M2 phenotype macrophages were mostly present within the hydrogel area (Fig. 6E).

Gene expression analysis induced by ECM hydrogels

Changes in the mRNA expression of genes related to inflammation (*Ptgs2*, *Ccl3*, *Ccl5*, *Il2*, *Il6*, *Il12b*), M1 macrophages (*Irf5*, *Cd86*, *Nos2*), M2 macrophages (*Mrc1*, *Cd163*, *Arg1*), growth factors (*NT-3*, *Fgf2*), axonal sprouting (*Gap43*), astrogliosis (*Gfap*), angiogenesis (*Vegfa*), and apoptosis (*Casp3*) were determined at 2, 4, and 8 weeks after hydrogel injection and compared to the control SCI lesion (Fig. 7, Supplementary Table S1).

The most profound host tissue response to the ECM hydrogels was observed 2 weeks after injury, when significant downregulation was found in the expression of *Fgf2*, *Cd163*, *Irf5*, *Ccl5*, and *Gap43* in both hydrogel groups, and of *Gfap* in the UB-ECM hydrogel group only, when compared to the control SCI lesion. At 4 weeks, no significant changes were detected between both hydrogel groups and the control group, except for a significant upregulation of *Arg1* in the UB-ECM hydrogel group compared to SC-ECM (Supplementary Table S2). A potential tissue-specific effect of SC-ECM was observed at 8 weeks, when significant upregulation of mRNA expression was detected for *NT-3*, *Fgf2*, *Irf5*, and *Casp3*. The expression of proinflammatory cytokines *IL-2*, *IL-6*, *Il12b*, and *Nos2* was undetectable in all groups.

The effect of hWJ-MSCs combined with SC-ECM hydrogels was determined 4 weeks after the scaffold implantation. The animals received immunosuppression to prevent rejection of the xenogeneic cells. Interestingly, the immunosuppression significantly decreased the mRNA expression of *Gfap* in both empty and cell-seeded hydrogels and of *Fgf2*, *Casp3*, *Ccl3*, and *Cd86* in empty hydrogels, when compared to the control lesion (Fig. 7, Supplementary
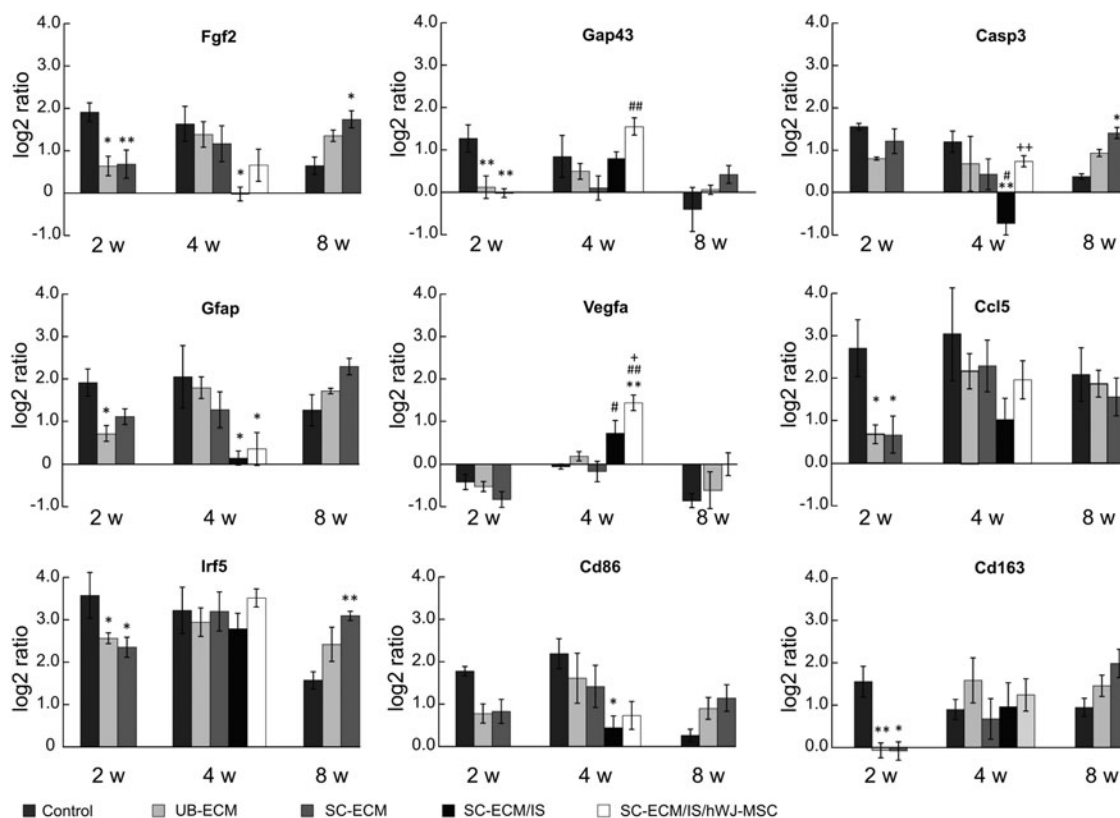
FIG. 7. Analysis of messenger RNA (mRNA) gene expression of several genes involved in inflammatory and reparative processes following spinal cord injury (SCI) treated with ECM hydrogels. The graphs show the log2-fold changes in gene expression over intact spinal cord tissue. IS, animal groups that received immunosuppression. $*p < 0.05$, $**p < 0.01$: ΔCt values of ECM hydrogel versus control lesion. $^{\#}p < 0.05$, $^{\#\#}p < 0.01$: ΔCt values of SC-ECM hydrogel with IS versus SC-ECM. $^{+}p < 0.05$, $^{++}p < 0.01$: ΔCt values of SC-ECM hydrogel with IS and hWJ-MSCs versus empty SC-ECM with IS.

Table S1). Moreover, a significant increase in the expression of *Vegfa* and *Gap43* was also found in cell-seeded hydrogels when compared to the empty hydrogels.

Discussion

In this study, we evaluated the *in vivo* neuroregenerative potential of two types of ECM hydrogels based on the CNS and non-CNS tissue, when injected into the spinal cord acutely after SCI. The ECM matrices were derived from porcine spinal cord and urinary bladder and processed into an injectable hydrogel form as was described previously.[19,21] Regarding the different tissue sources used, SC-ECM and UB-ECM hydrogels were prepared using different decellularization methods and differed in their composition as well as in their physical and biological properties.[19,21] Despite the lack of a native 3D ultrastructure from the source tissue, ECM hydrogels retain their biological activity and possess mechanical properties similar to that of soft neural tissue, with the advantage of injectability and *in situ* polymerization, which offer minimally invasive delivery techniques and facilitate the possibility of clinical translation.

When injected into the SCI, both hydrogel types were well integrated into the surrounding tissue, with persisting massive cell infiltration and neovascularization. A potentially important factor for tissue regeneration is tissue specificity

of the ECM hydrogel source. In this study, however, both studied materials proved to be advantageous for providing a supportive environment and revealed similar neurotrophic properties *in vitro* in the DRG explant culture as well as *in vivo* with regard to the ingrowth of NFs and neovascularization. These findings are consistent with those of a previous study, which showed no advantage of CNS-derived ECM materials versus non-CNS-derived ECM materials with respect to effects upon neural stem/progenitor cells.[24]

Macrophages were the predominant infiltrating cells within the grafts that participated in the ECM degradation. As was shown previously, degradation of ECM scaffolds is essential for the constructive tissue remodeling process, by which a degradable biomaterial serves as a temporary inductive niche, which is gradually replaced by anatomically appropriate and functional tissue as opposed to scar tissue.[11,25,26] Moreover, degradation of ECM scaffolds stimulates the release of matricryptic molecules; which possess a variety of bioactive properties, such as antimicrobial activity, angiogenic effects, as well as the recruitment of endogenous stem and progenitor cells.[26]

In the present study, however, despite the fact that the lesion cavity was filled with endogenous cell-populated ECM hydrogels 2 weeks after their injection, further progression in matrix degradation at later time points was not followed by full neural tissue replacement, but rather

resulted in the formation of a dense network of tissue containing axons, blood vessels, and other neural tissue elements interrupted by a number of small cysts.

According to the gene expression analysis, *in vivo* ECM degradation was associated with a significant decrease in mRNA expression of markers for proinflammatory/M1 macrophages (*Irf5*) and regulatory/M2 macrophages (*Cd163*), inflammation (*Ccl5/RANTES*), as well as genes for growth factor *Fgf2*, astrogliosis (*Gfap*), and neuronal growth cones (*Gap43*). The expression of other markers related to immune response, such as *Cd86*, *Mrc1*, and *Ptgs2*, also decreased, but these changes were not found to be significant. Interestingly, these effects were detected during the early phase after injury, but decreased or even reversed at later time points, suggesting that ECM hydrogel degradation played a significant role in the transient modulation of the innate immune and tissue repair response.

Previous reports have shown increased numbers of M2 macrophages and more positive polarization toward an M2 phenotype associated with ECM *in vivo* degradation and the promotion of constructive tissue remodeling.[15,27] Recent studies describe the M2 polarizing effects of ECM derived from several tissues.[28,29] In the present study, the expression of genes related to both M1 and M2 macrophages decreased at 2 weeks, which reflects that both inflammatory as well as anti-inflammatory responses were inhibited after ECM hydrogel treatment. Nevertheless, according to positive staining for CD206, ECM hydrogel treatment led to spatial differences of macrophage distribution within the lesion, where M2 macrophages were mostly accumulated within the hydrogel, and M1 macrophages were in the surrounding tissue.

The ability of ECM hydrogels to promote *in vitro* cell growth and proliferation was examined using hWJ-MSCs. The hWJ-MSCs currently represent a promising cell type in regenerative medicine and are already being evaluated in various clinical trials, including SCI.[30] The *in vitro* 2D cell culture demonstrated that both types of ECM hydrogels promoted adhesion and proliferation of hWJ-MSCs.

However, when seeded in 3D culture, hWJ-MSCs triggered rapid gel contraction. This well-known phenomenon is characteristic for collagen gels seeded with fibroblasts that generate tension on the matrix during both extension and retraction of pseudopodia.[31] A similar effect has also been described for ECM hydrogels derived from porcine dermis as well as urinary bladder seeded with fibroblasts.[21]

When used as a cell vehicle *in vivo* to fill the lesion cavity, the rapid gel contraction may then result in inhomogeneous scaffold distribution within the lesion. Moreover, when injected into the lesion, the ECM hydrogels may further contract over time as they are populated with various endogenous cells, such as fibroblasts or epithelial cells. Of note, a similar collagen concentration ($\sim 700\,\mu$g collagen/mg dry weight) as well as gel contraction rate was found for both SC-ECM and UB-ECM, while sulfated glycosaminoglycan concentration was higher for UB-ECM ($\sim 4\,\mu$g/mg dry weight) than for SC-ECM ($\sim 1\,\mu$g/mg dry weight).[19]

To evaluate ECM hydrogels for cell delivery, we prepared the cell seeded gels before their implantation into the lesions, which partly avoids the massive scaffold contraction within the lesion cavity. In spite of this, the inflammatory milieu of the acute lesion together with the massive infiltration of macrophages did not support cell survival. Furthermore, only few cells were detected within the lesion 4 weeks after the implantation. On the other hand, due to the limited volume of the implanted scaffold, the total number of implanted cells within the hydrogel was relatively small ($\sim 15,000$). By increasing the number of implanted cells a higher *in vivo* cell survival rate could be achieved, however, an increased degree of gel contraction may result in the enhanced formation of dense cell bulks within the lesion cavity.

Notably, immunosuppression significantly promoted axonal ingrowth, decreased expression of *Gfap*, *Fgf2*, *Casp3*, *Ccl3*, and *Cd86*, and increased expression of *Vegfa*, which confirmed the neurotrophic effect of immunosuppressive agents.[32]

In comparison with the synthetic nondegradable materials based on poly(2-hydroxyethyl methacrylate), which we previously developed and evaluated *in vivo*,[33,34] ECM hydrogels are undoubtedly advantageous, in terms of their injectability, degradability, as well as their biological activity, which is able to modulate the immune response and stimulate vascularization and axonal ingrowth. At the same time, there are also two impediments that hinder the use of ECM hydrogels in their current form as optimal materials for CNS repair: (1) progressive hydrogel contraction in combination with fibroblast-like cells, such as MSCs and (2) rapid *in vivo* hydrogel degradation, which was too fast to be followed by full tissue reconstruction in the lesion cavity.

When applied immediately into the SCI, the neuroregenerative potential of ECM hydrogels might be burdened by the hostility of the acute SCI lesion due to the acute inflammatory response, which in turn may significantly influence the speed of hydrogel degradation and thus the character of tissue replacement.

Remarkably, acute lateral hemisection, which we used to evaluate the feasibility of ECM hydrogels in CNS repair, is the least invasive and devastating SCI model. On the other hand, hemisection is a case of partial lesion with a high rate of spontaneous recovery and a high risk of inconsistencies in the injuries from one animal to the next, which might lead to misinterpretation of the behavioral evaluation.[35,36]

Further investigation using a subacute or chronic compression SCI model together with systematic functional evaluation is, therefore, the next step in establishing the link between *in vivo* biological properties of the ECM hydrogel in acute and chronic SCI.

To slow degradation, chemical crosslinking of the ECM hydrogel may offer longer scaffold persistence within the lesion and thus provide more time to complete the tissue remodeling. However, recent studies suggest that degradation of the ECM scaffold is an essential component of a rapid constructive remodeling response. Moreover, crosslinking of the ECM may reduce or eliminate the amount of cellular infiltration into the implant or even cause a foreign body reaction.[15] Alternatively, hydrogels composed of concentrations >8 mg/mL as used in the present study may slow the degradation process.

Conclusions

This study evaluated the *in vivo* function of two types of ECM hydrogels derived from decellularized porcine spinal cord and urinary bladder tissues as scaffolds for SCI repair. Both ECM hydrogels showed significant immunomodulatory

and neuroregenerative effects and provided the substrate for tissue bridging after SCI. Further studies concerning the optimization of hydrogel degradation time as well as the analysis of the ability to restore neuronal function after SCI in combination with a suitable cell type are needed to consider the potential of ECM hydrogels for clinical translation.

Acknowledgments

Disclosure Statement

No competing financial interests exist.

References

1. Young, W. Spinal cord regeneration. Cell Transplant **23,** 573, 2014.
2. Pego, A.P., Kubinova, S., Cizkova, D., Vanicky, I., Mar, F.M., Sousa, M.M., and Sykova, E. Regenerative medicine for the treatment of spinal cord injury: more than just promises? J Cell Mol Med **16,** 2564, 2012.
3. Kumar, P., Choonara, Y.E., Modi, G., Naidoo, D., and Pillay, V. Multifunctional therapeutic delivery strategies for effective neuro-regeneration following traumatic spinal cord injury. Curr Pharm Des **21,** 1517, 2015.
4. Kubinova, S., and Sykova, E. Biomaterials combined with cell therapy for treatment of spinal cord injury. Regen Med **7,** 207, 2012.
5. Assuncao-Silva, R.C., Gomes, E.D., Sousa, N., Silva, N.A., and Salgado, A.J. Hydrogels and cell based therapies in spinal cord injury regeneration. Stem Cells Int **2015,** 948040, 2015.
6. Macaya, D., and Spector, M. Injectable hydrogel materials for spinal cord regeneration: a review. Biomed Mater **7,** 012001, 2012.
7. Siebert, J.R., Eade, A.M., and Osterhout, D.J. Biomaterial approaches to enhancing neurorestoration after spinal cord injury: strategies for overcoming inherent biological obstacles. Biomed Res Int **2015,** 752572, 2015.
8. Ricks, C.B., Shin, S.S., Becker, C., and Grandhi, R. Extracellular matrices, artificial neural scaffolds and the promise of neural regeneration. Neural Regen Res **9,** 1573, 2014.
9. Crapo, P.M., Medberry, C.J., Reing, J.E., Tottey, S., van der Merwe, Y., Jones, K.E., and Badylak, S.F. Biologic scaffolds composed of central nervous system extracellular matrix. Biomaterials **33,** 3539, 2012.
10. Badylak, S.F. Decellularized allogeneic and xenogeneic tissue as a bioscaffold for regenerative medicine: factors that influence the host response. Ann Biomed Eng **42,** 1517, 2014.
11. Badylak, S.F., Freytes, D.O., and Gilbert, T.W. Extracellular matrix as a biological scaffold material: structure and function. Acta Biomater **5,** 1, 2009.
12. Nakayama, K.H., Lee, C.C., Batchelder, C.A., and Tarantal, A.F. Tissue specificity of decellularized rhesus monkey kidney and lung scaffolds. PLoS One **8,** e64134, 2013.
13. Adam Young, D., Bajaj, V., and Christman, K.L. Award winner for outstanding research in the PhD category, 2014 Society for Biomaterials annual meeting and exposition, Denver, Colorado, April 16–19, 2014: decellularized adipose matrix hydrogels stimulate in vivo neovascularization and adipose formation. J Biomed Mater Res A **102,** 1641, 2014.
14. Reing, J.E., Zhang, L., Myers-Irvin, J., Cordero, K.E., Freytes, D.O., Heber-Katz, E., Bedelbaeva, K., McIntosh, D., Dewilde, A., Braunhut, S.J., and Badylak, S.F. Degradation products of extracellular matrix affect cell migration and proliferation. Tissue Eng Part A **15,** 605, 2009.
15. Badylak, S.F., and Gilbert, T.W. Immune response to biologic scaffold materials. Semin Immunol **20,** 109, 2008.
16. Zhang, X.Y., Xue, H., Liu, J.M., and Chen, D. Chemically extracted acellular muscle: a new potential scaffold for spinal cord injury repair. J Biomed Mater Res **100,** 578, 2011.
17. Li, C., Zhang, X., Cao, R., Yu, B., Liang, H., Zhou, M., Li, D., Wang, Y., and Liu, E. Allografts of the acellular sciatic nerve and brain-derived neurotrophic factor repair spinal cord injury in adult rats. PLoS One **7,** e42813, 2012.
18. Liu, J., Chen, J., Liu, B., Yang, C., Xie, D., Zheng, X., Xu, S., Chen, T., Wang, L., Zhang, Z., Bai, X., and Jin, D. Acellular spinal cord scaffold seeded with mesenchymal stem cells promotes long-distance axon regeneration and functional recovery in spinal cord injured rats. J Neurol Sci **325,** 127, 2012.
19. Medberry, C.J., Crapo, P.M., Siu, B.F., Carruthers, C.A., Wolf, M.T., Nagarkar, S.P., Agrawal, V., Jones, K.E., Kelly, J., Johnson, S.A., Velankar, S.S., Watkins, S.C., Modo, M., and Badylak, S.F. Hydrogels derived from central nervous system extracellular matrix. Biomaterials **34,** 1033, 2013.
20. DeQuach, J.A., Yuan, S.H., Goldstein, L.S., and Christman, K.L. Decellularized porcine brain matrix for cell culture and tissue engineering scaffolds. Tissue Eng Part A **17,** 2583, 2011.
21. Wolf, M.T., Daly, K.A., Brennan-Pierce, E.P., Johnson, S.A., Carruthers, C.A., D'Amore, A., Nagarkar, S.P., Velankar, S.S., and Badylak, S.F. A hydrogel derived from decellularized dermal extracellular matrix. Biomaterials **33,** 7028, 2012.
22. Torres-Espin, A., Santos, D., Gonzalez-Perez, F., del Valle, J., and Navarro, X. Neurite-J: an image-J plug-in for axonal growth analysis in organotypic cultures. J Neurosci Methods **236,** 26, 2014.
23. Basso, D.M., Beattie, M.S., and Bresnahan, J.C. A sensitive and reliable locomotor rating scale for open field testing in rats. J Neurotrauma **12,** 1, 1995.
24. Crapo, P.M., Tottey, S., Slivka, P.F., and Badylak, S.F. Effects of biologic scaffolds on human stem cells and implications for CNS tissue engineering. Tissue Eng Part A **20,** 313, 2014.
25. Tottey, S., Corselli, M., Jeffries, E.M., Londono, R., Peault, B., and Badylak, S.F. Extracellular matrix degradation products and low-oxygen conditions enhance the regenerative potential of perivascular stem cells. Tissue Eng Part A **17,** 37, 2011.
26. Valentin, J.E., Stewart-Akers, A.M., Gilbert, T.W., and Badylak, S.F. Macrophage participation in the degradation and remodeling of extracellular matrix scaffolds. Tissue Eng Part A **15,** 1687, 2009.
27. Brown, B.N., Ratner, B.D., Goodman, S.B., Amar, S., and Badylak, S.F. Macrophage polarization: an opportunity for improved outcomes in biomaterials and regenerative medicine. Biomaterials **33,** 3792, 2012.

28. Sicari, B.M., Dziki, J.L., Siu, B.F., Medberry, C.J., Dearth, C.L., and Badylak, S.F. The promotion of a constructive macrophage phenotype by solubilized extracellular matrix. Biomaterials **35,** 8605, 2014.

29. Slivka, P.F., Dearth, C.L., Keane, T.J., Meng, F.W., Medberry, C.J., Riggio, R.T., Reing, J.E., and Badylak, S.F. Fractionation of an ECM hydrogel into structural and soluble components reveals distinctive roles in regulating macrophage behavior. Biomater Sci **2,** 1521, 2014.

30. Cheng, H., Liu, X., Hua, R., Dai, G., Wang, X., Gao, J., and An, Y. Clinical observation of umbilical cord mesenchymal stem cell transplantation in treatment for sequelae of thoracolumbar spinal cord injury. J Transl Med **12,** 253, 2014.

31. Brown, R.A. In the beginning there were soft collagen-cell gels: towards better 3D connective tissue models? Exp Cell Res **319,** 2460, 2013.

32. Sosa, I., Reyes, O., and Kuffler, D.P. Immunosuppressants: neuroprotection and promoting neurological recovery following peripheral nerve and spinal cord lesions. Exp Neurol **195,** 7, 2005.

33. Kubinova, S., Horak, D., Hejcl, A., Plichta, Z., Kotek, J., Proks, V., Forostyak, S., and Sykova, E. SIKVAV-modified highly superporous PHEMA scaffolds with oriented pores for spinal cord injury repair. J Tissue Eng Regen Med **9,** 1298, 2013.

34. Kubinova, S., Horak, D., Hejcl, A., Plichta, Z., Kotek, J., and Sykova, E. Highly superporous cholesterol-modified poly(2-hydroxyethyl methacrylate) scaffolds for spinal cord injury repair. J Biomed Mater Res **99,** 618, 2011.

35. Cloud, B.A., Ball, B.G., Chen, B.K., Knight, A.M., Hakim, J.S., Ortiz, A.M., and Windebank, A.J. Hemisection spinal cord injury in rat: the value of intraoperative somatosensory evoked potential monitoring. J Neurosci Methods **211,** 179, 2012.

36. Fouad, K., Hurd, C., and Magnuson, D.S. Functional testing in animal models of spinal cord injury: not as straight forward as one would think. Front Integr Neurosci **7,** 85, 2013.

Address correspondence to:
Sarka Kubinova, PhD
Institute of Experimental Medicine AS CR, v.v.i.
Vídeňská 1083
142 20 Prague 4-Krč
Czech Republic

E-mail: sarka.k@biomed.cas.cz

TISSUE ENGINEERING CONSTRUCTS AND CELL SUBSTRATES

Original Research

CrossMark

Dynamics of tissue ingrowth in SIKVAV-modified highly superporous PHEMA scaffolds with oriented pores after bridging a spinal cord transection

Aleš Hejčl [1,2] · Jiří Růžička[1,3] · Vladimír Proks[4] · Hana Macková[4] · Šárka Kubinová[1] · Dmitry Tukmachev[5] · Jiří Cihlář[6] · Daniel Horák[4] · Pavla Jendelová[1,3]

Abstract

While many types of biomaterials have been evaluated in experimental spinal cord injury (SCI) research, little is known about the time-related dynamics of the tissue infiltration of these scaffolds. We analyzed the ingrowth of connective tissue, axons and blood vessels inside the superporous poly (2-hydroxyethyl methacrylate) hydrogel with oriented pores. The hydrogels, either plain or seeded with mesenchymal stem cells (MSCs), were implanted in spinal cord transection at the level of Th8. The animals were sacrificed at days 2, 7, 14, 28, 49 and 6 months after SCI and histologically evaluated. We found that within the first week, the hydrogels were already infiltrated with connective tissue and blood vessels, which remained stable for the next 6 weeks. Axons slowly and gradually infiltrated the hydrogel within the first month, after which the numbers became stable. Six months after SCI we observed rare axons crossing the hydrogel bridge and infiltrating the caudal stump. There was no difference in the tissue infiltration between the plain hydrogels and those seeded with MSCs. We conclude that while connective tissue and blood vessels quickly infiltrate the scaffold within the first week, axons show a rather gradual infiltration over the first month, and this is not facilitated by the presence of MSCs inside the hydrogel pores. Further research which is focused on the permissive micro-environment of the hydrogel scaffold is needed, to promote continuous and long-lasting tissue regeneration across the spinal cord lesion.

1 Introduction

Spinal cord injury (SCI) is a devastating condition resulting in a disruption of the neuronal connections. After injury, the spinal cord lesion (SCL) develops into a combination of a pseudocystic cavity, glial and mesenchymal scar, resulting in a barrier for tissue repair and axonal regeneration [1]. Various types of experimental surgeries, that would either directly or indirectly reconstruct the lesion, have been investigated [2]. Building a bridge across the SCL using hydrogels, represents one of the therapeutic strategies in experimental SCI repair [1]. Several research groups, including ours, have shown that various hydrogels promote axonal ingrowth for a certain period of time [3–5]. Hydrogels are synthetic biomaterials providing the possibility to modify their physical and chemical properties, in order to better support and attract new tissue ingrowth inside the scaffold [4]. We can modify the chemical backbone of the scaffold, add functional groups or combine the hydrogels with other modalities, such as neurotrophic factors or stem cells [3, 4, 6, 7]. These adjustments may lead to an

✉ Aleš Hejčl
  ales.hejcl@gmail.com

1   Institute of Experimental Medicine, Academy of Sciences of the Czech Republic, Vídeňská 1083, 142 20 Prague, Czech Republic

2   Department of Neurosurgery, J. E. Purkinje University, Masaryk Hospital, Sociální péče 12A, 401 13 Ústí nad Labem, Czech Republic

3   Department of Neuroscience, 2nd Faculty of Medicine, Charles University, V Úvalu 84, 150 06 Prague 5, Czech Republic

4   Institute of Macromolecular Chemistry, Academy of Sciences of the Czech Republic, Heyrovského nám.2, 162 06 Praha 6, Břevnov, Czech Republic

5   Department of Neurosurgery, Motol University Hospital, V Úvalu 84, Prague 5 150 06, Czech Republic

6   Department of Mathematics, Faculty of Science, J. E. Purkyně University, České mládeže 8, 400 96 Ústí nad Labem, Czech Republic

improved ingrowth of axons, blood vessels or connective tissue into the bridge. However, little attention has been paid to the time-dependency of tissue infiltration into the scaffold. The design of most studies utilizing scaffolds in experimental SCI repair, leads to the evaluation of the axonal ingrowth at a single time point. According to our experience with hydrogel bridging in experimental SCI, we noticed that new axons do grow inside most scaffolds during the first weeks but, when evaluated at later time points, the amount of axons seems to be rather inadequate with respect to the earlier results (unpublished data). We therefore decided to study the time-dependent dynamics of tissue ingrowth inside the scaffold.

We used SIKVAV (Ser-Ile-Lys-Val-Ala-Val)-modified highly superporous poly (2-hydroxyethyl methacrylate) (HEMA) hydrogels with oriented pores to measure the time-dependent growth of axons across the scaffold [6]. These hydrogels had a moderate modulus of elasticity, which has been shown to best promote the aligned axonal ingrowth in that study; such aligned ingrowth being convenient for the ingrowth quantification.

2 Materials and methods

2.1 Hydrogel preparation

2.1.1 Reagents

Initiator, 2,2′-azobisisobutyronitrile (AIBN; Fluka, Buchs, Switzerland), was recrystallized from ethanol. The monomers, 2-hydroxyethyl methacrylate (HEMA; Wichterle-Vacík, Prague, Czech Republic) and ethylene dimethacrylate (EDMA; Ugilor S.A., France), were purified by vacuum distillation. Ammonium oxalate and 1,4-dioxane were obtained from Lach-Ner (Neratovice, Czech Republic). 2-Aminoethyl methacrylate hydrochloride (AEMA), ɣ-thiobutyrolactone, 2,2′-dithiodipyridine, imidazole and 1,1,1,3,3,3-hexafluoro-2-propanol were from Sigma-Aldrich (St. Louis, MO, USA) and used as received. Ultrapure Q-water ultrafiltered on a Milli-Q Gradient A10 System (Millipore, Molsheim, France) was used for all experiments. HS-CGGASIKVAVS-OH peptide was synthetized according to a published procedure [8].

2.2 Preparation of poly (2-hydroxyethyl methacrylate-*co*-2-aminoethyl methacrylate) P (HEMA-AEMA) hydrogel with oriented porosity

Preparation of the hydrogel is schematically shown in Fig. 1. Briefly, freshly crystalized 30–90 μm thick and 0.3–10 mm long ammonium oxalate needles of high aspect ratio were used as a porogen for the preparation of PHEMA-based

scaffolds. The ammonium oxalate crystals were parallel-oriented by shaking, which was followed by their slow sedimentation in a removable channel (12 mm in diameter) embedded in a narrow vessel on an orbital shaker (Fig. 1a). In order to maintain the crystal orientation, they were carefully transferred into the 5-ml polyethylene injection syringe with an inserted stainless sieve (32 μm), quickly washed with ethanol and dried in the air flow. The content of the crystals in the syringe was increased by the double filling of hot (90 °C) saturated oxalate solution, subsequent cooling and removing of redundant solution under vacuum (Fig. 1d). The ammonium oxalate in the syringe was then washed with ethanol and dried in an air flow and loaded with a polymerization mixture consisting of monomers (2.4 g HEMA, 0.025 g EDMA, 0.025 g AEMA), AIBN initiator (10 mg) and solvent (1,4-dioxane; 1.25 ml). The bottom of the syringe was then closed by the pressure cap and the mixture centrifuged (2000 rpm) to remove air bubbles and to homogenize the mixture. Finally, the syringe was completed with a rubber plunger and the mixture polymerized at 60 °C for 16 h. After the completion of the polymerization, the syringe was cut and the hydrogel removed (Fig. 1e). The resulting P(HEMA-AEMA) cylinder was immersed in 25% NaCl aqueous solution for 24 h to replace 1,4-dioxan and to protect the hydrogel from fast inhomogeneous swelling accompanied with hydrogel cracking. The cylinder was then transversely cut with a razor blade into discs 12 mm in diameter and 3 mm thick. Each disc was repeatedly washed with Q-water at room temperature to remove the ammonium oxalate.

2.3 Immobilization of HS-CGGASIKVAVS-OH on the P (HEMA-AEMA) discs

P(HEMA-AEMA) discs were immersed in 10 ml of aqueous 0.15 M imidazole solution and 2 ml of ethanol was added to improve the penetration of reagents in the hydrogels. 0.1 ml of ɣ-thiobutyrolactone was added under Ar and the mixture was gently shaken for 70 min. Discs were washed five times with Q-water and then transferred into 10 ml of 0.1 M phosphate buffer (pH 8) containing 3 ml of ethanol. A solution of 20 mg of 2,2′-dithiodipyridine in ethanol (2 ml) was added under Ar and the discs were incubated for 1 h. The discs were again repeatedly washed with the above described mixture of phosphate buffer and ethanol (10:3 v/v) under Ar. Finally, a solution of HS-CGGASIKVAVS-OH (2.5 mg) in 1,1,1,3,3,3-hexafluoro-2-propanol (0.25 ml) and phosphate buffer (pH 8; 6 ml) was added to the activated P(HEMA-AEMA) discs that were gently shaken for 60 min under Ar. The resulting HS-CGGASIKVAVS-modified P(HEMA-AEMA) discs were washed five times with Q-water, sterilized in 70% ethanol for 16 h and transferred in sterile 100-ml bottles.
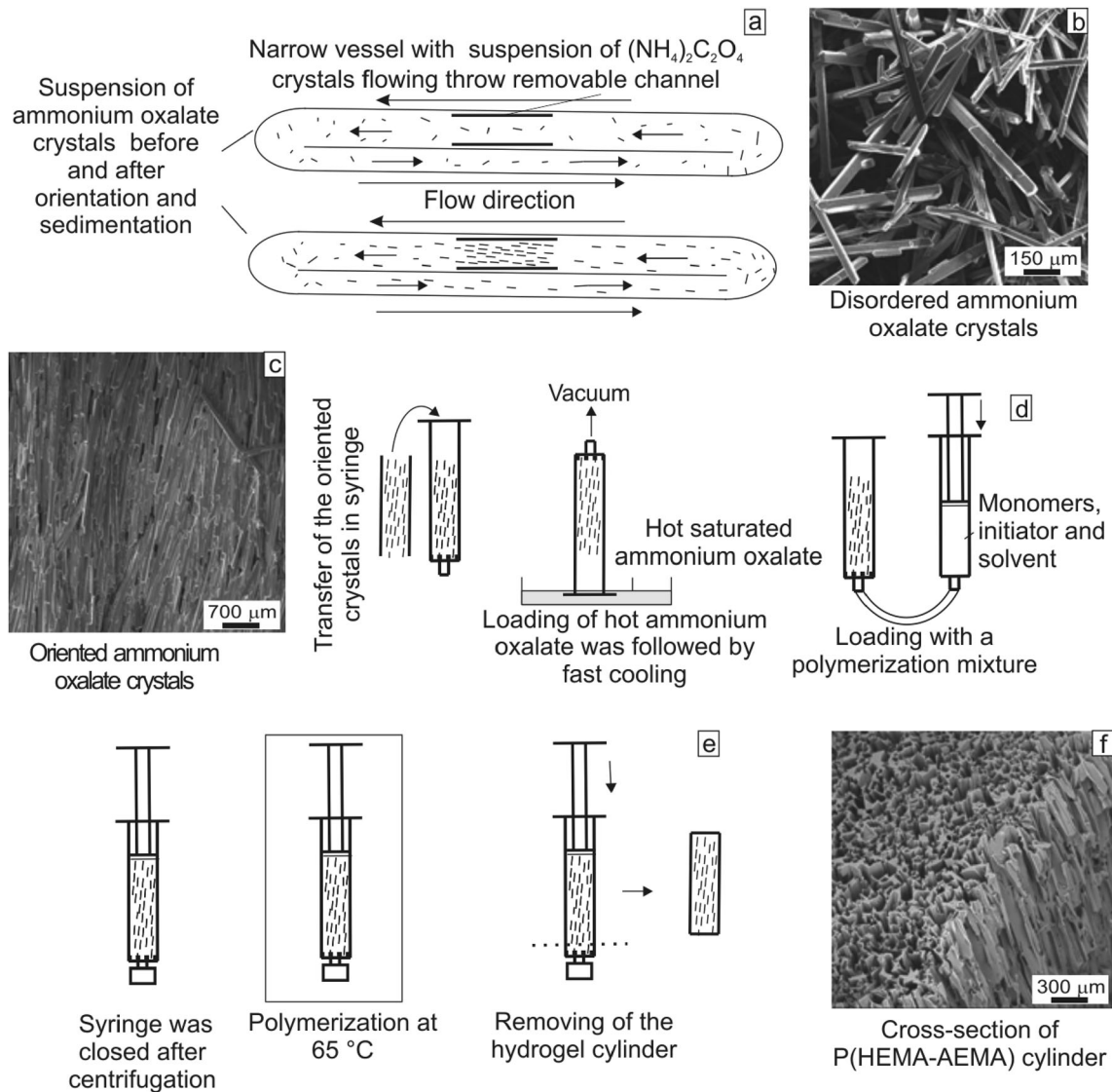
Fig. 1 Scheme of preparation of P(HEMA-AEMA) hydrogel. **a** Orientation of ammonium oxalate needles. SEM micrographs of **b** disorder and **c** oriented crystals. **d** Transfer of crystals and polymerization mixture to the syringe. **e** Preparation of P(HEMA-AEMA) cylinder. **f** SEM micrograph of P(HEMA-AEMA) hydrogel with oriented porosity

2.4 Characterization

P(HEMA-AEMA) discs were analyzed by a JSM 6400 scanning electron microscope (SEM; Jeol; Tokyo, Japan). The samples were sputter-coated with 4 nm Pt before imaging. The immobilization HS-CGGASIKVAVS-OH was indirectly determined by the observation of UV spectra of 2-thiopyridine, measured with a Lambda 20 spectrometer (Perkin-Elmer; Norwalk, CT, USA). Pascal 140 and 440 mercury porosimeter (ThermoFinigan; Rodano, Italy) was used for measuring the average pore size of the dry hydrogels in two pressure intervals, 0–400 kPa and 1–400 MPa [9]. A specific surface area of the dried hydrogels was measured by nitrogen adsorption, using a Gemini VII 2390 Analyzer (Micromeritics; Norcross, USA) at 77 K.

2.5 Seeding of MSCs on hydrogels

To enable the more easily distinguishable and stable tracking of the transplanted cells, rat MSCs expressing enhanced green fluorescent protein (GFP) isolated from GFP+ rats, were used in our experiments. The transgenic Sprague–Dawley rats [SD-Tg(CAG-EGFP)CZ-004Osb] were kindly provided by Dr. Masaru Okabe (Osaka University, Japan) [10], bred at the laboratory of Dr. Martin Marsala (University of California, San Diego, CA), then subsequently sent to our Institute, and bred in our animal facility.

The cells were isolated by extrusion of the bone marrow into a tissue culture Petri dish. The cells were plated in DMEM/10% fetal bovine serum with primocin (2 ml/ml). After 24 h, the non-adherent cells were removed by replacing the medium. When cells reached 75%–90% confluence, they were detached by trypsin/EDTA treatment and transferred into 75-cm^2 cell culture flasks. MSCs from passage 3 were used for in vitro and in vivo experiments. On the day of the hydrogel seeding, the cultures were trypsinized with a 0.25% trypsin/ethylenediaminetetraacetic acid (EDTA) solution. Two million cells per milliliter were then placed in a test tube along with a $2 \times 2 \times 2$ mm cube of hydrogel and put on a shaker (500 rpm) for 15 min in order to seed the 3D scaffold. We performed no quantitative analysis regarding the actual amount of seeded cells. However, our earlier study showed that the HEMA hydrogel provides good affinity to MSCs [4]. The hydrogels were implanted within 3 h after seeding.

2.6 Animal handling and surgery

This study was performed in accordance with the European Communities Council Directive of 22nd of September 2010 (2010/63/EU) regarding the use of animals in research, and was approved by the Ethics Committee of the Institute of Experimental Medicine, Academy of Sciences of the Czech Republic.

2.7 Spinal cord transection

Forty-six male rats (Wistar, Anlab, Czech Republic) with a weight of 300–350 g, underwent transection at the Th8 level. The animals were intraperitoneally injected with pentobarbital for anesthesia (0.06 g/1 kg i.p.); one dose of ATB (gentamicin 8 mg/1 kg i.m.), atropine (0.08 mg/1 kg s. c.), and mesocain to enhance local anesthesia (1 mg/1 kg s. c. + i.m.) was administered preoperatively. In addition, the rats received cyclosporine (Novartis; 10 mg/kg i.p.) before surgery and then daily until sacrifice. A linear skin incision was performed above the spinous processes of Th7-9; the paravertebral muscles were detached from the laminae Th7-9, and a Th8 laminectomy was performed. The dura was incised longitudinally in the midline and about a 2 mm-segment of spinal cord was dissected, creating a cavity resulting in complete spinal cord transection. The size and the character of the lesion were identical to our earlier study [11].

2.8 Hydrogel implantation

One week after the transection, we reopened the scar tissue from the skin to the spinal cord. We extracted the suture from the dura and removed the debris from the lesion. The

Table 1 Numbers of experimental animals

Days after hydrogel implantation	2	7	14	28	49	168
SIKVAV-HEMA	3	3	3	4	3	0
SIKVAV-HEMA with MSCs	3	4	5	6	3	3
Total	6	7	8	10	6	3

hydrogels were properly trimmed to adjust to the size and shape of the cavity. The hydrogel was taken from the EDTA solution and implanted wet in such a way as to ensure that it would firmly adhere to the edges of the transection cavity without causing any undue pressure onto the surrounding spinal cord tissue. Such approach ensures no further swelling of the hydrogel within the cavity. The muscles and skin were sutured again, and the animals were housed two in a cage with food and water ad libitum. The number of animals in each group regarding therapy (hydrogel with or without MSCs) and timing are summarized in Table 1.

2.9 Retrograde staining

Six months after SCI, under isoflurane anesthesia, a laminectomy of the lumbar vertebra 12 and 13 was performed and 2 µl of 2% hydroxystilbamidine (Fluorogold, Invitrogen, Carlsbad, CA) were stereotactically injected by a Nano-Injector (Stoelting Co., Wood Dale, IL) into the dorsal columns of 5 animals treated with hydrogel and MSCs. Two days later, the animals were perfused transcardially with phosphate-buffered saline (PBS) followed by 4% paraformaldehyde.

Sections were first incubated with anti-fluorogoldantibody (1:10,000; Chemicon International, Temecula, CA) then with biotinylated goat anti-rabbit secondary antibody (1:1000; Vector Labs, Burlingame, CA). They were processed using Vectastain ABC reagent (Vector Labs) and developed with diaminobenzidine (Vector Labs).

2.10 Tissue processing and histology

The animals were sacrificed 2, 7, 14, 28, 49 days and 6 months after hydrogel implantation. They were then deeply anesthetized with an intraperitoneal injection of overdose pentobarbital and perfused with physiological saline, followed by 4% paraformaldehyde in 0.1 M phosphate buffer. The spinal cord was left in the bone overnight, then removed and postfixed in the same fixative for at least 1 week.

A 4 cm-long segment of the spinal cord with the lesion site in the middle was dissected, and a series of 40 mm-thick longitudinal sections were collected. Hematoxylin–eosin staining was performed, using standard protocols, and the

slides were specifically evaluated using an Axio Observer D1 microscope (Carl Zeiss MicroimagingGmbH). For immunohistochemical studies, the following primary antibodies and dilutions were used: Cy3-conjugated anti-GFAP (1:200; Sigma-Aldrich) to identify astrocytes, anti-NF 160 (1:200; Sigma-Aldrich) to identify neurofilaments, and RECA-1 (1:50; Abcam) to identify endothelial cells of blood vessels. Alexa Fluor 594 goatanti–rabbit IgG (1:200; Invitrogen) and Cy3-conjugated anti-mouseIgM (1:100; Invitrogen) were used as secondary antibodies.

2.11 Tissue quantification

For each spinal cord, 4 to 5 slices were used for the quantification of axons. The hydrogels were divided into 3 parts: the cranial end, the central part and the caudal end. We calculated the number and the length of axons in each part of the scaffold, using the program Tissue Quest Analysis Software (Tissue Gnostics GmbH, Vienna, Austria). We then combined the data from the peripheral parts of the hydrogels (cranial and caudal ends) and evaluated them together. The central part was quantified and analyzed separately.

Blood vessels were evaluated via a semi-quantitative method using 4 slices for each spinal cord, as described in our previous paper [4]. We analyzed the number of green objects, regardless of the size of each object (number of areas), the total number of the green objects (sum of areas), and the intensity of the green color on each slice (densitometry) using Axio Vision 4.8 software (Carl Zeiss Microimaging GmbH, Jena, Germany). However, when the shape of the object was obviously not a blood vessel, it was manually excluded in order to avoid counting artifacts. By multiplying the "sum of areas" and the "densitometry" parameters, we obtained a semi-quantitative parameter, directly related to the number of blood vessels in the hydrogel *in vivo*.

The mean values are reported as mean ± SEM. Intergroup differences were analyzed using ANOVA,

and a Student's two-sample t-test (probability values <0.05 and <0.01 were considered statistically significant).

3 Results

3.1 Hydrogel scaffolds

Non-degradable PHEMA scaffolds were prepared by the radical polymerization of HEMA, EDMA and AEMA in the presence of a porogen-ammonium oxalatein small polyethylene syringes by a modification of the earlier described procedure [6]. The resulting hydrogel cylinders were subsequently cut on discs. The advantage of

polymerization in the syringes, consists mainly in minimizing contact of the hydrogel surface with the polymerization mold which could induce inhomogeneity of the hydrogel at the interface. A low concentration of EDMA (1 wt.%) was used to afford good mechanical properties of the hydrogel. Reactive amino groups were introduced by copolymerization of the monomers with 1 wt.% AEMA. To produce continuous pores in the hydrogel, which are required for the ingrowth of axons when implanted in the damaged spinal cord, it is necessary to orient the $(NH_4)_2C_2O_4$ crystals by gentle shaking on an orbital shaker. Figure 1b,c shows the $(NH_4)_2C_2O_4$ crystals before and after the orientation. The advantage of the $(NH_4)_2C_2O_4$ crystals consists in their needle-like shape, which in contrast to conventional porogens, such as cubic NaCl [12] or sucrose [13], provides connectivity between the pores and also enables a high level of filling due to the ordered crystal structure. Moreover, a double loading of saturated $(NH_4)_2C_2O_4$ solution raised crystal content in the syringe, as the crystals/cylinder volume ratio increased from 0.52 to 0.75. The SEM micrograph of a cross-section of the P(HEMA-AEMA) hydrogel, demonstrated that the orientation of the crystals during loading remained unchanged and a hydrogel with continuous pore channels was obtained after completion of the polymerization (Fig. 1e). The pore size (SEM) was identical to that of the original crystals, i.e., ~60 μm in diameter and a few mm in length. Mercury porosimetry confirmed the 70 μm pore size in the dry hydrogels. The large specific surface area of the P(HEMA-AEMA) hydrogel (82 m^2/g), determined by BET isotherm, documented the presence of macropores (<1 μm) in the polymer which could be beneficial for the prospective sufficient nourishment of the cells. In order to support cell adhesion, the P(HEMA-AEMA) hydrogel was coated with HS-CGGASIKVAVS-OH peptide. Its immobilization on the polymer surface was indirectly indicated by measuring the UV spectra of solutions before and after the reaction. Figure 2a shows characteristic adsorption bands of 2-thiopyrine in the spectrum at 272 and 337 nm, indicating 2-thiopyrine release from the activated P(HEMA-AEMA) discs in the supernatant after the reaction with peptide. After seeding MSCs attached and spread mostly parallel to the oriented pores of the hydrogels (2B).

3.2 Bridging the post-traumatic cavity with hydrogels

During the hydrogel manipulation and implantation, the scaffold was soft enough to adjust the shape and size of the post-transection cavity. The hydrogels bridged the transection cavity adequately. They adhered well to the spinal cord with minimal or no pseudocystic cavities. There was also no progression of pseudocystic cavities observed in time.
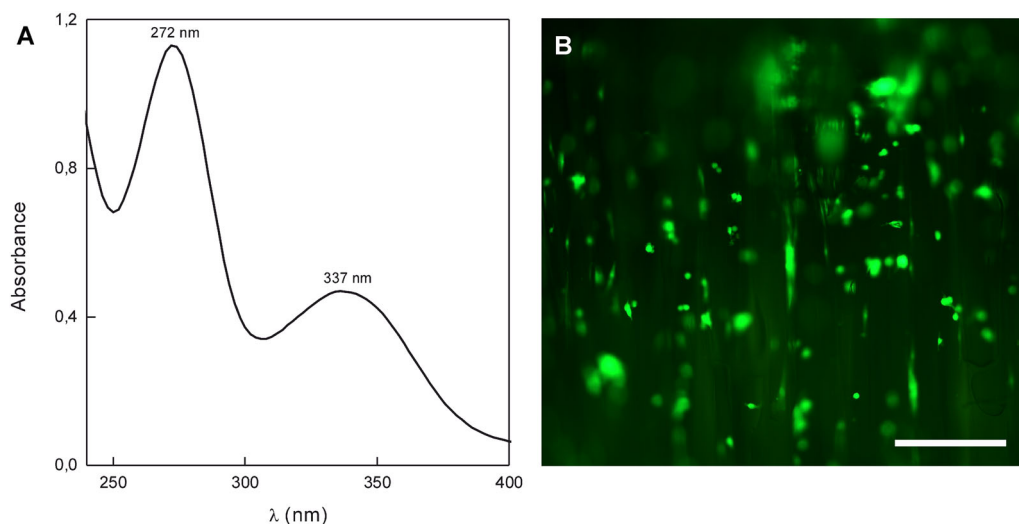
Fig. 2 **a** UV-spectrum of 2-thiopyridine released after immobilization of Ac-CGGASIKVAVS-OH on activated P(HEMA-AEMA) hydrogel. **b** MSCs attached to the hydrogel, many of them oriented along the pores of the scaffold

There were no signs of foreign body reactions observed in or around the hydrogels, either in the early or later stage after hydrogel implantation.

3.3 Connective tissue infiltration of the hydrogel scaffolds

Two days after hydrogel implantation, the pores of the hydrogels were dominantly filled with blood cells (Fig. 3a). There were no connective tissue elements observed in the pores, just a few myofibrils growing in the border zones of both groups of animals treated with hydrogels (with or without MSC). One week after hydrogel implantation, connective tissue elements infiltrated the whole volume of the hydrogel, both the periphery as well as the central part (Fig. 3b). MSCs were present in the pores of the hydrogel within the whole period, as long as 6 months after SCI (Fig. 3c). There was no difference in the amount of connective tissue between hydrogels seeded with MSC and without MSC. Also, we observed no change in the amount of connective tissue in the peripheral and central parts of the hydrogels from week 1 to week 7 after hydrogel implantation (Fig. 4).

3.4 Dynamics of axonal infiltration

Two days after hydrogel implantation, no axons were found either in the periphery or in the central part of the hydrogel. One week after hydrogel implantation, a few axons grew into the peripheral parts (mean total length $= 71 \pm 83 \,\mu m$) with none growing any further into the central part of the scaffold (Fig. 3d). Two weeks after hydrogel implantation, the number of axons grew significantly (mean total length

$= 188 \pm 76 \,\mu m$) into the peripheral parts of the hydrogel scaffold. The neural sprouts grew further and infiltrated the central parts of the hydrogel (mean total length $= 96 \pm 57$ μm). Four weeks after hydrogel implantation, the neural sprouts continued to infiltrate the peripheral part (mean total length $= 344 \pm 160 \,\mu m$). The axons also grew further into the central part of the scaffold with the mean total length of the axons $134 \pm 80 \,\mu m$. Seven weeks after the hydrogel implantation we observed a rather stable number of axons in the peripheral part with no further increase, compared to 4 weeks after implantation (mean total length $= 327 \pm 153$ μm), while in the central part the number of axons was $171 \pm 124 \,\mu m$ (Fig. 5).

Axons infiltrated the pores of the hydrogel in a slower and more gradual manner. Overall, they infiltrated about 2–4% of the whole volume of the scaffold in the peripheral parts and about 1.5–2% in the central part, guided in the cranio-caudal or caudo-cranial direction by the oriented pores of the hydrogel (Fig. 3e).

When we compared the axonal infiltration of hydrogels or hydrogels seeded with MSCs, we found no statistically significant difference between both groups at any time point, both in the peripheral as well as in the central parts of the hydrogel.

3.5 Dynamics of blood vessels ingrowth

There were no blood vessels in the scaffold 2 days after implantation, but the peripheral as well as the central parts of the hydrogels were filled with blood cells. The first blood vessels started to grow into the peripheral part of the hydrogels 1 week after implantation (Fig. 3f). However, the number of blood vessels did not increase between day 7 and

Fig. 3 SIKVAV-HEMA scaffolds bridging a posttraumatic cavity after spinal cord transection. **a** Left border region of the HEMA hydrogel 2 days after implantation in SCI. The pores are filled with blood elements, without any connective tissue (HE staining, scale bar = 100 μm). **b** One week after implantation of the HEMA scaffold the pores are completely filled with connective tissue (HE staining, scale bar = 100 μm). **c** GFP-positive MSCs 6 months after implantation of the HEMA scaffold seeded with MSCs (GFP staining, scale bar = 50 μm). **d** Neural sprouts invading pores of the bordering zone of the HEMA scaffold 2 weeks after implantation (NF160-g594 immunostaining, scale bar = 100 μm). **e** Axons in the central part of the HEMA scaffold seeded with MSCs 7 weeks after implantation are directed through the pores predominantly in the cranio-caudal or caudo-cranial direction (NF160-g594 immunostaining, scale bar = 100 μm). **f** Blood vessels infiltrating the pores of the HEMA scaffold (RECA-g594 immunostaining, scale bar = 100 μm). **g** Rare neurons were found to be fluorogold-positive in the spinal cord cranial from the tissue-scaffold border (white arrow, fluorogold staining, scale bar = 25 μm). **h** Astrocytes invading the peripheral part of the HEMA-scaffold 6 months after implantation (GFAP-Cy3, scale bar = 100 μm)
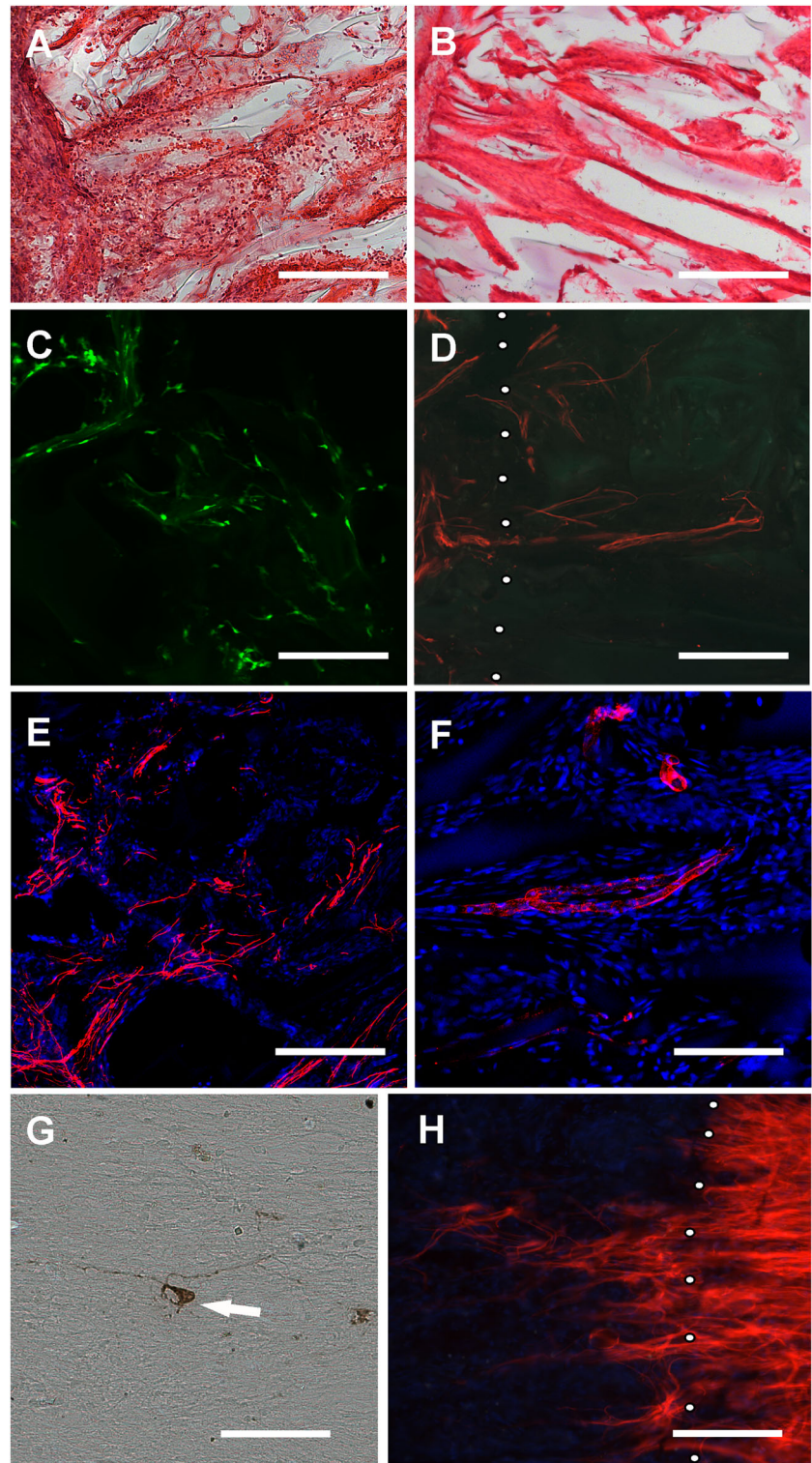

days 14, 28 or 49 and it became rather static until day 49 after SCI (Fig. 6). There were no statistically significant differences in the number of blood vessels observed during that time period. The blood vessels grew into the peripheral area and the same amount grew into the central parts of the hydrogel (Fig. 5). The same dynamics in the growth of blood vessels was observed in the hydrogels seeded with MSCs. We observed no statistically significant difference in the number of MSC between plain hydrogels and hydrogels seeded with MSCs.
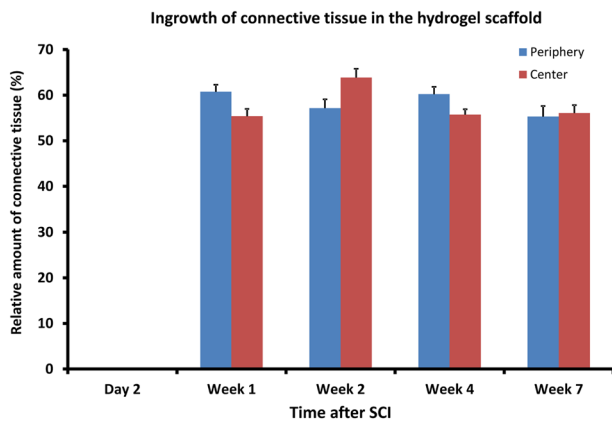
Fig. 4 Dynamics of connective tissue infiltration in the SIKVAV-HEMA scaffolds
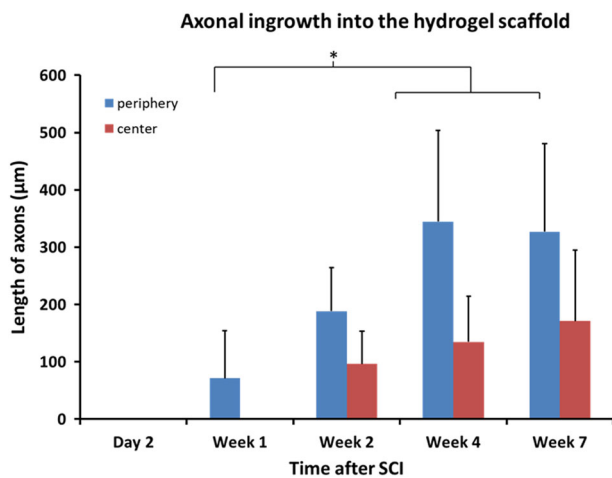
Fig. 5 Dynamics of axonal ingrowth in the SIKVAV-HEMA scaffold. A statistically significant increase in the number of axons is apparent between Day 7 and Weeks 4 and 7 after hydrogel implantation (*p < 0.05). There is a gradual increase in the number of axons infiltrating the scaffold
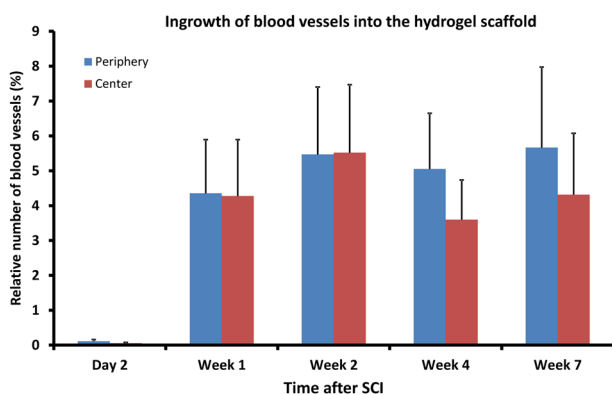
Fig. 6 Blood vessel ingrowth in the SIKVAV-HEMA scaffolds

3.6 Long-term results

Three rats were sacrificed 6 months after SCI. These were treated with hydrogels seeded with MSCs. MSCs were still abundantly present in the hydrogel scaffold 6 months after implantation (3 C). Six months after hydrogel implantation, most axons stopped at the tissue-hydrogel border, while some entered the hydrogel. We found only scarce positively-stained fluorogold neurons with projections in the cranial part of the spinal cord (Fig. 3g). In comparison to the early stage, we found that several astrocytes crossed into the hydrogel scaffold (Fig. 3h), however, their processes did not populate the hydrogel center.

4 Discussion

Complete SCI leads to disruption of the spinal cord tracts resulting in the formation of a pseudocystic cavity, glial and mesenchymal scar [14]. Implanting a hydrogel scaffold inside the post-traumatic cavity, represents one of the experimental approaches to reconstruct the spinal cord lesion [11]. Despite some progress, we have not yet achieved a complete bridging of the lesion with abundant axons crossing the barrier and forming functional connections. To do this, we would need to create an environment that would promote extensively progressive ingrowth of axons into and out of the hydrogel scaffold. However, no study has yet focused on the dynamics of tissue ingrowth into the hydrogel after implantation inside the spinal cord lesion.

In our previous research, we evaluated various types of hydrogel scaffolds [3, 4, 6, 7, 11, 15, 16] and noticed that after a few weeks of progressive ingrowth of axons, the results seemed rather disappointing in the long-term. We, therefore, decided to study the time-related ingrowth of axons into a hydrogel scaffold, using a SIKVAV-modified superporous PHEMA hydrogel with oriented pores. In our earlier study we found that moderate elastic modulus and porosity in these PHEMA scaffolds, showed a good combination of bridging properties, tissue infiltration and abundant axonal ingrowth [8]. Furthermore, we have shown that the oriented pores gave directed axonal guidance in the cranio-caudal and caudo-cranial direction, which allows an easy evaluation of the amount and the length of axons into the scaffold. We also seeded one group of the hydrogels with MSCs in order to assess whether these commonly used stem cells provide any advantage for the ingrowth of axons or blood vessels over time.

The hydrogels were implanted in a spinal cord transection cavity. This kind of experimental lesion mimics the most severe type of clinical SCI, in which the tissue is physically completely torn. Patients with complete spinal

cord injury (ASIA A) would be among the first to be included in clinical trials where the spinal cord lesion would be reconstructed utilizing non-injectable scaffolds, as there is no risk of losing any residual function [17]. At the same time, such an operation would be performed after some delay from the moment of injury, as the indication and the inclusion process require some time. We performed the implantation after a one week delay respecting the necessary time window. As we had also shown previously, such an approach may be even better than immediate surgery, as it improves adhesion to the edges of the spinal cord while minimizing the development of post-traumatic cavities [11].

4.1 Axonal growth into the hydrogel scaffold

The SIKVAV-HEMA-based hydrogel scaffold provided a permissive environment for the ingrowth of connective tissue, blood vessels and most importantly axons. While the ingrowth of connective tissue was rather fast, as it completely infiltrated the pores within the first week, axons infiltrated the scaffold in a slower and more gradual manner. The hydrogel scaffold attracted new axonal ingrowth but only for a limited period of time. Several factors could be considered to cause such a time-limited infiltration of the hydrogel scaffolds. One reason could be the spatial limitation in the hydrogel pores, due to the connective tissue infiltration. However, we demonstrated in our study that the connective tissue already fills the hydrogel pores within the first week, then remains stable for the next 2 months. However, the axons continued to grow progressively into the pores of the hydrogel during the first month after implantation. Therefore, the space limitation does not seem to be the decisive factor.

Another possible reason could be the lack of nutrients and growth factors in the hydrogel over time. We seeded some of our hydrogels with MSCs. MSCs may promote lesion repair and prevent neuronal apoptosis by secreting growth factors, such as the BDNF (brain-derived neurotrophic factor), VEGF (vascular endothelial growth factor), the NGF (nerve growth factor) or the GDNF (glial-derived neurotrophic factor) [18]. Furthermore, MSCs promote CNS plasticity [19]. In this study, however, we did not find any improvement in the number or in the growth dynamics of axons when the hydrogels were seeded with MSCs. Some other studies came to the same conclusion [20]. We showed that many MSCs were present within the scaffold as long as 6 months after SCI. Nonetheless, the number of present cells does not necessarily correlate with the extent of their metabolic activity [21]. Also, many groups, including ours, have shown neuroprotective and tissue preservation abilities of MSCs rather their influence on increased ingrowth of neural sprouts within the scaffold [3, 22, 23]. Using plain MSCs may be insufficient, but by

creating genetically engineered MSCs overexpressing some of the growth factors (BDNF or VEGF), we may achieve improved tissue repair including the promotion of axonal ingrowth [24]. The effect of MSCs also seems be facilitated by adding other supportive cells, e.g. Schwann cells [25]. For this reason, MSCs modifications may promote their positive effect on the neuronal repair after SCI.

One of the important factors is the micro-environmental milieu of the scaffold. The inner architecture of the hydrogel is one of the key components of the micro-environmental milieu. The inner structure is determined by the physical and chemical properties of the scaffold. In one of our previous studies, we found that the web-like architecture of the hydrogel, together with the HPMA-based backbone of the hydrogel, promotes the ingrowth of new axons despite promoting the adhesion of fewer MSCs compared to HEMA-based hydrogels [4]. The data from these two studies, suggests that the effect of MSCs seeded on hydrogels is less important than the inner milieu of the hydrogel, influenced by the chemical backbone and the architecture of the scaffold.

We also utilized a SIKVAV sequence attached to the hydrogels to promote cellular adhesion and growth-promoting properties. The SIKVAV sequence, a synthetic peptide from active regions of the A chain of basement membrane laminin, promotes cell adhesion and neural outgrowth by the binding of transmembrane integrin receptors [26]. The positive effect of the SIKVAV sequence on axonal regeneration and functional outcome sequence has been demonstrated previously [27, 28]. In one of our previous studies, PHEMA-based scaffolds modified with the SIKVAV sequence, promoted in vitro cell adhesion and axonal regeneration [8]. However, it still seems inadequate for a long-time promotion of axonal ingrowth. Therefore, the question remains of how to ensure long-term survival and promotion of axons in the hydrogel scaffolds. One of the strategies for axonal growth is the genetic manipulation of the injured axons. For migration, axonal growth cones require an adhesion complex that signals and links to the cytoskeleton. Integrins can belong to the targeted adhesion molecules, because axons regenerating through the CNS, particularly the scar tissue, must penetrate the extracellular matrix (ECM) for which integrins are the main receptors. Integrins, particularly $\alpha9\beta1$, are expressed in the CNS and PNS in embryogenesis, then downregulated and not re-expressed after injury [29]. Fawcett's group was able to obtain very extensive long-distance sensory axon regeneration in the spinal cord, by transducing sensory neurons with a tenascin-binding integrin and an integrin activator [30]. Our hydrogels can have different peptide sequences bound to the surface; however, the axons are not able to fully utilize the signals due to the missing integrin subunits. Therefore the potential of biomimetic materials can be

facilitated by modifying the axons to express a growth-promoting receptor for the matching sequence.

Another approach to promote the long-term growth and stability of axons, is to create a continuous milieu of trophic factors, such as the combination of olfactory ensheathing cells (OEC), together with olfactory nerve fibroblasts injected into the hydrogel scaffold, and with injections both in the rostral and caudal ends of the adhering spinal cord [31]. This leads to the promotion of cortico-spinal axons rostral to the lesion, but not across the lesion [32]. In a later study, a scaffold with guiding mini-channels seeded with GDNF-overexpressing Schwann cells, resulted in the growth of propriospinal axons across a bridge, their regeneration, formation of synapses and partial functional recovery [33].

4.2 Neovascularization in the hydrogel scaffold

Neovascularization at the site of the injury may provide oxygen and nutrition for axonal regeneration. Promoting the ingrowth of vasculature, may lead to improved axonal regrowth and functional recovery [34, 35]. Therefore manipulating the endogenous response towards promoting vascular repair is a logical step in tissue engineering. Our study showed that the blood vessels started to grow a few days after the lesion and were found not only in the peripheral part, but already grew long enough into the central part of the hydrogel 7 days after the SCI. However, there was no significant increase in the amount of blood vessels after the first week. This study also shows that the presence of MSCs does not increase the ingrowth of new blood vessels into the hydrogel scaffold, although many studies have shown that MSCs induce angiogenesis in injured tissues [36]. It is promoted by the paracrine release of the VEGF [37]. We have shown previously that new blood vessels often grow into the pores of the scaffold in close proximity to MSCs seeded in hydrogel scaffolds [3].

Various adhesion promoting approaches have been applied to promote angiogenesis [4, 38]. In one of our former studies, we found that the RGD peptide sequence promotes vascular growth into the hydrogel scaffolds when implanted in a spinal cord lesion [4]. The exogenous growth factors (GF) usually need to be applied at the site of injury in a supraphysiological level as they degrade quickly. Conversely, the tissue itself reacts to injury by increasing the levels of the vascular endothelial growth factor (VEGF) and the implantation of biomaterials activates the secretion of several cytokines [39, 40]. Feng et al. therefore propose taking advantage of such endogenous processes [41]. Using properly engineered injectable hydrogels, they activated macrophages to secrete pro-angiogenic cytokines, and released endogenous angiogenesis promoting growth factors inside the hydrogel. The manipulation with growth factors seems to be a stronger pro-angiogenetic tool than the presence of MSCs.

5 Conclusions

After hydrogel implantation inside a spinal cord lesion, the pores of the SIKVAV-HEMA scaffold are completely filled with connective tissue elements within the first week. Also, blood vessels infiltrate about 5% of the total hydrogel volume within the first week and the amount stays stable for the next 2 months. Axons, on the other hand, infiltrate the hydrogel scaffold in a gradual manner. The amount progresses within the first 4 weeks in the hydrogel scaffold and then remains stable. Rare axons were found to cross the bridge into the distal stump of the spinal cord. MSCs did not show any effect on the hydrogel infiltration over time with respect to the speed or the amount of any tissue infiltration. We need to investigate modifications and additional therapies that would enable long-time progressive infiltration of axons into the scaffold, which would be sufficient enough to cross the bridge and create new synapses leading to functional restoration.

Compliance with ethical standards

Conflict of interest The authors declare that they have no conflict of interest.

References

1. Geller HM, Fawcett JW. Building a bridge: engineering spinal cord repair. Exp Neurol. 2002;174:125–36. https://doi.org/10.1006/exnr.2002.7865.

2. Hejčl AJ, Sameš P, Syková M. Experimental treatment of spinal cord injuries. Cesk Slov Neurol N. 2015;78/111:377–93.

3. Hejcl A, Sedy J, Kapcalova M, Toro DA, Amemori T, Lesny P, et al. HPMA-RGD hydrogels seeded with mesenchymal stem cells improve functional outcome in chronic spinal cord injury. Stem Cells Dev. 2010;19:1535–46. https://doi.org/10.1089/scd.2009.0378.

4. Hejcl A, Ruzicka J, Kapcalova M, Turnovcova K, Krumbholcova E, Pradny M, et al. Adjusting the chemical and physical properties of hydrogels leads to improved stem cell survival and tissue ingrowth in spinal cord injury reconstruction: a comparative study of four methacrylate hydrogels. Stem Cells Dev. 2013;22:2794–805. https://doi.org/10.1089/scd.2012.0616.

5. Nomura H, Baladie B, Katayama Y, Morshead CM, Shoichet MS, Tator CH. Delayed implantation of intramedullary chitosan channels containing nerve grafts promotes extensive axonal regeneration after spinal cord injury. Neurosurgery. 2008;63:127–41. https://doi.org/10.1227/01.NEU.0000335080.47352.31.

6. Kubinova S, Horak D, Hejcl A, Plichta Z, Kotek J, Proks V, et al. SIKVAV-modified highly superporous PHEMA scaffolds with oriented pores for spinal cord injury repair. J Tissue Eng Regen Med. 2015;9:1298–309. https://doi.org/10.1002/term.1694.

7. Hejcl A, Lesny P, Pradny M, Sedy J, Zamecnik J, Jendelova P, et al. Macroporous hydrogels based on 2-hydroxyethyl methacrylate. Part 6: 3D hydrogels with positive and negative surface charges and polyelectrolyte complexes in spinal cord injury repair. J Mater Sci Mater Med. 2009;20:1571–7. https://doi.org/10.1007/s10856-009-3714-4.

8. Kubinova S, Horak D, Kozubenko N, Vanecek V, Proks V, Price J, et al. The use of superporous Ac-CGGASIKVAVS-OH-modified PHEMA scaffolds to promote cell adhesion and the differentiation of human fetal neural precursors. Biomaterials. 2010;31:5966–75. https://doi.org/10.1016/j.biomaterials.2010.04.040.

9. Salek P, Korecka L, Horak D, Petrovsky E, Kovarova J, Metelka R, et al. Immunomagnetic sulfonated hypercrosslinked polystyrene microspheres for electrochemical detection of proteins. J Mater Chem. 2011;21:14783–92. https://doi.org/10.1039/c1jm12475g.

10. Okabe M, Ikawa M, Kominami K, Nakanishi T, Nishimune Y. 'Green mice' as a source of ubiquitous green cells. FEBS Lett. 1997;407:313–9.

11. Hejcl A, Urdzikova L, Sedy J, Lesny P, Pradny M, Michalek J, et al. Acute and delayed implantation of positively charged 2-hydroxyethyl methacrylate scaffolds in spinal cord injury in the rat. J Neurosurg Spine. 2008;8:67–73. https://doi.org/10.3171/SPI-08/01/067.

12. Horák D, Hradil H, Lapčíková M, Šlouf M. Superporous poly(2-hydroxyethyl methacrylate) based scaffolds: preparation and characterization. Polymer. 2008;49:2046–54.

13. Horak D, Kroupova J, Slouf M, Dvorak P. Poly(2-hydroxyethyl methacrylate)-based slabs as a mouse embryonic stem cell support. Biomaterials. 2004;25:5249–60. https://doi.org/10.1016/j.biomaterials.2003.12.031.

14. Fitch MT, Doller C, Combs CK, Landreth GE, Silver J. Cellular and molecular mechanisms of glial scarring and progressive cavitation: in vivo and in vitro analysis of inflammation-induced secondary injury after CNS trauma. J Neurosci. 1999;19:8182–98.

15. Ruzicka J, Romanyuk N, Hejcl A, Vetrik M, Hruby M, Cocks G, et al. Treating spinal cord injury in rats with a combination of human fetal neural stem cells and hydrogels modified with serotonin. Acta Neurobiol Exp. 2013;73:102–15.

16. Hejcl A, Lesny P, Pradny M, Michalek J, Jendelova P, Stulik J, et al. Biocompatible hydrogels in spinal cord injury repair. Physiol Res. 2008;57(Suppl 3):S121–32.

17. Amr SM, Gouda A, Koptan WT, Galal AA, Abdel-Fattah DS, Rashed LA, et al. Bridging defects in chronic spinal cord injury using peripheral nerve grafts combined with a chitosan-laminin scaffold and enhancing regeneration through them by co-transplantation with bone-marrow-derived mesenchymal stem cells: case series of 14 patients. J Spinal Cord Med. 2014;37:54–71. https://doi.org/10.1179/2045772312Y.0000000069.

18. Li N, Sarojini H, An J, Wang E. Prosaposin in the secretome of marrow stroma-derived neural progenitor cells protects neural cells from apoptotic death. J Neurochem. 2010;112:1527–38. https://doi.org/10.1111/j.1471-4159.2009.06565.x.

19. Hao P, Liang Z, Piao H, Ji X, Wang Y, Liu Y, et al. Conditioned medium of human adipose-derived mesenchymal stem cells mediates protection in neurons following glutamate excitotoxicity by regulating energy metabolism and GAP-43 expression. Metab

Brain Dis. 2014;29:193–205. https://doi.org/10.1007/s11011-014-9490-y.

20. Gunther MI, Weidner N, Muller R, Blesch A. Cell-seeded alginate hydrogel scaffolds promote directed linear axonal regeneration in the injured rat spinal cord. Acta Biomater. 2015;27:140–50. https://doi.org/10.1016/j.actbio.2015.09.001.

21. Oliveira E, Assuncao-Silva RC, Ziv-Polat O, Gomes ED, Teixeira FG, Silva NA, et al. Influence of different ECM-like hydrogels on neurite outgrowth induced by adipose tissue-derived stem cells. Stem Cells Int. 2017;2017:6319129 https://doi.org/10.1155/2017/6319129.

22. Papa S, Vismara I, Mariani A, Barilani M, Rimondo S, De Paola M, et al. Mesenchymal stem cells encapsulated into biomimetic hydrogel scaffold gradually release CCL2 chemokine in situ preserving cytoarchitecture and promoting functional recovery in spinal cord injury. J Control Release. 2018;278:49–56. https://doi.org/10.1016/j.jconrel.2018.03.034.

23. Qu J, Zhang H. Roles of mesenchymal stem cells in spinal cord injury. Stem Cells Int. 2017;2017:5251313 https://doi.org/10.1155/2017/5251313.

24. Stewart AN, Matyas JJ, Welchko RM, Goldsmith AD, Zeiler SE, Hochgeschwender U, et al. SDF-1 overexpression by mesenchymal stem cells enhances GAP-43-positive axonal growth following spinal cord injury. Restor Neurol Neurosci. 2017;35:395–411. https://doi.org/10.3233/RNN-160678.

25. Yang EZ, Zhang GW, Xu JG, Chen S, Wang H, Cao LL, et al. Multichannel polymer scaffold seeded with activated Schwann cells and bone mesenchymal stem cells improves axonal regeneration and functional recovery after rat spinal cord injury. Acta Pharmacol Sin. 2017;38:623–37. https://doi.org/10.1038/aps.2017.11.

26. Tashiro K, Sephel GC, Weeks B, Sasaki M, Martin GR, Kleinman HK, et al. A synthetic peptide containing the IKVAV sequence from the A chain of laminin mediates cell attachment, migration, and neurite outgrowth. J Biol Chem. 1989;264:16174–82.

27. Tysseling-Mattiace VM, Sahni V, Niece KL, Birch D, Czeisler C, Fehlings MG, et al. Self-assembling nanofibers inhibit glial scar formation and promote axon elongation after spinal cord injury. J Neurosci. 2008;28:3814–23. https://doi.org/10.1523/JNEUROSCI.0143-08.2008.

28. Tysseling VM, Sahni V, Pashuck ET, Birch D, Hebert A, Czeisler C, et al. Self-assembling peptide amphiphile promotes plasticity of serotonergic fibers following spinal cord injury. J Neurosci Res. 2010;88:3161–70. https://doi.org/10.1002/jnr.22472.

29. Andrews MR, Czvitkovich S, Dassie E, Vogelaar CF, Faissner A, Blits B, et al. Alpha9 integrin promotes neurite outgrowth on tenascin-C and enhances sensory axon regeneration. J Neurosci. 2009;29:5546–57. https://doi.org/10.1523/JNEUROSCI.0759-09.2009.

30. Cheah M, Andrews MR, Chew DJ, Moloney EB, Verhaagen J, Fassler R, et al. Expression of an activated integrin promotes long-distance sensory axon regeneration in the spinal cord. J Neurosci. 2016;36:7283–97. https://doi.org/10.1523/JNEUROSCI.0901-16.2016.

31. Deumens R, Koopmans GC, Honig WM, Hamers FP, Maquet V, Jerome R, et al. Olfactory ensheathing cells, olfactory nerve fibroblasts and biomatrices to promote long-distance axon regrowth and functional recovery in the dorsally hemisected adult rat spinal cord. Exp Neurol. 2006;200:89–103. https://doi.org/10.1016/j.expneurol.2006.01.030.

32. Deumens R, Koopmans GC, Honig WM, Maquet V, Jerome R, Steinbusch HW, et al. Limitations in transplantation of astroglia-biomatrix bridges to stimulate corticospinal axon regrowth across large spinal lesion gaps. Neurosci Lett. 2006;400:208–12. https://doi.org/10.1016/j.neulet.2006.02.050.

33. Deng LX, Deng P, Ruan Y, Xu ZC, Liu NK, Wen X, et al. A novel growth-promoting pathway formed by GDNF-overexpressing Schwann cells promotes propriospinal axonal regeneration, synapse formation, and partial recovery of function after spinal cord injury. J Neurosci. 2013;33:5655–67. https://doi.org/10.1523/JNEUROSCI.2973-12.2013.

34. Iida T, Nakagawa M, Asano T, Fukushima C, Tachi K. Free vascularized lateral femoral cutaneous nerve graft with anterolateral thigh flap for reconstruction of facial nerve defects. J Reconstr Microsurg. 2006;22:343–8. https://doi.org/10.1055/s-2006-946711.

35. Glaser J, Gonzalez R, Sadr E, Keirstead HS. Neutralization of the chemokine CXCL10 reduces apoptosis and increases axon sprouting after spinal cord injury. J Neurosci Res. 2006;84:724–34. https://doi.org/10.1002/jnr.20982.

36. Gao XR, Xu HJ, Wang LF, Liu CB, Yu F. Mesenchymal stem cell transplantation carried in SVVYGLR modified self-assembling peptide promoted cardiac repair and angiogenesis after myocardial infarction. Biochem Biophys Res Commun. 2017;491:112–8. https://doi.org/10.1016/j.bbrc.2017.07.056.

37. Hou Y, Ryu CH, Jun JA, Kim SM, Jeong CH, Jeun SS. IL-8 enhances the angiogenic potential of human bone marrow mesenchymal stem cells by increasing vascular endothelial growth factor. Cell Biol Int. 2014;38:1050–9. https://doi.org/10.1002/cbin.10294.

38. Wang C, Poon S, Murali S, Koo CY, Bell TJ, Hinkley SF, et al. Engineering a vascular endothelial growth factor 165-binding heparan sulfate for vascular therapy. Biomaterials. 2014;35:6776–86. https://doi.org/10.1016/j.biomaterials.2014.04.084.

39. Golebiewska EM, Poole AW. Platelet secretion: from haemostasis to wound healing and beyond. Blood Rev. 2015;29:153–62. https://doi.org/10.1016/j.blre.2014.10.003.

40. Ullm S, Kruger A, Tondera C, Gebauer TP, Neffe AT, Lendlein A, et al. Biocompatibility and inflammatory response in vitro and in vivo to gelatin-based biomaterials with tailorable elastic properties. Biomaterials. 2014;35:9755–66. https://doi.org/10.1016/j.biomaterials.2014.08.023.

41. Feng Y, Li Q, Wu D, Niu Y, Yang C, Dong L, et al. A macrophage-activating, injectable hydrogel to sequester endogenous growth factors for in situ angiogenesis. Biomaterials. 2017;134:128–42. https://doi.org/10.1016/j.biomaterials.2017.04.042.

Injectable hydroxyphenyl derivative of hyaluronic acid hydrogel modified with RGD as scaffold for spinal cord injury repair

Kristyna Zaviskova [ORCID],[1,2] Dmitry Tukmachev,[1,2] Jana Dubisova,[1,2] Irena Vackova,[1] Ales Hejcl,[1]
Julie Bystronova,[3] Martin Pravda,[3] Ivana Scigalkova,[3] Romana Sulakova,[3] Vladimir Velebny,[3]
Lucie Wolfova,[1,3] Sarka Kubinova[1]

[1]Department of Biomaterials and Biophysical Methods, Institute of Experimental Medicine of the Czech Academy of Sciences, Prague, Czech Republic
[2]2nd Medical Faculty, Charles University, Prague, Czech Republic
[3]Department of Tissue Engineering, Contipro a.s., Dolni Dobrouc, Czech Republic

Abstract: Hydrogel scaffolds which bridge the lesion, together with stem cell therapy represent a promising approach for spinal cord injury (SCI) repair. In this study, a hydroxyphenyl derivative of hyaluronic acid (HA-PH) was modified with the integrin-binding peptide arginine-glycine-aspartic acid (RGD), and enzymatically crosslinked to obtain a soft injectable hydrogel. Moreover, addition of fibrinogen was used to enhance proliferation of human Wharton's jelly-derived mesenchymal stem cells (hWJ-MSCs) on HA-PH-RGD hydrogel. The neuroregenerative potential of HA-PH-RGD hydrogel was evaluated *in vivo* in acute and subacute models of SCI. Both HA-PH-RGD hydrogel injection and implantation into the acute spinal cord hemisection cavity resulted in the same axonal and blood vessel density in the lesion area after 2 and 8 weeks. HA-PH-RGD hydrogel alone or combined with fibrinogen (HA-PH-RGD/F) and seeded with hWJ-MSCs was then injected into subacute SCI and evaluated after 8 weeks using behavioural, histological and gene expression analysis. A subacute injection of both HA-PH-RGD and HA-PH-RGD/F hydrogels similarly promoted axonal ingrowth into the lesion and this effect was further enhanced when the HA-PH-RGD/F was combined with hWJ-MSCs. On the other hand, no effect was found on locomotor recovery or the blood vessel ingrowth and density of glial scar around the lesion. In conclusion, we have developed and characterized injectable HA-PH-RGD based hydrogel, which represents a suitable material for further combinatorial therapies in neural tissue engineering. © 2018 Wiley Periodicals, Inc. J Biomed Mater Res Part A: 106A: 1129–1140, 2018.

Key Words: hyaluronic acid, spinal cord injury, scaffold, mesenchymal stem cells, regenerative medicine

INTRODUCTION

Spinal cord injury (SCI) often results in permanent neurological defects as a consequence of the inability of axons to regenerate across the lesion. Despite progress, which has been made in promoting SCI repair in experimental models, there is still no effective therapy available for the patients.[1] A promising treatment approach is represented by the use of supportive and stimulatory biomaterial, which can serve as a bridge for axonal regrowth and endogenous cell migration as well as a carrier for cell transplantation.[2–4] A convenient way for the development of materials suitable for tissue regeneration is to mimic the structure and components of extracellular matrix (ECM) of the target tissue. Moreover, physical or chemical cues can be incorporated into the biomaterial to influence specific cell behavior.[5]

Natural hydrogels are extensively developed materials for SCI repair. They can be based on an ECM component, such as collagen,[6] fibronectin,[7] hyaluronic acid (HA),[8–12] or other naturally occurring polysaccharides or their combination.[13,14] In addition, hydrogels that retain the composition of tissue-specific ECM can be prepared by the decellularization of various tissues.[15,16]

HA is an important structural component of ECM and it is widely used due to its biocompatibility, biodegradability, and non-immunogenicity as biomaterial in clinical settings. Among its structural functions, HA also acts as a signaling molecule via specific HA receptors to actively modulate tissue regeneration.[17,18]

In neural tissue engineering, HA-based materials have been studied *in vitro* as substrates for neural stem cell cultures,[19] as well as *in vivo*, alone or as carriers for cell delivery
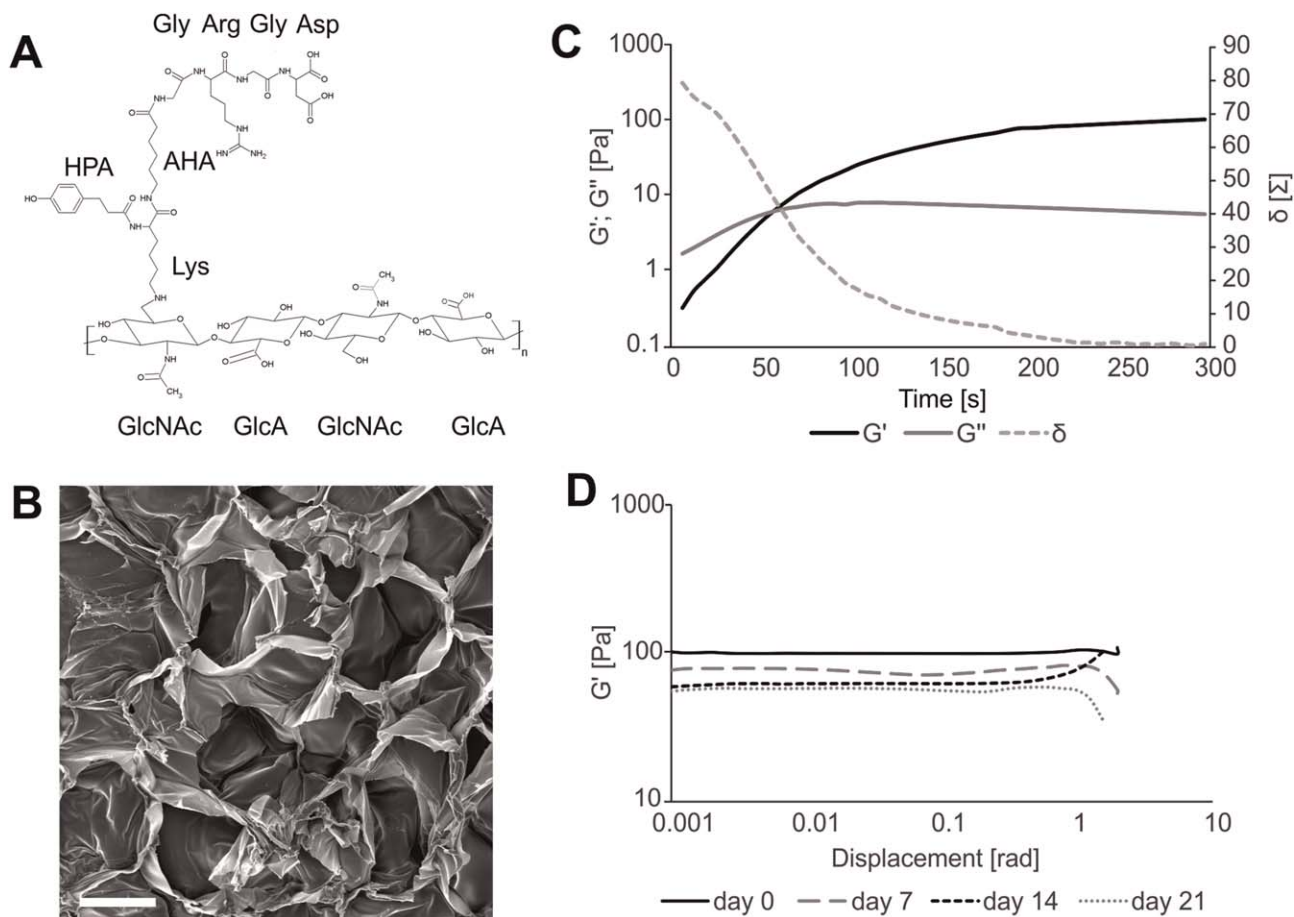
FIGURE 1. A: Scheme of hydroxyphenyl derivative of HA with attached RGD peptide sequence. B: SEM image of the HA-PH-RGD hydrogel structure. C: Gelation kinetic of the HA-PH-RGD crosslinked with 0.04 U/mL of HRP and 0.165 mM H$_2$O$_2$. D: The influence of HA-PH-RGD swelling on the elastic modulus. Scale bar: 100 μm.

to improve cell retention and integration.[10,20,21] Injectable HA-based hydrogels were also developed for localized intrathecal delivery of bioactive molecules into the SCI.[22,23]

Native HA does not form a gel nor support cell adhesion. Therefore, it is necessary to chemically modify the functional groups of HA and tune its chemical, physical or biological properties according to the special demands of the particular application. Concerning the gel formation, various HA derivatives can be stabilized by crosslinking, such as dihydrazide crosslink of HA polyaldehyde, thiol-en click crosslinking of norbornene-HA derivative, initiated by UV light, copper catalyzed 1,3-dipolar cycloaddition reaction, or UV initiated crosslinking of methacrylated HA.[18] To enable cell adhesion, functionalization of HA-based materials has been achieved using a variety of techniques, such as the incorporation of poly-L-lysine,[24] laminin,[25] fibronectin,[26] fibrinogen,[27] blending with methylcellulose,[14] or modifying HA with integrin ligands derived from ECM, such as arginine-glycine-aspartic acid (RGD) sequence.[28]

One of such promising HA-based materials capable to form covalently cross-linked hydrogel with the required mechanical properties, is the hydroxyphenyl derivative of HA (HA-PH).[29,30] The cross-linking reaction of this HA-PH derivative can be triggered by enzyme horseradish peroxidase (HRP) and hydrogen peroxide (H$_2$O$_2$) under physiological conditions, without a negative effect on encapsulated cells during cross-linking reaction and gel forming.[31] Previously, we demonstrated the chondrogenic potential of HA-PH derivative based hydrogel in vitro as well as in vivo in cartilage defects.[31,32]

In this study, we have used the HA-PH derivative bearing the newly developed 3–(4-hydroxyphenyl) propionic acid (PH)—L-lysine—aminohexanoic acid—L-glycine—L-arginine—L-glycine—L-aspartic acid (HA-PH-RGD) sequence [Fig. 1(A)], which allows the attachment of PH moiety and RGD cell adhesive motive to polymer backbone in one synthetic step. The mechanical properties of HA-PH-RGD hydrogel were then optimized to be suitable for the soft neural tissue with an optimal time of gelation, to enable a hydrogel injection into the site of the defect.

The biocompatibility of this material was evaluated in vitro in cell culture as well as in vivo in an experimental model of SCI in rats. First, we compared two ways of hydrogel delivery into the lesion cavity after acute spinal cord hemisection, where we did not observe any remarkable differences in tissue repair, when the hydrogel was formed

ex vivo and then implanted or injected into the lesion and crosslinked *in situ*. Then, we evaluated the neuroregenerative potential of HA-PH-RGD hydrogel alone or in combination with human Wharton's jelly-derived mesenchymal stem cells (hWJ-MSCs) after its injection into the subacute spinal cord hemisection. To further promote hWJ-MSCs adhesion, HA-PH-RGD was combined with fibrinogen (HA-PH-RGD/F), which contains integrin binding sites, such as RGD, and has been widely used as a promising additive to enhance cell survival, growth, and proliferation.[33,34] Moreover, fibrinogen is abundant in a blood plasma and can be easily extracted from the donors for the autologous use. We used hWJ-MSCs, as these cells represent an easily accessible source, with high potential for clinical applications. Moreover, a therapeutic benefit of hWJ-MSCs in SCI alone as well as in combination with a biomaterial has been shown previously in several experimental and clinical studies.[35–37]

MATERIALS AND METHODS
Hyaluronan RGD modification
HPA-K-AHA-GRGD oligopeptide sequence was synthesized by solid phase synthesis using Fmoc-SPPS protocol.[38] Briefly, N-termini of the RGD adhesive peptide was modified by subsequent attachment of lysine, 6-aminohexanoic acid (Ahx) and glycine. Furthermore, α-amino group of lysine was acylated by 3-(4-hydroxyphenyl) propionic acid (HPA). This peptide sequence (HPA-K-Ahx-GRGD) was purified and characterized by ^{1}H NMR and Mass Spectroscopy.

The RGD sequence was further conjugated with hyaluronan polyaldehyde (HA-CHO; DS = 10%; Mw = 400 kDa; purchased from Contipro a. s.) via reductive amination.[39,40] HA-CHO (1.00 g, 2.50 mmol dimers of HA) was dissolved in 100 mL of demineralized water. Then, HPA-K-Ahx-GRGD (0.25 mmol) was added to the reaction mixture and the mixture was further stirred for 1 h at room temperature. Subsequently, a solution of picoline-borane complex (PIC-BOR; 0.625 mmol) in 10 mL of 50% propan-2-ol was added to the mixture. The reaction mixture was stirred for another 12 h at room temperature. The final product was obtained after precipitation by propan-2-ol. The degree of substitution (DS) of HPA-K-Ahx-GRGD of such modified HA-PH-RGD derivative was 2.5%.

Chemical characterization of HA-PHA-RGD derivative
^{1}H NMR and HSQC spectroscopy was carried out on a Bruker Advance III 500 MHz instrument operating at a proton frequency of 500.25 MHz, and elaborated by Bruker 2.1 Topspin software. Samples were dissolved in a mixture of D2O and NaOD (0.75 mL) and transferred into 5 mm NMR quartz tubes. ^{1}H NMR was also used to determinate the DSs of the prepared HA-PHA-RGD derivative. The DS was calculated from the ratio of the signal intensity of aromatic protons of the HPA (doublets 6.47 and 6.89 ppm) with respect to the signal of hydrogens of the *N*-acetyl group (singlet 2.01 ppm) (Supporting Information Figs. S1–S3).

LCMS-2020 Single Quadrupole Liquid Chromatograph Mass Spectrometer (LC/MS) with the column C18 (250 $\times$ 10.00 mm, Jupiter 4 u Proteo 90 A) was used for RGD sequence isolation. Gradient elution was used for peptide purification (phase A 0.1% formic acid; phase B – acetonitrile). The gradient was set as follows: 0–8 min 30% B, 8–15 min 30–50 min % B, 15–16 min 50–95% B, 16–20 min 95% B, 20–22 min 95–30% B, 22–32 min 30% B. Chromatographs and the MS detector record are shown in Supporting Information Figure 4.

Size exclusion chromatography combined with a multi-angle laser light scattering detector was used to determine the molecular weight of the HA-PH-RGD. A refractive index increment (dn/dC) of 0.155 mL g^{-1} was used to calculate the molecular weight and polydispersity (Mw/Mn).

Hydrogel preparation and crosslinking
The HA-PH-RGD (20 mg/mL) was dissolved in 0.9% NaCl and stirred for a period of at least 6 h at room temperature to gain homogenous solutions. The crosslinking of HA-PH-RGD solution and hydrogel formation was initiated by the addition of 0.04 U/mL HPR (Sigma) and 0.165 mM H_2O_2 (Merck, Germany) to the HA-PH-RGD solution. Cylindric teflon moulds with a volume of 0.4 mL were used for gel forming and maturing.

Hydrogel characterization
Rheological measurements were performed using TA Instruments AR-G2 rheometer and Rheology Advantage Data Analysis software. The device settings were as follows: parallel plate (40 mm), gap 400 μm, dose volume 500 μL and temperature 37°C. For evaluation of the viscoelastic properties of material, that is, storage modulus G′, loss modulus G″ and shear loss angle δ (tan δ = G″/G′), strain sweep mode was used (frequency 1 Hz and displacement from 0.001 to 2 rad). Crosshatched geometry was used to avoid slippage of the samples. The time of gelation was evaluated from the intersection of the G′ and G″ moduli using time sweep step mode (frequency 1 Hz and displacement 0.001 rad).

Hydrogels used for the stability study were prepared using the teflon moulds. The samples with a volume of 0.4 mL were immersed in phosphate-buffered saline (PBS) for 7, 14 and 21 days. Then, the swollen hydrogel disks were gently blotted dry and measured on a rheometer in strain sweep mode. The increasing deformation—displacement set from 0.001 to 2 rad was performed at 1 Hz, in order to achieve elastic modulus of the material. Crosshatched geometry was used to avoid slippage of the samples. The swelling ratio of the samples could not be properly evaluated. Due to the swollen hydrogel consistency, it was not possible to completely and equivalently blot up the swollen samples, which would have affected the obtained values. Moreover, this procedure would cause destruction of the sample structure. Scanning electron microscope (SEM) was used to show the hydrogel structure (Supporting Information).

Cell isolation and culture
Human umbilical cord samples were collected from healthy full-term neonates after spontaneous delivery at the Department of Obsterics and Gynecology, University Hospital of

Pilsen, Czech Republic. The samples were obtained upon written informed consent from mothers using the guidelines approved by the Institutional Ethics Committee. The proximal part of the umbilical cord close to the placenta (10–15 cm), was cut and immersed into the sterile PBS (IKEM, Czech Republic) with antibiotic-antimycotic solution (Sigma). Samples were transferred to the laboratory on ice to be processed within 24 h from partum. After washing in PBS and betadine (EGIS Pharmaceuticals PLC, Hungary) and the removal of blood vessels and amniotic membrane, the remaining tissue (Wharton's jelly) was chopped into small pieces (1–2 mm^3), and the pieces were transferred to culture dishes (Nunc; Schoeller, Czech Republic) containing the alpha-Minimum Essential Medium (East Port, Czech Republic) supplemented with 5% platelet lysate (IKEM, Czech Republic) and gentamicin 10 mg/mL (Sandoz, Czech Republic), and cultivated at 37°C in a humidified atmosphere containing 5% CO_2. On day 10, the explants were removed from the culture dishes, and the remaining adherent cells were cultured until 90% confluence and passaged using 0.05% Trypsin/EDTA (Life Technologies, USA). After passaging, the cells were seeded into culture flasks (Nunc) at a density of 5×10^3 cells/cm^2. The medium was changed twice a week. hWJ-MSCs from passage three were used for both *in vitro* and *in vivo* studies. The mesenchymal stem cell phenotype was characterized using fluorescence-activated cell sorting (FACS) analysis of surface marker profiles (FACSAria; Becton Dickinson, USA) and adipogenic, osteogenic and chondrogenic differentiation (Supporting Information).

Cell proliferation

To enhance cell proliferation, the initial HA-PH or HA-PH-RGD solutions were mixed with fibrinogen (1 mg/mL, Sigma) in 0.9% NaCl and formed into hydrogel film to cover the 24-well culture plate. The culture wells were seeded by 1.5×10^5 of hWJ-MSCs per well. After 3, 7, or 12 days of cultivation, the cell proliferation was evaluated using CellTiter-Glo reagent.

Proliferation of hWJ-MSCs in the presence of HA-PH-RGD hydrogel, combined with fibrinogen (HA-PH-RGD/F) was further determined after 3 h, 1, and 3 days in culture using WST-1 reagent (Roche, Germany). hWJ-MSCs were mixed with HA-PH-RGD/F hydrogel to form 3D culture (20 μL, 8 $\times 10^4$ cells) in 1 mL of medium in a 24-well plate. The same volume of hydrogel without cells served as a background. At the measured time points, WST-1 reagent was added to each well and the plates were incubated for 2 h at 37°C. The absorbance was measured using a Tecan Spectra ELISA plate reader (Tecan Trading) at 450 nm with a reference reading at 620 nm.

The morphology of hWJ-MSCs grown in HA-PH-RGD and HA-PH-RGD/F hydrogel was examined by fluorescent staining for actin filaments. After fixation in 4% paraformaldehyde in 0.1 M PBS for 10 min, the cells were stained with Alexa-Fluor 568 phalloidin (1:400, Molecular Probes, USA), and the nuclei were visualized by using 4,6-diamidino-2-phenylindole (DAPI) fluorescent dye (1:1000, Invitrogen, UK).

Hydrogel application into the SCI lesion

Male Wistar rats (250–300 g, Velaz, Czech Republic) underwent a hemisection on the right side at the level of the eighth thoracic vertebra (Th8). The surgical procedure was described previously in.[16] Briefly, the animals were induced with pentobarbital anesthesia (60 mg/kg), then the skin above the Th8 was cut and muscles were detached from the spine. The laminectomy at Th8 was performed and dura was incised with micro-scissors. The right half of one spinal cord segment (2-mm long) was dissected to generate a hemisection cavity.

In the animals with acute application of hydrogel ($n = 3$, in each time point and group), the cavity was filled with hydrogel immediately after the hemisection was performed. Two methods of hydrogel application were used. First, HA-PH-RGD solution (20 mg/mL) was mixed with crosslinking components to form a gel in the teflon mold as described above. The adjusted hydrogel volume was then implanted into the lesion to fill the hemisection cavity. In the second approach, approximately 5 μL of HA-PH-RGD hydrogel solution mixed with crosslinking agents was immediately injected by Omnican Insulin syringe for U-100 Insulin (B.Braun, Germany) into the lesion cavity, where the complete *in situ* gelation occurred. The control lesion was filled with saline.

Animals with a subacute lesion underwent hemisection one week before hydrogel injection. The liquid pre-gel solution of HA-PH-RGD hydrogel ($n = 6$), HA-PH-RGD/F ($n = 6$) and HA-PH-RGD/F combined with hWJ-MSCs (3 million/0.5 mL, approximately 3×10^4 transplanted cells in 5 μL of the hydrogel) ($n = 7$), was mixed with crosslinking agents and immediately injected into the hemisection cavity by Omnican Insulin syringe for U-100 Insulin (B.Braun, Germany), to form gel *in situ*. In the control SCI group ($n = 8$), the hemisection defect was filled with saline. From 5 days after the hemisection induction, all animal groups with a subacute hydrogel injection and controls received a daily injection of the immunosuppressant cyclosporinA (10 mg/kg, i.p.) (Sandimmune; Novartis, Switzerland), azathioprine (2 mg/kg, p.o.) (Imuran; Aspen Europe GmbH, Germany) and methylprednisolone (2 mg/kg, i.m.) (Solu-Medrol; Pfizer Manufacturing, Belgium), to prevent rejection of the transplanted cells.[16] All animals were housed two rats per cage with food and water ad libitum. All experiments were performed in accordance with the European Communities Council Directive of 24 November 1986 (86/609/EEC), regarding the use of animals in research and were approved by the Ethics Committee of the Institute of Experimental Medicine, Academy of Sciences Czech Republic, Prague, Czech Republic.

Tissue processing and histology

Two and eight weeks after the acute hydrogel application, and 8 weeks after subacute hydrogel injection, the animals were deeply anesthetized with an intraperitoneal injection of overdose chloral hydrate (Sigma) and intracardially perfused with PBS, followed by 4% paraformaldehyde in 0.1 M PBS. The spinal cord was left in the bone for 1 week in 4%

paraformaldehyde in 0.1 M PBS. A 3 cm long segment of the spinal cord containing the lesioned site was dissected out, transferred to sucrose and frozen. Then, a series of 40 µm thick longitudinal sections were collected.

Non-specific immunohistological staining was avoided by the application of blocking goat or donkey serum (1:10; G9023 or D9663, Sigma) depending on the secondary antibody host organism. Triton X-100 (0.1% in 0.1 M PBS; Sigma) was used for the permeabilization of cell membranes. Samples were stained with antibodies against neurofilaments 160 kDa (NF-160, 1:200), glial fibrillary acidic protein (GFAP, conjugated with Cy3, 1:800; all from Sigma); growth associated protein 43 (GAP43, 1:100), M2 macrophages (CD206, 1:250; all from Santa Cruz); endothelial cell (RECA-1, 1:500), microglia/macrophages (ED1, 1:150), human mitochondria (MTCO2, 1:250; all from Abcam, UK); and oligodendrocytes (1:200; CE-1, Merck-Millipore, Germany). Donkey anti-mouse IgG AlexaFluor 488, donkey anti-goat IgG AlexaFluor 594, goat anti-mouse IgG Alexa Fluor 488, goat anti-mouse IgG Alexa Fluor 594 (all 1:400; Life Technologies, USA), and goat anti-mouse IgM Cy3 (1:200; Merck-Millipore, Germany) were used as secondary antibodies. The nuclei were visualized by using DAPI fluorescent dye (1:1000; Invitrogen, UK).

Fluorescent micrographs were taken using fluorescence microscope Observer D1 with AxioVision 4.8.2 software (Zeiss, Germany), LEICA DMI6000B (Leica, Germany) with TissueFAXS software (TissueGnostics GmbH, Austria) and a laser scanning confocal microscope LSM 5 DUO (Zeiss, Germany).

For analysis of axonal and blood vessels ingrowth, three images across the lesion (cranial side, central and caudal side) from three longitudinal sections for each animal were taken using a 20× objective. The relative area of the axons (NF160 staining) and blood vessels (RECA staining) within the images was analyzed using ImageJ software (NIH, Bethesda, USA). Quantification analysis expressed the percentage of NF160 or RECA positive area from a total lesion area.

To evaluate glial scarring, three mosaic images of GFAP staining for each animal was taken using a 20× objective. Integrated density and mean gray value of three areas around the lesion (cranial side, central and caudal side) and background (uninjured part of spinal cord) were measured by ImageJ software. Results were expressed as the corrected total cell fluorescence (CTCF), while CTCF = Integrated Density – (Area × Mean gray value of background).[41]

Gene expression analysis

Changes in the mRNA expression of genes related to M1 macrophages (*Irf5, Cd86*), M2 macrophages (*Mrc1, Cd163*), axonal growth (*Gap43*), angiogenesis (*Vegfa*), growth factor (*Fgf2*), apoptosis (*Casp3*), inflammation (*Ccl3, Ccl5*), astrogliosis (*Gfap*), and glial scar related chondroitin sulfate proteoglycans (CSPGs) (*Ncan, Ptprz1, Cspg4*) were determined 8 weeks after subacute injection of HA-PH-RGD hydrogels by quantitative real-time PCR (qPCR), and plotted against the control lesion. RNA was isolated from paraformaldehyde-fixed frozen

tissue sections using the High Pure RNA Paraffin Kit (Roche, Germany) and RNA amounts were quantified using NanoPhotometer P 330 (Implen, Germany). The isolated RNA was reverse transcribed into complementary DNA using the Transcriptor Universal cDNA Master (Roche, Germany) and T100 Thermal Cycler (Bio-Rad, USA). The qPCR reactions were performed using cDNA solution, FastStart Universal Probe Master (Roche, Germany) and TaqMan Gene Expression Assays (Thermo Fisher Scientific) (Supplementary Table 1). The qPCR was carried out in a final volume of 10 µL containing 20 ng of extracted RNA. Amplification was performed on the real-time PCR cycler (StepOnePlus, Life Technologies). All amplifications were run under the same cycling conditions: 2 min at 50°C, 10 min at 95°C, followed by 40 cycles of 15 s at 95°C and 1 min at 60°C. All samples were run in duplicate and a negative control (water) was included in each array; with *Gapdh* as a reference gene. Results were expressed as log2-fold changes of ΔΔCt values relative to control spinal cord lesions treated with saline.

Analysis of locomotor functions

To investigate the effect of the hydrogel treatment on the gait of the rat, locomotor functions were quantitatively evaluated using MotoRater 303030 and TSE Motion 8.5.11 software (TSE-systems, Germany) (Supporting Information).

Statistical evaluation

Statistical significance of the differences in histological analysis between the groups with acute hydrogel application at two time points was determined using two-way ANOVA. A one-way ANOVA with Holm-Sidak method for all pairwise multiple comparison was used for the comparisons of histological analysis and gene expression between the groups with subacute injection of hydrogels at 8 weeks (SigmaPlot V13; Systat Software Inc., USA). All data in graphs are expressed as mean ± SEM.

RESULTS

Characterization of HA-PH-RGD hydrogel

In this study, we developed new peptide sequences composed of HPA-K-AHA-GRGD (PH-RGD). The structure of this sequences allows to attach to the polymer backbone both PH moiety and RGD cell-adhesive motive in one synthetic step. The conjugation of this sequence with hyaluronan polyaldehyde was performed via reductive amination. The DS of the prepared conjugate was determined by ^{1}H NMR as 2.5%, and thus the achieved concentration of the RGD sequence was 1 µmol/mL in hydrogel, containing 20 mg/mL HA-PH-RGD derivative (NMR spectra in Supporting Information Figs. S1–S3).

HA-PH-RGD derivative was crosslinked by the use of HRP and H_2O_2, and the gelation rate was evaluated by the rheological measurement. The dosing of the crosslinking agents (HRP, H_2O_2) was optimized to 0.04 U/mL HRP and 0.165 mM H_2O_2, to obtain a compressive modulus similar to the native neural tissue and gelation time of 61 ± 4 s ($n = 3$), which is appropriate to achieve a safe application of
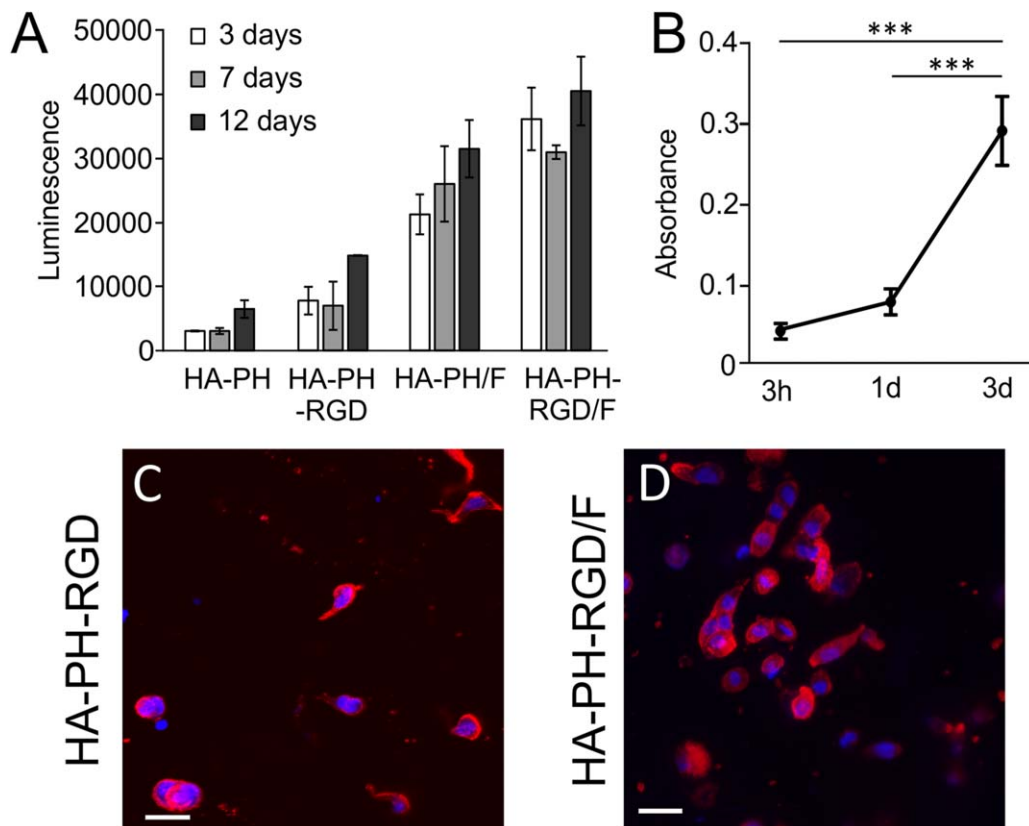
FIGURE 2. A: Proliferation of hWJ-MSCs in HA-PH hydrogels on different adhesive substrates (RGD peptide, F-fibrinogen) measured by luminescence of ATP. Statistical differences between the groups are shown in Supporting Information Table S3. B: Proliferation of hWJ-MSCs in 3D culture of HA-PH-RGD/F hydrogel measured by WST-1 assay. ***$p < 0.001$, ($n = 3$). C,D: The morphology of hWJ-MSCs in 3D culture in HA-PH-RGD and HA-PH-RGD/F hydrogel after 1 day of cultivation stained for phalloidin (red) and DAPI (blue). Scale bar: 25 μm.

the viscous pre-gel solution into the site of the defect using a syringe [Fig. 1(C)].

The effect of hydrogel swelling on mechanical strength is shown in Figure 1(D). The mechanical strength of the material slightly decreased, which corresponded to the decreasing of G′ modulus of the samples.

In vitro cell culture

The toxicity of crosslinking agents (HRP and H_2O_2) was tested by their addition to hWJ-MSC culture, while no cytotoxic effects were observed at concentrations which were used for the hydrogel gelation (Supporting Information Table S2). Proliferation of hWJ-MSCs seeded on HA-PH, and HA-PH-RGD hydrogel, combined with fibrinogen (F) is shown in Figure 2(A). Low cell proliferation was found on the unmodified HA-PH hydrogel, which was further increased on the HA-PH modified with RGD. A remarkable increase in the cell proliferation rate was then achieved when the HA-PH and HA-PH-RGD hydrogels were combined with fibrinogen. Therefore, for cell encapsulation, fibrinogen (1 mg/mL) was added into the HA-PH-RGD hydrogel. The ability of HA-PH-RGD/F to support cell proliferation in 3D culture was further verified by the WST-1 method after 3 h, 1, and 3 days [Fig. 2(B)]. Despite of enhanced cell proliferation, the morphology of hWJ-MSCs after 1 day in 3D culture

was found similar in HA-PH-RGD and HA-PH-RGD/F [Fig. 2(C,D)].

Evaluation of HA-PH-RGD hydrogels in acute SCI lesions

Two ways of hydrogel application were compared in the acute SCI lesion; implantation of the *in vitro* crosslinked HA-PH-RGD hydrogel and injection of the HA-PH-RGD together with crosslinking agents to form a hydrogel *in situ*. Both implanted and injected HA-PH-RGD hydrogels filled the lesion cavity and were highly populated with endogenous cells. The dense ingrowth of neurofilaments [Fig. 3(A)], as well as blood vessels [Fig. 3(B)] into the hydrogel-treated lesion was observed throughout the whole implant after 2 weeks, and persisted with no considerable changes 8 weeks after application. Quantitative analysis revealed a higher density of neurofilaments [Fig. 3(C)] and blood vessels [Fig. 3(D)] in both hydrogel groups compared with the control lesion, while no differences were found between the lesion treated by hydrogel implantation or injection at any time point. Figure 3(F,G) then depicted migrating astrocytes (staining for GFAP) and Figure 3(H) newly formatted axonal growth cones (staining for GAP43) invading into the hydrogel treated lesion. The results show that the hydrogel injection into the lesion and its subsequent crosslinking *in situ* is not harmful to the surrounding tissue and represents a
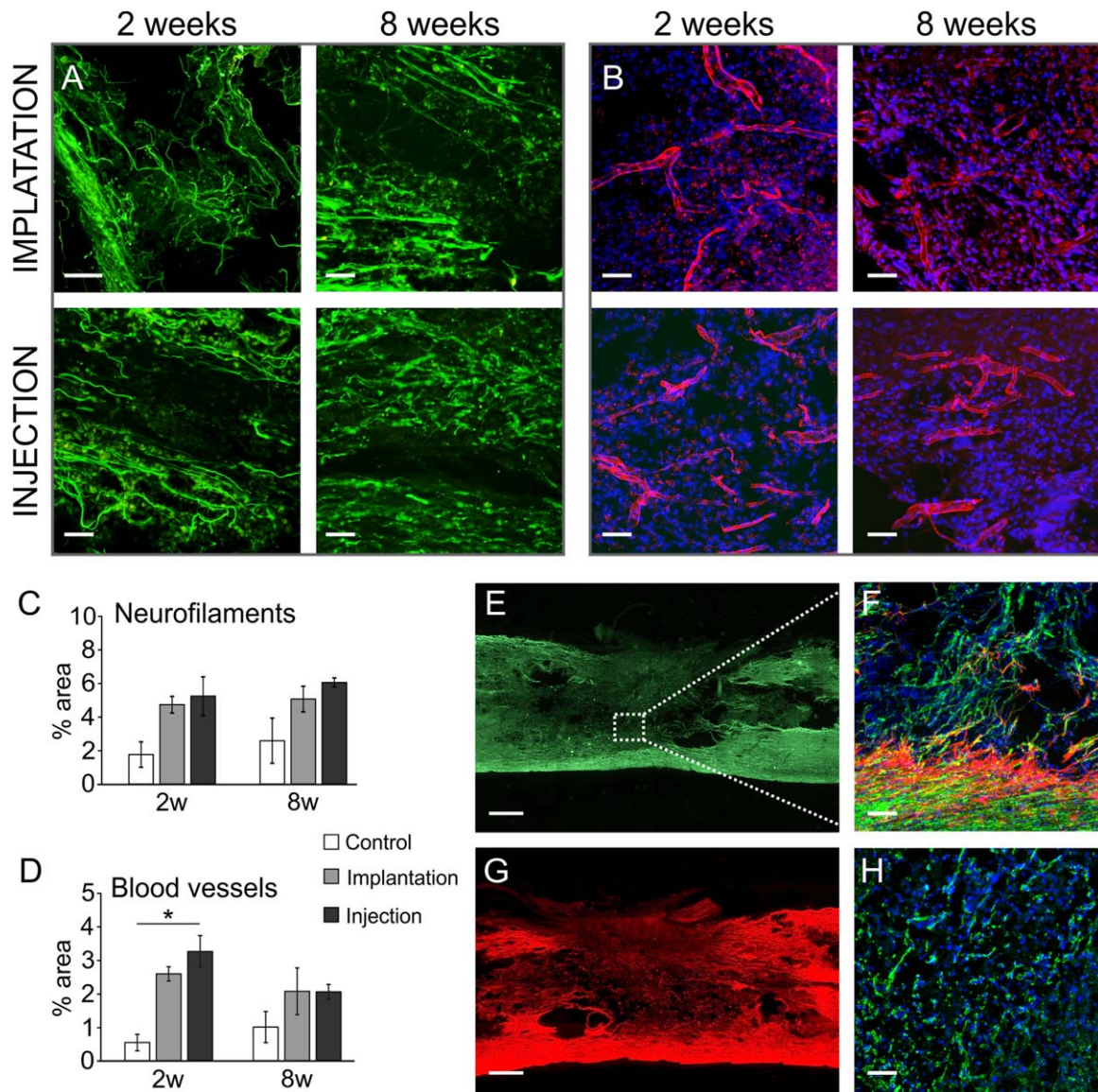
FIGURE 3. Representative images of longitudinal sections of the spinal cord lesion 2 and 8 weeks after the acute HA-PH-RGD hydrogel injection or implantation into the hemisection cavity: Staining for (A) neurofilaments (NF-160, green) and (B) blood vessels (RECA, red; DAPI, blue). Quantitative analysis of the ingrowth of (C) neurofilaments and (D) blood vessels into the lesion area 2 and 8 weeks after the injection or implantation of HA-PH-RGD hydrogel. The values are expressed as the percentage of (C) NF-160 or (D) RECA positive area from a total lesion area. ($n = 3$), *$p < 0.05$. E: Immunofluorescent staining for neurofilaments (NF-160); square in (E) is shown under the higher magnification inset in (F); (F) immunofluorescent staining for neurofilaments (NF-160, green), astrocytes (GFAP, red) and cell nuclei (DAPI, blue) and (G) immunofluorescent staining for astrocytes (GFAP) 2 weeks after HA-PH-RGD injection. (H) Immunofluorescent staining for growth associated protein 43 (GAP43, green) and cell nuclei (DAPI, blue) 8 weeks after HA-PH-RGD hydrogel implantation. Scale bar: 500 μm (E, G), 50 μm (A, B, F, H).

non-invasive and effective way of hydrogel delivery resulting in tissue repair.

Histological evaluation of HA-PH-RGD hydrogels in subacute SCI lesion

The tissue response of the subacute injection of HA-PH-RGD, HA-PH-RGD/F, and HA-PH-RGD/F combined with hWJ-MSCs was evaluated after 8 weeks. As is apparent from Figure 4, both HA-PH-RGD and HA-PH-RGD/F hydrogels significantly improved the density of neurofilaments within the lesion when compared to the control untreated lesion, and this effect was further enhanced by the addition of hWJ-

MSCs. Because immunohistochemical results of HA-PH-RGD/F did not significantly differ from the results obtained with HA-PH-RGD, we did not show the immunohistochemistry of this group.

Astrocytes, detected by immunofluorescence staining for GFAP (Fig. 5), migrated from the lesion border to the lesion area treated by hydrogel, which suggests the formation of a permissive environment promoting glial cell infiltration [Fig. 5(D,F)]. Quantitative evaluation of the GFAP staining density around the lesion, which should reflect the density of the glial scar, did not reveal significant differences between the control and hydrogel treated groups [Fig. 5(G)]. Blood vessels densely
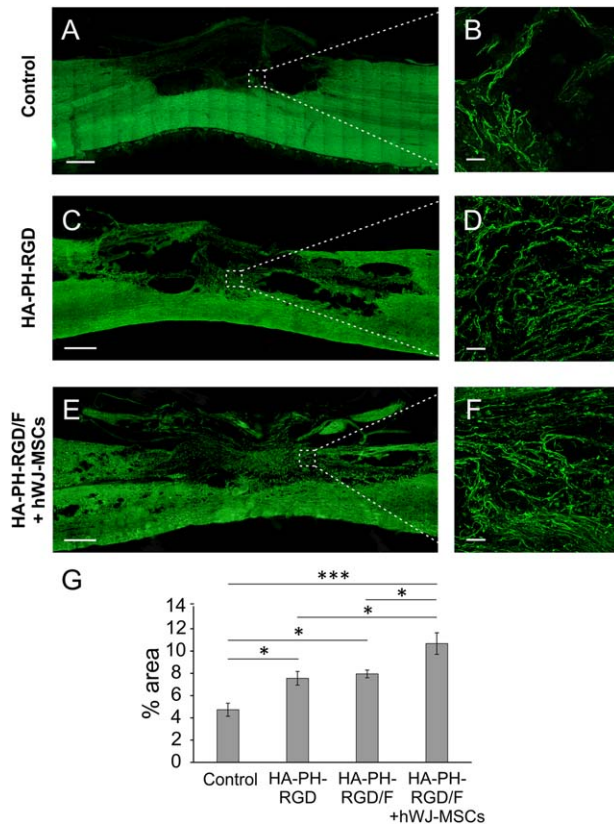
FIGURE 4. Representative images of the longitudinal sections of the spinal cord lesion in (A,B) controls and at 8 weeks after the subacute injection of (C,D) HA-PH-RGD and (E,F) HA-PH-RGD/F hydrogels combined with hWJ-MSCs, stained for neurofilaments (NF-160). Squares (A,C,E) are also shown under the higher magnification insets (B,D,F). G: Quantitative analysis of axonal ingrowth is expressed as the percentage of NF-160 positive area from a total lesion area ($n = 6$). $*p < 0.05$, $***p < 0.001$. Scale bar: 500 μm (A,C,E), 50 μm (B,D,F).

FIGURE 5. Representative images of the longitudinal sections of the spinal cord lesion in (A,B) control and at 8 weeks after subacute injection of (C,D) HA-PH-RGD and (E,F) HA-PH-RGD/F hydrogels combined with hWJ-MSCs, stained for astrocytes (GFAP). Squares (A,C,E) are also shown under the higher magnification insets (B,D,F). G: Quantitative analysis of the glial scar density around the lesion was expressed as the CTCF of GFAP staining ($n = 6$). Scale bar: 500 μm (A,C,E), 50 μm (B,D,F).

infiltrated the hydrogel treated lesion, however the increase in blood vessel density was not found to be significant when compared with the control lesion (Fig. 6).
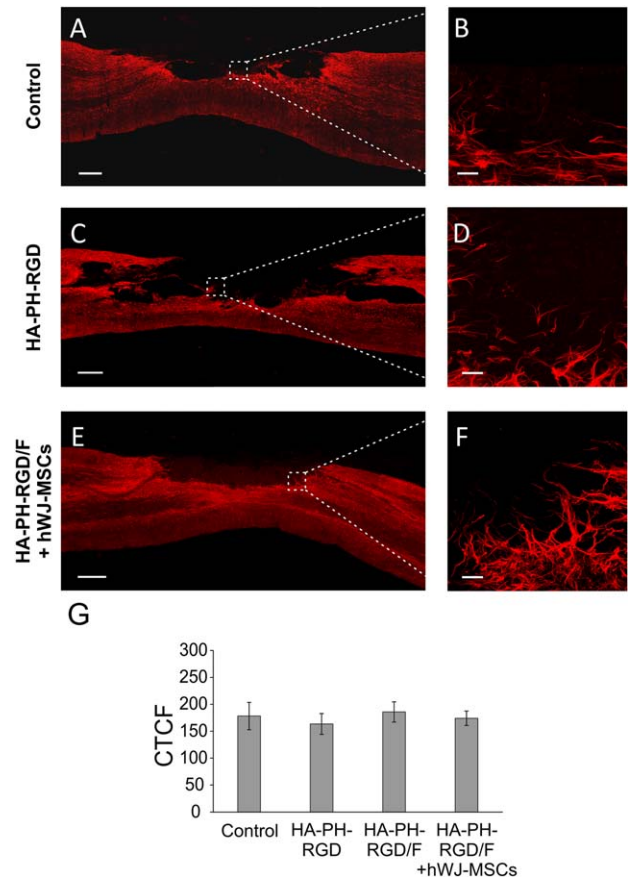
ED1 staining, specific for microglia/macrophages, combined with CD206 staining specific for M2 macrophages confirmed the migration of both M1 and M2 macrophages into the hydrogel treated lesion, however, no quantification was performed to detect the M1/M2 ratio [Fig. 7(A–D)]. Oligodendrocytes were detected in the area of hydrogel treated lesions, but not in the control lesion [Fig. 7(E–H)].

Of note, we did not observe any hWJ-MSCs in the spinal cord tissue eight weeks after cell application, on the basis of staining for the human mitochondria (MTCO2) marker used for the detection of human MSCs in the host tissue.

Gene expression analysis in subacute SCI lesions
Changes in the mRNA expression of selected genes were determined 8 weeks after the injection of HA-PH-RGD, HA-PH-RGD/F and HA-PH-RGD/F hydrogel combined with hWJ-MSCs (Fig. 8).

Both the HA-PH-RGD and HA-PH-RGD/F hydrogel injections resulted in a decrease in mRNA expression of genes related to macrophages (*Irf5, Cd86*), inflammation (*Ccl3*) or

glial scar formation (*Gfap, Ptprz1*), but these changes were not significant. Significant downregulation was then found for the expression of *Gap43* when compared with the untreated control lesion. On the contrary, the expression of *Gap43* was significantly increased when the HA-PH-RGD/F was combined with hWJ-MSCs. Similarly, a combination with hWJ-MSCs led to significant upregulation of both M1 (*Irf5, Cd86*) and M2 macrophages markers (*Mrc1*).

Analysis of locomotor functions in subacute SCI lesions
The effect of the hydrogel treatment on the locomotor functions, such as knee and ankle angles and hind limb retraction and protraction (distance on x-axis of metatarsophalangeal joint in relation to iliac crest), was measured using the TSE Motion 8.5.11. No statistical differences between the control and hydrogel treated animals was found at 2, 5 and 8 weeks (Supporting Information Fig. S7).

DISCUSSION
HA-based hydrogels have great potential as scaffold materials for cell delivery in various tissue engineering applications.
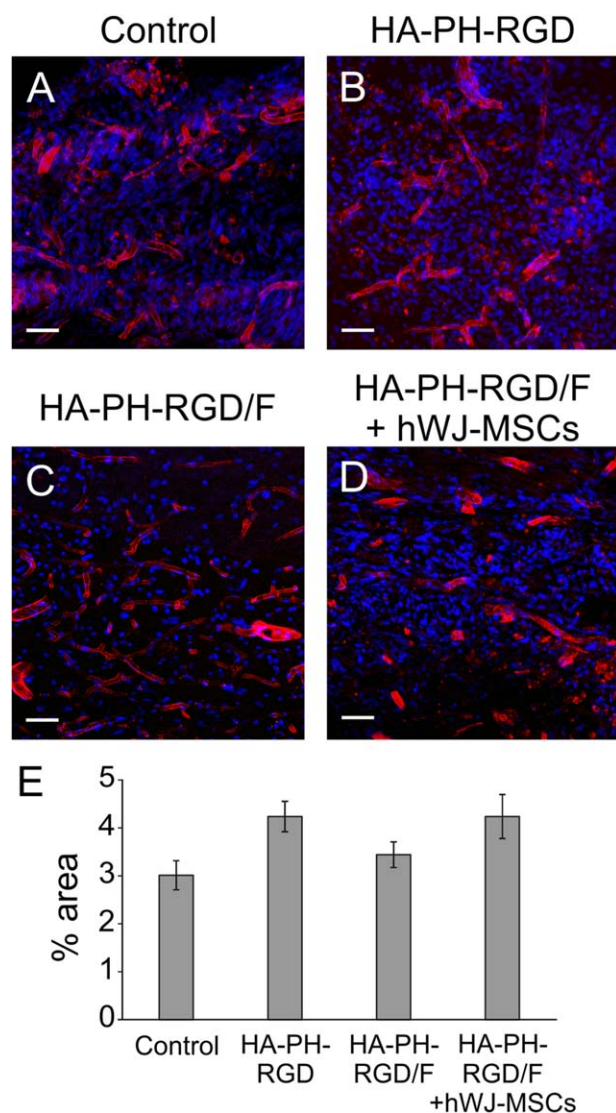
FIGURE 6. Representative images of the longitudinal sections of the spinal cord lesion in (A) control and at 8 weeks after subacute injection of (B) HA-PH-RGD, (C) HA-PH-RGD/F and (D) HA-PH-RGD/F hydrogel combined with hWJ-MSCs, stained for blood vessels (RECA, red) and DAPI (blue). E: Quantitative analysis of blood vessel ingrowth is expressed as the percentage of RECA positive area from a total lesion area ($n = 6$). Scale bar: 50 μm.

In the present study, we prepared and characterized injectable HA-PH derivative based hydrogel, specifically developed for neural tissue repair. The big advantage of this material over the others is that it can be manufactured in a reproducible manner under GMP (Good Manufacture Practice) conditions, which are required to allow the transfer of its production from bench-to-bedside in clinical practise.

To form a hydrogel, we used an enzymatic crosslink reaction initiated by HRP and H_2O_2. The concentration of the cross-linking agents was optimized to set mechanical properties comparable to the native spinal cord tissue, and to get the optimal time of gelation for material application into the site of the defect. Moreover, the used crosslink reaction is non-cytotoxic and enabled to form cell-laden hydrogel under physiological conditions.

To enhance cell adhesion and migration into implants, the HA-PH was functionalized with RGD oligopeptide sequence, which has affinity for multiple integrin receptors, and has been previously shown to support effective cell spreading and cytoskeletal organization, as well as cell proliferation.[42] However, an important factor in the establishment of cell adhesion is ligand density, which is, in the case of used HA-PH-RGD derivative, limited to the DS of PH-RGD oligopeptide. Hydrogel containing 20 mg/mL of the new designed HA-PH-RGD conjugate with a DS of 2.5% achieved a concentration of RGD sequence 1 μmol/mL of hydrogel. As was shown in the experiments *in vitro*, the presence of the RGD motive in the HA-PH hydrogel structure improved its cell affinity, but in a limited way. Therefore, for the cell encapsulation, the bioadhesive properties of the HA-PH-RGD hydrogel were further enhanced by the incorporation of fibrinogen which offers cellular adhesive domains and has been previously proved as a natural additive to enhance cell survival, growth and proliferation.[33,34]

On the other hand, the addition of fibrinogen to HA-PH-RGD hydrogel had no effect on the assessed tissue repair parameters in subacute SCI. Notably, when exposed to *in vivo* conditions within the SCI lesion, the hydrogel is infiltrated with extracellular fluid containing various proteins which together with endogenous cell infiltration and degradation of the hydrogel implant may overlap the potential benefit of fibrinogen in HA-PH-RGD/F hydrogel.

To evaluate the repair potential of the HA based hydrogels, the subacute SCI lesion was treated by injection of HA-PH-RGD, HA-PH-RGD/F and HA-PH-RGD/F combined with hWJ-MSCs one week after the lesion induction, and compared with the control injection of saline. Notably, despite the tissue removal after hemisection, the lesion cavity did not remain empty and was commonly filled with debris and connective tissue that enable vascularization with poor axonal infiltration. However, after injection of both HA-PH-RGD and HA-PH-RGD/F, the density of NF-positive fibers in the lesion cavity significantly increased, and this effect was further enhanced when the HA-PH-RGD/F was combined with hWJ-MSCs. Contradictorily, the robust axonal ingrowth into HA-PH-RGD and HA-PH-RGD/F revealed by the histological analysis did not correlate with decreased mRNA expression of gene related to axonal growth (*Gap43*). On the other hand, *Gap43* was upregulated in group with hWJ-MSCs. Gap43, which is expressed at high levels in newly created neuronal growth cones during axonal regeneration, is considered a crucial component of effective regenerative response in the nervous system. It is likely that axonal sprouting into HA-PH-RGD and HA-PH-RGD/F hydrogels might culminate during an earlier period after injury, while still persist in the group with hWJ-MSCs. Therefore, NF160 staining of HA-PH-RGD and HA-PH-RGD/F hydrogel groups carried out at 8 weeks revealed already matured sprouting neurons.

Similarly, the expression of both markers of M1 and M2 macrophage/microglia has been increased when the HA-PH-RGD/F was combined with hWJ-MSCs. It suggests that tissue repair processes, facilitated by the stem cells treatment,
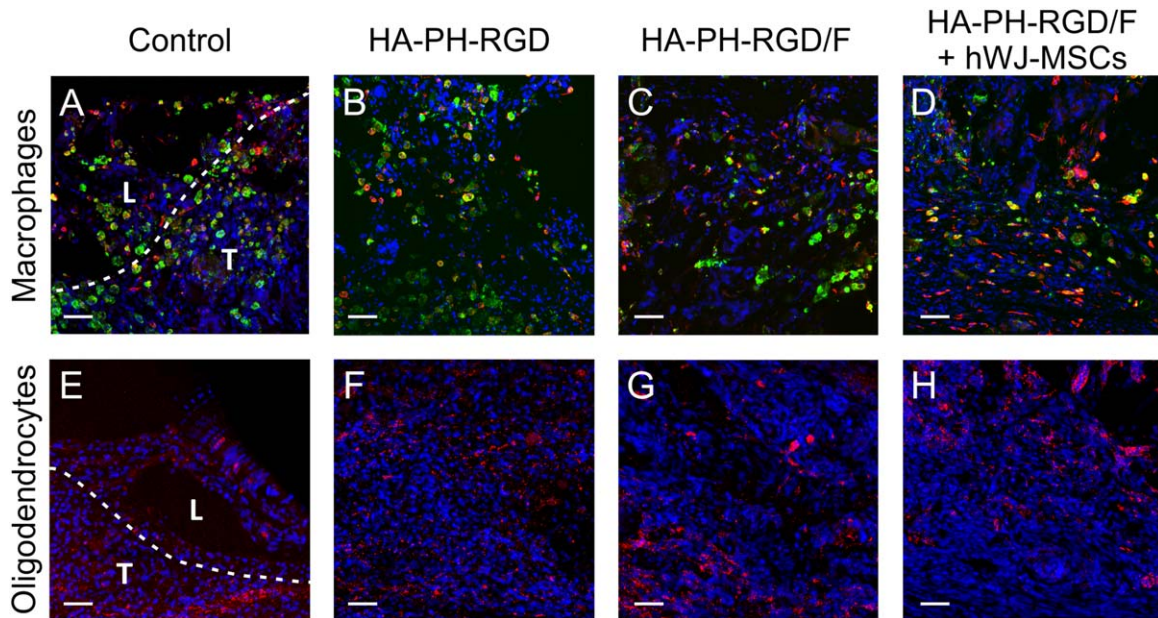
FIGURE 7. Representative images of the longitudinal sections of the spinal cord lesion in (A,E) control and at 8 weeks after subacute injection of (B,F) HA-PH-RGD, (C,G) HA-PH-RGD/F and (D,H) HA-PH-RGD/F hydrogel combined with hWJ-MSCs. Staining for (A–D) macrophages (ED1, green) and M2 macrophages (CD206, red), (E–H) oligodendrocytes (MOSP, red) and (A–H) DAPI (blue). The dotted lines in (A,E) outline the border of the tissue (T) and the lesion area (L). Other images are taken from the center of the lesion. Scale bar: 50 μm.

involves orchestrated activation of different macrophage phenotype.[43]

Despite immunosuppression using the combination of three agents, hWJ-MSCs did not survive in the host tissue over the period of 8 weeks. On the other hand, we proved the effect of the cells using immunohistochemical and qPCR analysis, which supports the commonly proposed hypothesis that transplanted cells release trophic factors that provide long lasting neurotrophic and immunomodulatory effects.[44–46]

In contrast to improvement in tissue repair parameters, no significant improvement in locomotor functions was observed in animals treated with both hydrogel alone or in combination with hWJ-MSCs. Although it is unlikely that HA scaffolds alone can lead to behavioral restoration without additional treatment, the combination of hydrogels with various stem cells may have beneficial effects on the repair of the injured spinal cord by providing trophic support.[2–4] However, an important factor which significantly affects the
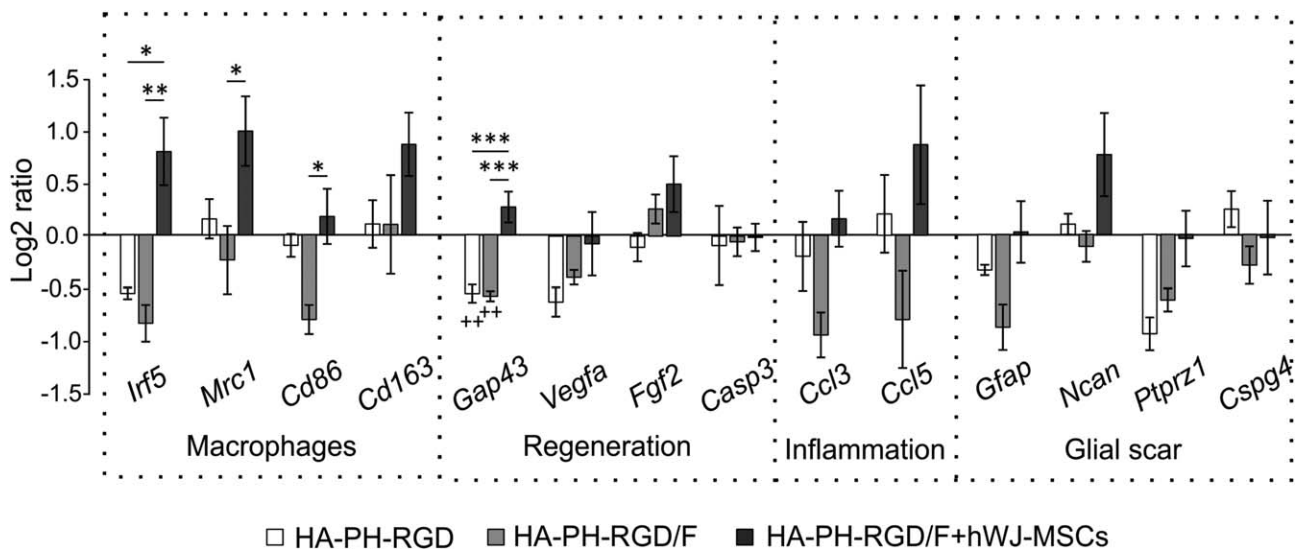
FIGURE 8. Analysis of mRNA gene expression of selected genes involved in the reparative processes following SCI treated with HA-PH-RGD, HA-PH-RGD/F, and HA-PH-RGD/F hydrogel combined with hWJ-MSCs. The graph shows the log2-fold changes in gene expression over the control lesion with saline. Significance is calculated between ΔCt values. $++p < 0.01$: versus control lesion, $*p < 0.05$, $**p < 0.01$, $***p < 0.001$, ($n = 5$).

behavioral outcome after SCI is the number of transplanted cells.

In our previous study, an effective hWJ-MSC dose, necessary to induce functional improvement after contusion SCI, was determined as 1.5 million cells in a single intrathecal application (unpublished data). The higher dose of transplanted cells would probably increase number of surviving cells as well as behavioural outcome. However, in this study, we primarily evaluate the feasibility of HA-PH-RGD hydrogel for neural tissue repair and as a cell carrier per se. Therefore, the number of transplanted cells (approximately 3×10^4 cells) was limited by the size of the lesion and hydrogel volume (approximately 5 μL), and did not exceed the level at which the functional locomotor improvement could be achieved. To overcome the limitation of the number of cells that can be implanted with the hydrogel, we propose a combination of hydrogel with additional cell application via direct cell injection into the lesion site or via intrathecal application.

To test the therapeutic approach, we used a spinal cord hemisection, because it is the least invasive and devastating SCI model for the evaluation of new biomaterials, allows filling the lesion cavity with the material and clear analysis of the endogenous infiltration into the implant.[16,47,48] On the other hand, this model is a case of partial lesions with a high rate of spontaneous recovery and a high risk of inconsistencies in the injuries from one animal to the next, which might lead to misinterpretation of the behavioral evaluation.[49] Further investigation using the SCI model, which completely cuts a projecting system of axons together with systematic functional evaluation is therefore the next step in establishing the HA-PH-RGD hydrogel as a scaffold for SCI repair.

In conclusion, many types of scaffolds are able to support axonal growth and spouting after SCI, but are unable to achieve significant functional recovery, due to the reduced regeneration of long-tract axons through sites of SCI. Besides the development of optimal materials for bridging the lesion, modifying the extrinsic and intrinsic factors limiting regrowth after SCI represent the current challenge of how to overcome the inhibitory properties of the axon–scar environment. Combinatorial therapies will probably be essential to achieve such functional connectivity.[50]

CONCLUSION

This study showed that injectable HA-PH-RGD based hydrogel may be a promising material for SCI repair in rats. Injection of HA-PH-RGD hydrogels bridged the lesion cavity, supported vascularization and increased axonal sprouting into the lesion, which was further improved by its combination with hWJ-MSC. However, enhancement of transplanted cell survival as well as additional treatments that would further stimulate axonal reconnection, are required to overcome HA-PH-RGD hydrogel limitation in functional SCI restoration.

ACKNOWLEDGMENTS

DISCLOSURE

Kristyna Zaviskova, Dmitry Tukmachev, Jana Dubisova, Irena Vackova, Ales Hejcl, and Sarka Kubinova have no affiliations with or involvement in any organization or entity with any financial interest, or non-financial interest in the subject matter or materials discussed in this article. Julie Bystronova, Martin Pravda, Ivana Scigalkova, Romana Sulakova, and Lucie Wolfova are employees of Contipro a.s. which is a producer of HA and derivatives of HA, and which provided hyaluronan based materials for the article.

REFERENCES

1. Hill CE. A view from the ending: axonal dieback and regeneration following SCI. Neurosci Lett 2016;652:11–24.
2. Kubinova S, Sykova E. Biomaterials combined with cell therapy for treatment of spinal cord injury. Regen Med 2012;7:207–224.
3. Pego AP, Kubinova S, Cizkova D, Vanicky I, Mar FM, Sousa MM, Sykova E. Regenerative medicine for the treatment of spinal cord injury: more than just promises? J Cell Mol Med 2012;16:2564–2582.
4. Shrestha B, Coykendall K, Li YC, Moon A, Priyadarshani P, Yao L. Repair of injured spinal cord using biomaterial scaffolds and stem cells. Stem Cell Res Ther 2014;5:91.
5. Park J, Lim E, Back S, Na H, Park Y, Sun K. Nerve regeneration following spinal cord injury using matrix metalloproteinase-sensitive, hyaluronic acid-based biomimetic hydrogel scaffold containing brain-derived neurotrophic factor. J Biomed Mater Res A 2010;93:1091–1099.
6. Li X, Zhao Y, Cheng S, Han S, Shu M, Chen B, Chen X, Tang F, Wang N, Tu Y, Wang B, Xiao Z, Zhang S, Dai J. Cetuximab modified collagen scaffold directs neurogenesis of injury-activated endogenous neural stem cells for acute spinal cord injury repair. Biomaterials 2017;137:73–86.
7. King VR, Hewazy D, Alovskaya A, Phillips JB, Brown RA, Priestley JV. The neuroprotective effects of fibronectin mats and fibronectin peptides following spinal cord injury in the rat. Neuroscience 2010;168:523–530.
8. Khaing ZZ, Milman BD, Vanscoy JE, Seidlits SK, Grill RJ, Schmidt CE. High molecular weight hyaluronic acid limits astrocyte activation and scar formation after spinal cord injury. J Neural Eng 2011;8:046033.
9. Kushchayev SV, Giers MB, Hom Eng D, Martirosyan NL, Eschbacher JM, Mortazavi MM, Theodore N, Panitch A, Preul MC. Hyaluronic acid scaffold has a neuroprotective effect in hemisection spinal cord injury. J Neurosurg Spine 2016;25:114–124.
10. Mothe AJ, Tam RY, Zahir T, Tator CH, Shoichet MS. Repair of the injured spinal cord by transplantation of neural stem cells in a hyaluronan-based hydrogel. Biomaterials 2013;34:3775–3783.
11. Raynald, Li Y, Yu H, Huang H, Guo M, Hua R, Jiang F, Zhang K, Li H, Wang F, Li L, Cui F, An Y. The hetero-transplantation of human bone marrow stromal cells carried by hydrogel unexpectedly demonstrates a significant role in the functional recovery in the injured spinal cord of rats. Brain Res 2016;1634:21–33.
12. Wang X, He J, Wang Y, Cui FZ. Hyaluronic acid-based scaffold for central neural tissue engineering. Interface Focus 2012;2:278–291.
13. Gomes ED, Mendes SS, Leite-Almeida H, Gimble JM, Tam RY, Shoichet MS, Sousa N, Silva NA, Salgado AJ. Combination of a peptide-modified gellan gum hydrogel with cell therapy in a lumbar spinal cord injury animal model. Biomaterials 2016;105:38–51.
14. Caicco MJ, Zahir T, Mothe AJ, Ballios BG, Kihm AJ, Tator CH, Shoichet MS. Characterization of hyaluronan-methylcellulose hydrogels for cell delivery to the injured spinal cord. J Biomed Mater Res A 2013;101:1472–1477.
15. Koci Z, Vyborny K, Dubisova J, Vackova I, Jager A, Lunov O, Jirakova K, Kubinova S. ECM hydrogel derived from human umbilical cord as a scaffold for neural tissue repair and its comparison to ECM from CNS and non-CNS porcine tissues. Tissue Eng Part C Methods 2017;23:333–345.
16. Tukmachev D, Forostyak S, Koci Z, Zaviskova K, Vackova I, Vyborny K, Sandvig I, Sandvig A, Medberry CJ, Badylak SF, Sykova E,

Kubinova S. Injectable extracellular matrix hydrogels as scaffolds for spinal cord injury repair. Tissue Eng A 2016;22:306–317.

17. Litwiniuk M, Krejner A, Speyrer MS, Gauto AR, Grzela T. Hyaluronic acid in inflammation and tissue regeneration. Wounds 2016;28:78–88.

18. Knopf-Marques H, Pravda M, Wolfova L, Velebny V, Schaaf P, Vrana NE, Lavalle P. Hyaluronic acid and its derivatives in coating and delivery systems: applications in tissue engineering, regenerative medicine and immunomodulation. Adv Healthcare Mater 2016;5:2841–2855.

19. Seidlits SK, Khaing ZZ, Petersen RR, Nickels JD, Vanscoy JE, Shear JB, Schmidt CE. The effects of hyaluronic acid hydrogels with tunable mechanical properties on neural progenitor cell differentiation. Biomaterials 2010;31:3930–3940.

20. Liang Y, Walczak P, Bulte JW. The survival of engrafted neural stem cells within hyaluronic acid hydrogels. Biomaterials 2013;34: 5521–5529.

21. Li L-M, Han M, Jiang X-C, Yin X-Z, Chen F, Zhang T-Y, Ren H, Zhang J-W, Hou T-J, Chen Z, Ou-Yang H-W, Tabata Y, Shen Y-Q, Gao J-Q. Peptide-tethered hydrogel scaffold promotes recovery from spinal cord transection via synergism with mesenchymal stem cells. ACS Appl Mater Interfaces 2017;9:3330–3342.

22. Fuhrmann T, Obermeyer J, Tator CH, Shoichet MS. Click-cross-linked injectable hyaluronic acid hydrogel is safe and biocompatible in the intrathecal space for ultimate use in regenerative strategies of the injured spinal cord. Methods 2015;84:60–69.

23. Gupta D, Tator CH, Shoichet MS. Fast-gelling injectable blend of hyaluronan and methylcellulose for intrathecal, localized delivery to the injured spinal cord. Biomaterials 2006;27:2370–2379.

24. Wei YT, He Y, Xu CL, Wang Y, Liu BF, Wang XM, Sun XD, Cui FZ, Xu QY. Hyaluronic acid hydrogel modified with nogo-66 receptor antibody and poly-L-lysine to promote axon regrowth after spinal cord injury. J Biomed Mater Res B Appl Biomater 2010;95:110–117.

25. Hou S, Xu Q, Tian W, Cui F, Cai Q, Ma J, Lee IS. The repair of brain lesion by implantation of hyaluronic acid hydrogels modified with laminin. J Neurosci Methods 2005;148:60–70.

26. Seidlits SK, Drinnan CT, Petersen RR, Shear JB, Suggs LJ, Schmidt CE. Fibronectin-hyaluronic acid composite hydrogels for three-dimensional endothelial cell culture. Acta Biomater 2011;7: 2401–2409.

27. Snyder TN, Madhavan K, Intrator M, Dregalla RC, Park D. A fibrin/hyaluronic acid hydrogel for the delivery of mesenchymal stem cells and potential for articular cartilage repair. J Biol Eng 2014;8:10.

28. Cui FZ, Tian WM, Hou SP, Xu QY, Lee IS. Hyaluronic acid hydrogel immobilized with RGD peptides for brain tissue engineering. J Mater Sci Mater Med 2006;17:1393–1401.

29. Darr A, Calabro A. Synthesis and characterization of tyramine-based hyaluronan hydrogels. J Mater Sci Mater Med 2009;20:33–44.

30. Wolfova L, Pravda M, Foglarova M, Memcova M, Niedoba K, Velebny V. Derivates based on hyaluronic acid, capable of forming hydrogels, method of preparation thereof, hydrogels based on said derivatives, method of preparation thereof and use. Patent WO2013127374 A1; 2013.

31. Kučera L, Weinfurterová R, Dvořáková J, Kučera J, Pravda M, Foglarová M, Švík K, Klein P, Velebný V, Kubala L. Chondrocyte cultivation in hyaluronan-tyramine cross-linked hydrogel. Int J Polymer Mater PolymerBiomaterials 2015;64:661–674.

32. Dvořáková J, Kučera L, Kučera J, Švík K, Foglarová M, Muthný T, Pravda M, Němcová M, Velebný V, Kubala L. Chondrogenic differentiation of mesenchymal stem cells in a hydrogel system based on an enzymatically crosslinked tyramine derivative of hyaluronan. J Biomed Mater Res A 2014;102:3523–3530.

33. Karoubi G, Ormiston ML, Stewart DJ, Courtman DW. Single-cell hydrogel encapsulation for enhanced survival of human marrow stromal cells. Biomaterials 2009;30:5445–5455.

34. Zapotocky V, Pospisilova M, Janouchova K, Svadlak D, Batova J, Sogorkova J, Cepa M, Betak J, Stepankova V, Sulakova R, Kulhanek J, Pitucha T, Vranova J, Duffy G, Velebny V. Fabrication of biodegradable textile scaffold based on hydrophobized hyaluronic acid. Int J Biol Macromol 2017;95:903–909.

35. Cheng H, Liu X, Hua R, Dai G, Wang X, Gao J, An Y. Clinical observation of umbilical cord mesenchymal stem cell transplantation in treatment for sequelae of thoracolumbar spinal cord injury. J Transl Med 2014;12:253.

36. Li X, Tan J, Xiao Z, Zhao Y, Han S, Liu D, Yin W, Li J, Li J, Wanggou S, Chen B, Ren C, Jiang X, Dai J. Transplantation of hUC-MSCs seeded collagen scaffolds reduces scar formation and promotes functional recovery in canines with chronic spinal cord injury. Sci Rep 2017;7:43559.

37. Zhao Y, Tang F, Xiao Z, Han G, Wang N, Yin N, Chen B, Jiang X, Yun C, Han W, Zhao C, Cheng S, Zhang S, Dai J. Clinical study of neuroregen scaffold combined with human mesenchymal stem cells for the repair of chronic complete spinal cord injury. Cell Transplant 2017;26:891–900.

38. Amblard M, Fehrentz J-A, Martinez J, Subra G. Methods and protocols of modern solid phase peptide synthesis. Mol Biotechnol 2006;33:239–254.

39. Huerta-Angeles G, Němcová M, Příkopová E, Šmejkalová D, Pravda M, Kučera L, Velebný V. Reductive alkylation of hyaluronic acid for the synthesis of biocompatible hydrogels by click chemistry. Carbohydr Polym 2012;90:1704–1711.

40. Šedová P, Buffa R, Kettou S, Huerta-Angeles G, Hermannová M, Leierová V, Šmejkalová D, Moravcová M, Velebný V. Preparation of hyaluronan polyaldehyde—a precursor of biopolymer conjugates. Carbohydr Res 2013;371:8–15.

41. McCloy RA, Rogers S, Caldon CE, Lorca T, Castro A, Burgess A. Partial inhibition of Cdk1 in G 2 phase overrides the SAC and decouples mitotic events. Cell Cycle 2014;13:1400–1412.

42. Mackova H, Plichta Z, Proks V, Kotelnikov I, Kucka J, Hlidkova H, Horak D, Kubinova S, Jirakova K. RGDS- and SIKVAVS-modified superporous poly(2-hydroxyethyl methacrylate) scaffolds for tissue engineering applications. Macromol Biosci 2016;16:1621–1631.

43. Gensel JC, Zhang B. Macrophage activation and its role in repair and pathology after spinal cord injury. Brain Res 2015;1619:1–11.

44. Urdzíková L, Růžička J, LaBagnara M, Kárová K, Kubinová Š, Jiráková K, Murali R, Syková E, Jhanwar-Uniyal M, Jendelová P. Human mesenchymal stem cells modulate inflammatory cytokines after spinal cord injury in rat. Int J Mol Sci 2014;15:11275–11293.

45. Petrenko Y, Sykova E, Kubinova S. The therapeutic potential of three-dimensional multipotent mesenchymal stromal cell spheroids. Stem Cell Res Ther 2017;8:94.

46. Assinck P, Duncan GJ, Hilton BJ, Plemel JR, Tetzlaff W. Cell transplantation therapy for spinal cord injury. Nat Neurosci 2017;20: 637–647.

47. Kubinova S, Horak D, Hejcl A, Plichta Z, Kotek J, Proks V, Forostyak S, Sykova E. SIKVAV-modified highly superporous PHEMA scaffolds with oriented pores for spinal cord injury repair. J Tissue Eng Regen Med 2015;9:1298–1309.

48. Kubinova S, Horak D, Hejcl A, Plichta Z, Kotek J, Sykova E. Highly superporous cholesterol-modified poly(2-hydroxyethyl methacrylate) scaffolds for spinal cord injury repair. J Biomed Mater Res A 2011;99:618–629.

49. Fouad K, Hurd C, Magnuson DS. Functional testing in animal models of spinal cord injury: not as straight forward as one would think. Front Integr Neurosci 2013;7:85.

50. Chew DJ, Fawcett JW, Andrews MR. The challenges of long-distance axon regeneration in the injured CNS. Prog Brain Res 2012;201:253–294.